Modelling Arctic Sea Ice: On the Relationship between Ice Thickness Distributions and the Ice Strength

Modelle für arktisches Meereis:

Zusammenhänge zwischen Eisdickenverteilungen und der

Eisstärke

PhD thesis

by

Mischa Ungermann

Department 1

Physics and Electrical Engineering

Universität Bremen

September 22, 2017

First reviewer: Prof. Dr. Thomas Jung
                    Alfred Wegener Institute
                    Helmholtz Centre for Polar and Marine Research
Second reviewer: Prof. Dr. Christian Haas
                    Alfred Wegener Institute
                    Helmholtz Centre for Polar and Marine Research

Abstract

The effects of anthropogenic climate change are most drastic in the Arctic. This amplification of climate change signals is strongly connected to the sea ice in the Arctic Ocean. This thesis presents an analysis of the sea ice cover in numerical ocean – sea ice models with a focus on two different parameterizations: an active ice thickness distribution and an ice strength parameterization that is based on this additional thickness information. The research questions are: (1) can the parameterizations improve the reproduction of Arctic-wide sea ice observations? (2) Do the parameterizations actually reproduce physically observed behavior? (3) How can the parameterizations and their use in basin-scale models be improved further?

In a first step, model quality is assessed by a quantitative measure of the reproduction of satellite observations of sea ice concentration, thickness and drift. Including a full ice thickness distribution in each grid cell instead of only two ice categories clearly improves the model results. At the same time, a strength parameterization based on a two-category approach produces better model results than a multi-category strength parameterization.

In a next step, the two parameterizations are evaluated in more detail. The ice thickness distribution parameterization reproduces local observations in the Arctic to a large degree and simulates faithfully regional and seasonal differences found in observed distributions. The poor performance of the multi-category ice strength parameterization is explained by the physical assumptions that were made in its original derivation and that do not agree with the current understanding of the ice cover.

In conclusion, using an ice thickness distribution improves model performance, but a multi-category parameterization of the ice strength should be avoided. In future work, a new ice strength parameterization could be derived from the physical properties of the ice pack that are demonstrated in this work.

Zusammenfassung

Die stärksten Effekte des globalen Klimawandels werden in der Arktis beobachtet. Diese Arktische Verstärkung des Klimawandels is eng mit dem Meereis im Arktischen Ozean verbunden. In dieser Dissertation wird die Beschreibung und Reproduktion von Meereis in numerischen Ozean – Meereis Modellen analysiert, speziell der Einfluss von zwei physikalischen Parameterisierungen: einer aktive Eisdickenverteilung und einem Modell der Eisstärke, das auf diesen zusätzlichen Informationen über die Eisdicke basiert. Die Forschungsfragen sind: (1) Können die Parameterisierungen die Reproduktion von Meereisbeobachtungen Arktis-weit verbessern? (2) Reproduzieren die Parameterisierungen das physikalische Verhalten, welches sie eigentlich beschreiben sollen? (3) Wie können die Parameterisierungen und ihre Verwendung in Ozean- und Klimamodellen weiter verbessert werden?

Als Maß der Qualität der Modelle wird die Übereinstimmung von Modellergebnissen und Satellitenbeobachtungen von Meereiskonzentration, -dicke und -drift quantitativ gemessen. Eine Eisdickenverteilung in jeder einzelnen Gitterzelle anstelle von nur zwei Kategorien für Eisdicke verbessern die Modellergebnisse deutlich. Allerdings führt eine Eisstärkenparameterisierung auf Basis von zwei Kategorien zu besseren Ergebnissen als eine Mehr-Kategorien-Eisstärke.

Als nächstes werden die beiden Parameterisierungen im Detail ausgewertet. Örtliche Eisdickenverteilungen in arktischen Beobachtungen werden realistisch wiedergegeben und das Modell reproduziert Unterschiede zwischen den beobachteten Verteilungen aus verschiedenen Regionen oder Jahreszeiten. Die schlechten Ergebnisse der Mehr-Kategorien-Eisstärke können mit den physikalischen Annahmen erklärt werden, die für die urspüngliche Herleitung aufgestellt wurden: nach heutigem Wissensstand sind diese unvollständig.

Als Fazit dieser Arbeit bleibt, dass eine Eisdickenverteilung in mehre-

ren Kategorien zu einer Verbesserung von Meereismodellen führt, aber eine Mehr-Kategorien-Eisstärke vermieden werden sollte. In Weiterführung dieser Arbeit könnte eine neue Eisstärkenparameterisierung auf Basis der hier vorgestellten physikalischen Eigenschaften des Packeises hergeleitet werden.

Contents

CONTENTS

1. Introduction

Anthropogenic climate change can easily be seen as one of the largest challenges humanity ever had to face. As a short, introductory example, the total heat uptake of the upper 2000m of the world ocean from $1955 - 2010$ was $24 \pm 1.9 \times 10^{22}$J (Levitus *et al.*, 2012). To put these immense scales into perspective, the total energy consumption of the European Union in the year 2015 was 4.5×10^{19}J (Eurostat, 2017). So even if we wanted to reproduce a change in the oceans similar to the one we caused unwillingly and spent every effort of our whole society towards this goal, we would still need over $5,000$ years to produce a comparable amount of energy. Our task as climate scientists is set on learning how the climate system works with all its components, so we can understand and predict the changes that are happening and that are yet to come. The most complete collection of this understanding is collected and summarized in the reports of the International Panel on Climate Change (2013).

One striking feature in this report are the changes observed and predicted in the Arctic (Figure 1.1). The surface temperature in the Arctic increases two times faster than the global average (Blunden & Arndt, 2017) and the area covered by sea ice at the end of summer has reduced by 50% since the beginning of reliable satellite data for sea ice concentration in 1979 (Windnagel *et al.*, 2016). With this rapid summer sea ice reduction, the Arctic is estimated to be nearly ice free in summer before the second half of this century (Overland & Wang, 2013).

Manabe & Stouffer (1980) found much stronger changes in the polar regions than in lower latitudes in model simulations with increased greenhouse gas forcing. This so-called "polar amplification" of climatic changes is the combined result of many different factors. Pithan & Mauritsen (2014) found the largest changes in Arctic surface temperature caused by a temperature feedback loop in climate simulations. Further, decadal variability in the
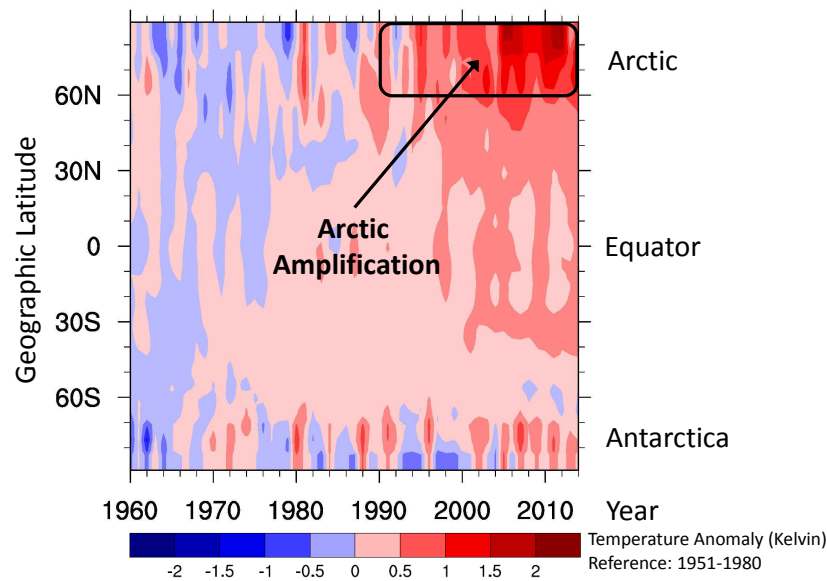
Figure 1.1: Average surface air temperature anomaly (compared to 1951-1980 mean) by year and latitude. Both global warming and the increased warming in the Arctic are clearly visible. Figure taken from (Wendisch *et al.*, 2017)

Pacific Ocean, changing circulation patterns in the Atlantic Ocean and high-latitude atmospheric circulation patterns affect the drastic changes found in observations of the Arctic (Screen & Francis, 2016; Polyakov *et al.*, 2017; Ding *et al.*, 2017). But in addition to these individual factors, all these studies identify the sea ice covering the Arctic Ocean as one of the most important causes of the Arctic amplification.

1.1   Sea Ice in the Arctic

In this section I give a short overview of the different properties and aspects of sea ice. A more detailed description and further sources are given by Thomas & Dieckmann (2009).

The most obvious and defining processes that are relevant for the sea ice are thermodynamic in nature: when it is cold enough, the water in the ocean will freeze into sea ice, when it gets too warm, this sea ice will melt again. When the surface ocean starts to freeze, small ice crystals form in the water. As they get larger, these combine into small platelets, which in turn can coagulate into small ice floes. If there are already ice floes floating on the ocean, the water can freeze onto these floes at the bottom or the edges. Similarly, ice floes do not melt uniformly. Deep reaching features like keels

Figure 1.2: Sea Ice in the central Arctic late in the melting Season. (Picture: M. Hoppmann)

and ridges are eroded more quickly by warm air or ocean currents. When the surface of ice floes melts, the meltwater collects in small ponds on the floe and changes the topography and the albedo.

In addition, the ice pack is in perpetual motion. Arctic sea ice is not a single, uniform pack of ice, but consists of many different floes. While these floes come in all sizes from smaller than a meter to multiple kilometers, they are all floating on the ocean surface where they are pushed at by the wind, the ocean currents, and by each other. Following the dominant wind patterns, the ice travels over the whole Arctic.[1]

All this motion of the ice can lead to floes getting pushed against each other in various angles. The stresses created in such situations are high enough to break the ice. Depending on the thickness of the participating floes, the ice can raft over each other or, if the ice is too thick, break into pieces and pile up into pressure ridges. Similarly, if the stresses are divergent, floes can break apart and create leads of open water in the ice, ranging from small cracks to linear kinematic features spanning the whole Arctic basin.

The final aspect that needs mentioning are the many different scales that are relevant when describing and researching sea ice behavior. The Arctic ice pack measures thousands of kilometers horizontally, but is rarely thicker than

---

[1]As shown probably most impressively by Fridtjof Nansen in the year 1893, who, in an effort to reach the North Pole, let his expedition ship freeze into the ice pack north of the coast of Siberia and waited until the transpolar ice drift moved him closer to the pole.

10m. Additionally, the properties of the ice can be very heterogeneous on the meter scale (Figure 1.2). Ice that has grown without deforming in a similar region has a more or less uniform thickness. But commonly, after only a few weeks, this ice is covered with refrozen leads where the ice is substantially thinner, or pressure ridges where it is much thicker. When moving through the Arctic, ice floes of different source regions mix, so that neighboring floes can have different thicknesses and ice types. And each year that an ice floe survives in the Arctic leaves more scars on its surface from former melt ponds, now maybe drained into empty pools, or old pressure ridges.

Sea ice can be studied from many different points of view. First, it plays a large role in the biological net in the Arctic. It plays a key role in the growth patterns of algae, or more general phytoplankton. These are the foundation of the food web in the oceans and combined with the high amount of nutrients in the Arctic Ocean, they provide food for the large amounts of fish living in the cold waters. But sea ice also provides a habitat for large marine mammals. Changes in the ice cover will not only impact the flora and fauna in and around the ocean, but also the native communities living in the Arctic. In their traditional lifestyle, a closed sea ice cover is important for transportation and hunting (Meier *et al.*, 2014).

Second, a reduction of the sea ice cover allows to develop new possibilities for humans to live and work in the Arctic. Reduced amounts of sea ice will open up new shipping routes with new risks for the Arctic in case of accidents, but also the possibility to reduce the global fuel consumption by shipping (Pizzolato *et al.*, 2016). Similarly, there are new options for fishing and natural resource extraction in the ocean that bring their own particular risks and rewards (Meier *et al.*, 2014).

And finally, the sea ice can be studied as a key factor in the global climate system, which will be the main motivation in this thesis. As mentioned above, it is crucial in the Arctic amplification of climate change. Additionally, there is evidence that the reduction in sea ice can impact the large-scale atmospheric pressure patterns and the amount of summer precipitation in large parts of the northern hemisphere (Vihma, 2014). Extreme weather events in the northern mid-latitudes are thought to be connected to changes in the sea ice cover, although the exact dependence of these highly chaotic events on single factors is still a matter of intense research (Overland *et al.*, 2016).

Multiple reasons make the sea ice so important for the climate in the Arctic and beyond: (1) Sea ice is a highly effective insulator between the atmosphere and the ocean. The drag of the Arctic winds on the surface ocean, the sensible heat transfer between air and water and the radiative exchanges between ocean and atmosphere are all drastically reduced when an ice cover separates the two. (2) In summer, the ice not only changes the distribution of the sunlight by reflecting it before it can reach the ocean, but it also changes the total amount of sunlight that is taken up. Due to the lighter surface of ice compared to the ocean, a larger amount of the incoming radiation is finally reflected back into space (after some scattering in the atmosphere) and does not heat any part of the earth. (3) All these properties often interact and form feedback loops, the major reason for the large effect sea ice has on climate change scenarios.

1.2 Sea Ice Modeling

I use computer models to investigate the properties of sea ice. There are multiple arguments in favor of using models in sea ice research: (1) models provide the sea ice state in every point of the model domain and during the whole time of the model integration. This provides information also in those areas and situations, where no observations are available. (2) Models allow for experiments with globally unique systems like the global climate or the polar cryosphere. (3) Models are not bound to real time, so simulations of multiple decades can be calculated in mere hours or days.

Note however, that despite these advantages of models, observations of the physical state of sea ice are the necessary basis of this research. Without observations, it is impossible to say if a model describes sea ice realistically, or if it has some specific biases, or if it describes some fantasy that has almost nothing to do with the physical reality. Unfortunately, there are far fewer reliable observations of sea ice than there are for example reliable observations of the surface air temperature in central Germany. First of all, expeditions into the Arctic are expensive and require large amounts of time and preparation. Next, the harsh conditions in the Arctic make in-situ observations difficult and pose large challenges in the development of autonomous measuring devices. And finally, the different relevant scales in sea ice make it necessary to cover large areas and resolve at the same time

small details in observations.

For these reasons, I focus in my work on sea ice models as they are used currently in many different ocean and climate models. Such models are used in global or at least basin-wide simulations and need to cover large horizontal areas. For the numerical description, the model areas are partitioned into grids, where each grid cell is described by one datapoint in the model. Typical grid spacings in climate models are between 100km and 10km, while high resolution models today reach grid spacings of only few kilometers for the whole Arctic (Stroeve *et al.*, 2014; Wang *et al.*, 2016). Note that there are many different types of numerical models used in sea ice research, from one-dimensional models of a column in the ice (e.g. Savage, 2008; Godlovitch *et al.*, 2012) over process models for individual ridging events (e.g. Hopkins, 1998; Herman, 2016) up to the basin-scale models used in climate simulations (Stroeve *et al.*, 2014). But for the remainder of this work, I will focus only on the latter kind and use the words "sea ice model" to denote exclusively this category.

Sea ice models using horizontal grids describe the integrated properties of the ice pack over each grid cell. This information can differ from the exact physical properties of an ice floe (Hibler, 1977). Usually, a single grid cell contains multiple floes and a certain fraction of open water. So the properties of the "ice" in the model like thickness, albedo or drift speed are always approximations for the properties of the specific mixture of different physical ice in the specific grid cell.

In climate simulations, sea ice models are often coupled to an ocean model and possibly also an atmosphere model. In this coupled case, they need to regulate the interaction between atmosphere and ocean additionally. The exchange of momentum, energy and freshwater between the air and the sea is a major driver for the global circulation patterns in both. If there is sea ice present, these exchanges must be adapted and the adaptions must be communicated to the respective model components. In such coupled models, the design of the sea ice components is closely connected to the design of ocean and atmosphere components or a possible coupler (Hunke *et al.*, 2011).

In general, sea ice models solve two large systems of equations for these tasks: (1) the dynamics of the ice pack are calculated as a result of different forcing terms. Most important are the wind blowing over the ice, the ocean currents flowing under it, and the ice pushing against itself. The results determine the motion and the deformation of the ice in each point (Feltham,

2008). (2) The thermodynamics are calculated for each grid cell individually. The exact combination of incoming radiation, the temperatures of air and ocean, and the thickness of ice and snow determine for each point if ice melts or freezes and the amount of heat transferred between ocean, ice and atmosphere (Fichefet & Morales Maqueda, 1997).

As a consequence of this approach, many crucial small-scale processes can not be resolved in these models. Instead, their effects are included in parameterizations. Ideally, the mean effect of the sub-grid processes can be described as a simple function of the large-scale parameters that are available in the model. When the first sea ice models were designed, these parameterizations described the effects of all processes taking place in a single grid cell containing a huge amount of different floes. And even if current very-high resolution models start to resolve the largest floes individually, features like pressure ridges and leads are often only a few meters wide, so the need for parameterizations still remains (Hunke *et al.*, 2011).

The earliest parameterizations were concerned with the ice properties most important for the ice itself and its impact on the Arctic climate. Computationally simple schemes were developed to describe the effective albedo of the ice pack, the distribution of different thicknesses in a given grid cell, and the strength of the ice to resist deformation (Maykut & Untersteiner, 1971; Coon *et al.*, 1974). Later, physical processes impacting the behavior of the ice were described in increasing detail. For example, by now there are individual parameterizations for melt ponds, the vertical salinity profile in the ice or the form drag created by ridges, keels, and floe edges (Flocco *et al.*, 2010; Turner & Hunke, 2015; Tsamados *et al.*, 2014).

Unfortunately, this increase in model complexity makes the evaluation of sea ice models even more difficult. Even the most basic models today have a large amount of free parameters that are supposed to adjust the conceptual equations of the model to the situations found in reality. And with every additional parameterization, more of these free parameters are added. Since the effects of most of these parameterizations are closely connected, this makes it difficult to correctly adjust the free parameters. On the one hand, it is necessary to tune the models towards the available observations, that is, to adjust the free parameters so that they best describe the known reality (Hourdin *et al.*, 2017). On the other hand, the complexity of current sea ice models allows for similar adjustments to model behavior via different sets of parameters and therefore allows also to reduce effects of one parameterization

by adjusting a different one (Hunke, 2010). In this way tuning can also hide properties of new parameterizations that are both positive or negative for the overall model.

This would be only a small problem, if the effects described by each parameterization were documented well. But as mentioned above, there is only a relatively small amount of sea ice observations available in the Arctic. New parameterizations are often based on only few observations of the specific properties they are to represent (Hunke, 2014). And coinciding observations of the described small-scale behavior and the matching large-scale properties that are used for the parameterization are even less frequent. For this reason, many parameterizations today are still evaluated only rudimentarily. This means that for many parameterizations, the understanding of their effect on the large-scale model variables, their representation of the physical processes they ought to describe and their interaction with other model components is still limited.

1.2.1 The Ice Thickness Distribution in Models

One of the oldest and at the same time one of the most commonly used parameterizations is the active Ice Thickness Distribution (ITD) (Thorndike *et al.*, 1975). It describes the thickness of the ice in a given model grid cell by a distribution in different thickness categories. For each of these categories, it keeps track of the individual changes to ice thickness and the resulting changes in the relative amounts of ice in each category. This thickness distribution allows then to calculate more precisely the many properties of the ice that depend on the thin ice fraction or the amount of thick ice in pressure ridges. Due to the high local variability of thickness in the ice and the large impact of especially the thin ice fraction on both the amount of energy transported vertically through the ice and the horizontal pressure necessary to deform the ice, this parameterization was and is seen as crucial for a realistic description of the large-scale properties of the ice pack (Massonnet *et al.*, 2011). A common alternative is to calculate only the total volume of the ice in a grid cell and the relative amount of the area covered by thick ice (Hibler, 1979). But while this variant is simpler and computationally cheaper, it is obviously limited in the amount of thickness information available for all other parameterizations.

Since the introduction of the ice thickness distribution parameterization,

it has been closely connected to the ice strength. The ice strength is defined as the maximum pressure the ice can support before deforming permanently. Rothrock (1975) argued that the ice deforms in compression by getting pushed into pressure ridges and calculated the ice strength from the energy necessary to form those pressure ridges. With the assumption that the thinnest ice will ridge most easily, his derivation depended heavily on the ice thickness distribution of the ice in question. Therefore his parameterization for the ice strength that is derived from first principles is only applicable to sea ice models using the ice thickness distribution parameterization.

The strong physical arguments present in the derivation of the ice thickness distribution parameterization make it still attractive for use in sea ice models. While the numerical implementation of this parameterization changed over the years (Hibler, 1980; Bitz *et al.*, 2001; Lipscomb, 2001), the underlying physical principles are still unchanged. Of the current climate models, a large part implements some version of it (Stroeve *et al.*, 2014). But as for so many other parameterizations, many questions about this foundational parameterization are still unanswered.

Over the last decades, researchers have provided not only an increase in model parameterizations and complexity, but also an increase in sea ice observations. Motivated by the drastic changes in the Arctic, the new millennium has seen an increase in sea ice observations with both established and newly developed methods. Especially the amount of observations of thickness distributions in specific Arctic regions has increased strongly. This allows to revisit the ice thickness distribution and the ice strength, two cornerstones of sea ice modeling, in more detail and finally untangle and answer some of the open questions.

1.3 Scope and Structure of this Thesis

This thesis gives a detailed evaluation of sea ice physics based on a multicategory thickness representation, especially the ice thickness parameterization and the ice strength parameterization, in an Arctic sea ice model. The effects of the two parameterizations are disentangled and distinguished from confounding effects of model tuning; and their advantages and disadvantages are discussed. As a consequence of this evaluation, recommendations for best practices and future development regarding these two parameterizations can

be given for climate models.

In a first step, I investigate if multicategory physics improve Arctic-wide simulations of sea ice. Firstly, I present a precise and quantitative measure of model quality for such an evaluation Secondly, the effects of multicategory physics in general are split up into the individual contributions of the representation of ITDs in single grid cells, of an ice strength parameterization based on the thin ice fraction, and of the ability to tune these two parameterizations towards a given target. This investigation focuses on large-scale model results and evaluates only the integrated effects of these parameterizations on basin-wide sea ice properties.

In a second step, I investigate both parameterizations in more physical detail. This means for one part to compare modeled ITDs to observations. The model reproduces certain parts of individual observed distributions, while it struggles with others. An analysis of these details allows to identify which physical mechanisms are implemented in a satisfactory way and which physical mechanisms demand new numerical approximations. Then, the different ice strength parameterizations are compared in more detail to find out exactly which parameter choices, which numerical implementations and finally which physical assumptions work best in the context of Arctic-wide sea ice models.

The key research questions addressed in this thesis can be summarized in the following way:

Key research questions

- **Q1**: Do physical parameterizations based on a multicategory description of sea ice thickness help to improve sea ice models in the Arctic?

- **Q2**: Which parts of the involved parameterizations work as they are supposed to and which parts do not?

- **Q3**: How can the inaccurate parts of these parameterizations be improved? Both in terms of model configuration and changes to the parameterizations?

The thesis is structured as follows. I investigate in how far parameterizations based on multicategory ice thickness can improve the reproduction of large-scale observations of Arctic sea ice in chapter 2. I develop a clear method to determine model quality in which an automated parameter optimization is combined with a quantitative measure how well satellite observations of different sea ice properties in the Arctic are reproduced. Chapter 2 has been published in the *Journal of Geophysical Research* by Ungermann, M., Tremblay, L. B., Martin, T., & Losch, M. (2017) under the title '*Impact of the Ice Strength Formulation on the Performance of a Sea Ice Thickness Distribution Model in the Arctic*'.

I analyze the ITD parameterization and its ability to produce realistic thickness distributions in more detail in chapter 3. Model results are compared to a large amount of ITD observations in the Arctic with a focus on regional, seasonal and decadal variability. For a thorough evaluation of the parameterization, both the reproductions of regional mean distributions and local distributions in single grid cells are evaluated and the most important model parameters shaping the modeled ITDs are highlighted.

Then, I analyze the ice strength parameterization based on a thickness distribution in chapter 4. The relevant equations are recast in the context of a two-category thickness model to facilitate direct comparisons of different ice strength parameterizations and clearly separate effects of different choices of functional dependencies from the effects of different physical mechanisms relevant to the parameterization. The resulting evaluation links shortcomings in individual ice strength parameterizations to the physical assumptions made in their original derivation.

Finally, I summarize the main results of this thesis, draw final conclusions, and give an outlook over possible future work in chapter 5.

Remark Chapter 2 constitutes a published paper, while chapters 3 and 4 were written as manuscripts ready for submission to scientific journals. For this reason, each chapter is designed to be understandable on its own, even though this leads to a few small repetitions, especially in the model descriptions. The respective roles of my co-authors are noted in the beginning of chapter 2 and explain inconsistencies regarding the use of the first person plural or singular in this thesis.

2. Impact of the Ice Strength Formulation on the Performance of a Sea Ice Thickness Distribution Model in the Arctic [1]

Abstract The impact of a subgrid-scale ice thickness distribution (ITD) and two standard ice strength formulations on simulated Arctic sea ice climate is investigated. To this end different model configurations with and without an ITD were tuned by minimizing the weighted mean error between the simulated and observed sea ice concentration, thickness and drift speed with an semi-automatic parameter optimization routine. The standard ITD and ice strength parameterization lead to larger errors when compared to the simple single-category model with an ice strength parameterization based on the mean ice thickness. Interestingly, the simpler ice strength formulation, which depends linearly on the mean ice thickness, also reduces the model-observation error when using an ITD. For the ice strength parameterization that makes use of the ITD, the effective ice strength depends strongly on the number of thickness categories, so that introducing more categories can lead to overall thicker ice that is more easily deformed.

2.1 Introduction

Reliable sea ice models are an essential ingredient of climate models, but also of accurate sea ice forecasts that are required by the increasing shipping activities in the Arctic. The requirement of accuracy, together with advances in computing power, has led to an increase in sea ice model complexity over the last decades. With the rising amount of available observational data of Arctic sea ice, many new physical processes have been included in additional model parameterizations (Hunke *et al.*, 2011). For the development of future model systems a thorough scrutiny of each component of a sea ice model as well as its interaction with other components seems necessary (e.g. Hunke, 2014).

One of the most commonly used parameterizations in current sea ice models employs a subgrid-scale ice thickness distribution (ITD) to describe the ice thickness in each grid cell. Most implementations today are based on Thorndike *et al.* (1975). There are two main reasons that motivated this parameterization: First, the conductive heat flux through sea ice is dominated by the contributions of thin ice and open water, even if they cover only a small fraction of the total area. Second, most of the ice deformation processes, especially of a thicker and stronger pack, are ridging of the thinner ice fraction and shearing along leads (also characterized by thin or no ice).

Hence, an ITD is used in many sea ice models and many new parameterizations — such as an ice enthalpy distribution (Zhang & Rothrock, 2001) or an anisotropic rheology of discrete failure regimes (Wilchinsky & Feltham, 2012) — are based on an ITD model. Although ITD models seem to be well established, many questions about the exact mechanics of the involved processes and about the ITD's impact on model simulations remain.

Already when the ITD parameterization originally was developed, two main problems were identified that are still the biggest sources of uncertainty today: (1) the redistribution of ice between different ice thickness categories by ridging processes (Thorndike et al., 1975) and (2) the assumption that the deformation energy is either lost to friction or converted to potential energy as ice floes ridge and raft (Rothrock, 1975). Both Thorndike et al. (1975) and Rothrock (1975) make assumptions about the mechanical processes that govern sea ice ridge formation, but Pritchard (1981) already showed that they were missing important parts of the energy balance. At the time there were only a few observations of thickness and ridge profiles available (see e.g. Parmerter & Coon, 1972, and references therein), and dynamical modeling studies provided the most reliable understanding of ridging processes (Parmerter & Coon, 1973). The amount of available data has increased since. After discrete element models of the ridging process (Hopkins, 1998), laboratory experiments of ridging (Tuhkuri, 2002), and in-situ measurements of stresses in ice floes (Tucker & Perovich, 1992; Richter-Menge & Elder, 1998), the analysis of ridging properties is still an important field of ongoing research. Methods range from evaluating airborne observations (Herzfeld et al., 2015) and basin-wide process-oriented model simulations (Hopkins & Thorndike, 2006) to the analysis of conceptual models (Godlovitch et al., 2011). A common notion is that the details of the physical processes during ridging and their large-scale statistical properties, that is, the key features in shaping an ITD and determining the amount of energy necessary for deformation, are still not sufficiently well understood.

To evaluate an ITD model in view of uncertain theory, one of the first approaches was to compare the results to observed ice thickness. Such assessments are impeded by the sparsity of observational data for ice thickness. Still, Thorndike et al. (1975) could successfully simulate thickness distributions with a column ITD model that were similar to upward looking sonar measurements from submarines sailing under the Arctic sea ice. Bitz et al. (2001) reproduced this result in their global coupled model against a much

larger set of similar upward looking sonar data. In spite of this partial success, high uncertainties remain in ice thickness data both from models and observations (Schweiger *et al.*, 2011). Schweiger *et al.* (2011) also emphasize the importance of model parameterizations such as an ITD or the ice strength and the difficulty in evaluating their impact. One way forward is to combine different datasets. For example, Lindsay & Schweiger (2015) used ice thickness observations from different sources to reduce the uncertainty in Arctic-wide trends; Stroeve *et al.* (2014) compared models of the Climate Model Intercomparison Project Phase 5 (CMIP5) with a similar collection of thickness data and showed that these models still cannot accurately reproduce statistics, regional distributions and trends of ice thickness; Chevallier *et al.* (2016) reported that observed concentrations are modeled accurately in global ocean reanalysis products, but that errors with respect to observed drift speeds remain and that there were large differences between the models in the regional ice thickness fields with no product standing out.

With the availability of data being a limiting factor, a common method to assess the impact of an ITD parameterization on sea ice models is to compare model configurations with and without this parameterization. Bitz *et al.* (2001) found in a coupled global climate model that including an ITD increases the mean ice thickness. This increase improved the fit to upward-looking sonar observations for mainly thick, ridged ice in the central Arctic, but deteriorated the fit in the peripheral seas. In addition, the interannual variability of both the sea ice export through Fram Strait and the ocean meridional overturning circulation increased with an ITD model. Feedback mechanisms were found to have a stronger effect on the sea ice in climate simulations with an ITD model (Holland *et al.*, 2006). Komuro & Suzuki (2013) show the positive impact of this parameterization on the reproduction of realistic heat fluxes through the pack ice. Maslowski & Lipscomb (2003) compared two successive versions of a sea ice model and found that the later version improved the reproduction of sea ice observations significantly for which they stated the inclusion of an ITD parameterization into the model as the main reason. Massonnet *et al.* (2011) compared NEMO-LIM2 and NEMO-LIM3 model output to a much more exhaustive set of observations, but arrived at the same conclusions that the inclusion of an ITD parameterization into the model is one of the main reasons for a much improved model performance. All studies clearly show the positive impact of including an ITD model, but all evaluations are either limited by the lack

of reliable observational data (again) or the simultaneous change of multiple model components confounds the conclusions.

Here we attempt a systematic investigation of the impact of an ITD parameterization on the reproduction of different large-scale observations of sea ice. We are supported by the ever increasing amount of available observational data. Our approach to systematic comparisons contains three steps: (1) We construct a cost function with error-weighted satellite data for sea ice concentration, thickness and drift as a robust measure of model performance; (2) We use this cost function to systematically tune different model configurations with and without an ITD model separately; that is, we explicitly do not use the same model parameters when using an ITD or a single-category model to avoid biases introduced by different parameterizations as much as possible. (3) We distinguish clearly between the effects of changing the ice thickness representation and the effects of changing the ice strength formulation.

The remainder of the paper is structured as follows: First we describe how we evaluate the different model configurations in section 2.2. This section contains an overview over the cost function, the optimization technique, the most important model equations, and the approach to tuning the different model configurations. The results of these comparisons are presented in section 2.3. The results are discussed in section 2.4 and the most important conclusions can be found in section 2.5.

2.2 Method

2.2.1 Cost Function

To evaluate our model results quantitatively we construct a cost function from satellite observations as a measure for model quality. We follow Kauker *et al.* (2015) and use four different datasets: (1) the reprocessed concentration dataset and error estimates from OSISAF (EUMETSAT Ocean and Sea Ice Satellite Application Facility, 2011) (1979 - 2009); (2) the ICESat-JPL thickness product (Kwok & Cunningham, 2008) with a local error estimated as in Kauker *et al.* (2015) yet with an upper limit of 1m for the uncertainty (March and October/November, 2003 - 2008); (3) the OSISAF sea ice drift (Lavergne *et al.*, 2010) (October to April, 2002 - 2006) and (4) the sea ice drift of Kimura *et al.* (2013) (May to July, 2003 - 2007). All of the drift

data are derived from passive-microwave satellite data, with error estimates provided by Sumata *et al.* (2014, 2015).

The cost function F is defined as

$$F = \sum_{i=1}^{N} \frac{(y_i - x_i)^2}{N_d(y_i)\xi_i^2} \tag{2.1}$$

where y_i is an observational data point with measurement uncertainty ξ_i, x_i the simulated value of the corresponding model variable, $N_d(y_i)$ the number of data points in each of the four datasets, and N the total number of observations. In equation (2.1) each data point y_i is weighted by $1/N_d$ in order to give equal weight to all four datasets. For instance, if the error for each data point $(x_i - y_i)$ was exactly equal to the measurement uncertainty ξ_i, the cost function for each dataset would be equal to one, summing up to a total value of $F = 4$. Note that the cost function is an average misfit of all included points, so that even for cost function values of less than four there can (and indeed do) exist regions where further improvement is still possible without overfitting.

2.2.2 Green's Function Approach

For a meaningful comparison of two model configurations, both configurations are tuned individually to minimize the differences between simulated and observed concentration, thickness and drift fields from 1979 to 2009. We use an semi-automatic optimization approach for a set of parameters with large impact on the ITD. The adjoint capabilities of the MITgcm (e.g. Heimbach *et al.*, 2010) cannot be used to optimally estimate the parameters, because our experiments span multiple decades. Instead we use Green's functions to linearize the problem and obtain a maximum likelihood estimate for a set of optimal parameters. A detailed mathematical background for the Green's function approach can be found in textbooks (e.g. Menke, 2012), while the short description below follows Menemenlis *et al.* (2005).

The relationship between the vector of observational data $\mathbf{y}$ and the model can be expressed as

$$\mathbf{y} = M(\boldsymbol{\nu}) + \boldsymbol{\varphi} \tag{2.2}$$

where the operator M combines the integration of the model and the sampling of the output at the specific locations. The model depends on a set of

control parameters, for which $\boldsymbol{\nu}$ is a vector of perturbations around a reference $\boldsymbol{\nu_0}$. $\boldsymbol{\varphi}$ is the remaining error due to non-perfect parameter choices and systematic errors in the model. To get an optimal estimate of the control parameters $\boldsymbol{\nu_0} + \boldsymbol{\nu}$, a cost function

$$F = \boldsymbol{\varphi}^T \mathbf{R}^{-1} \boldsymbol{\varphi} \qquad (2.3)$$

is minimized that measures a least-squares error weighted by a symmetric matrix $\mathbf{R}^{-1}$. For the special cost function (2.1) in section 2.2.1, the error is the model-data misfit $\varphi_i = y_i - x_i$ and $\mathbf{R}^{-1}$ is diagonal with elements $R_{ii}^{-1} = (N_d(y_i)\xi_i^2)^{-1}$. Equation (2.3) is minimized after linearizing operator M with a matrix $\mathbf{M}$. $\mathbf{M}$ is constructed by writing the Green's function for each of the control parameters into a new column. This first order approximation allows to write equation (2.2) as

$$\Delta\mathbf{y} = \mathbf{y} - M(\mathbf{0}) \;=\; \mathbf{M}\boldsymbol{\nu} + \boldsymbol{\varphi} \qquad (2.4)$$

with the model data misfit $\Delta\mathbf{y}$. In this notation, $M(\mathbf{0})$ is the sampled output of a model integration with the reference set of control parameters $\boldsymbol{\nu_0}$, that is, the vector of perturbations is $\mathbf{0}$. Differentiating (2.3) with respect to the control vector $\boldsymbol{\nu}$ and equating the resulting gradient to zero, we obtain

$$\frac{\partial F(\boldsymbol{\nu}_{\mathrm{opt}})}{\partial \boldsymbol{\nu}} = -\mathbf{M}^T \mathbf{R}^{-1} 2 \left(\Delta\mathbf{y} - \mathbf{M}\boldsymbol{\nu}_{\mathrm{opt}} \right) = 0. \qquad (2.5)$$

Solving for the perturbation

$$\boldsymbol{\nu}_{\mathrm{opt}} = \left(\mathbf{M}^T \mathbf{R}^{-1} \mathbf{M}\right)^{-1} \mathbf{M}^T \mathbf{R}^{-1} \Delta\mathbf{y} \qquad (2.6)$$

gives a set of optimal control parameters $\boldsymbol{\nu_0} + \boldsymbol{\nu}_{\mathrm{opt}}$. As a criterion for a successful optimization, the linearization error by this approach should be much smaller than the vector $\boldsymbol{\xi}$ consisting of the measurement uncertainties ξ_i

$$\|M(\boldsymbol{\nu}_{\mathrm{opt}}) - \mathbf{M}\boldsymbol{\nu}_{\mathrm{opt}}\| \ll \|\boldsymbol{\xi}\|. \qquad (2.7)$$

Because each of the Green's functions is calculated by one sensitivity experiment, the total computational effort necessary to construct $\mathbf{M}$ limits the number of control parameters.

2.2.3 Model Equations

Momentum Equations and Thermodynamics

For the dynamic part of the model we assume a viscous-plastic rheology with an elliptical yield curve and a normal flow rule (Hibler, 1979). The ice velocities are calculated from the momentum balance:

$$m\frac{\partial \mathbf{u}}{\partial t} = m f_C \mathbf{k} \times \mathbf{u} + \boldsymbol{\tau}_a + \boldsymbol{\tau}_w - m\hat{g}\boldsymbol{\Delta}_H + \nabla \cdot \boldsymbol{\sigma}, \tag{2.8}$$

where $m = \rho_i h$ is the ice mass per unit area, h is the ice thickness, ρ_i is the ice density, $\mathbf{u}$ is the sea ice velocity vector, f_C is the Coriolis parameter, $\mathbf{k}$ is a unit vector pointing vertically upward, $\boldsymbol{\Delta}_H$ is the sea surface tilt, $\hat{g}$ is the gravitational acceleration and $\boldsymbol{\sigma}$ is the internal ice stress. The surface stress $\boldsymbol{\tau}_a$ and the water drag $\boldsymbol{\tau}_w$ can be written as

$$\tau_a = \rho_a C_a |\mathbf{u}_a - \mathbf{u}| \mathbf{R}_a (\mathbf{u}_a - \mathbf{u}) \tag{2.9}$$

$$\tau_o = \rho_o C_o |\mathbf{u}_o - \mathbf{u}| \mathbf{R}_o (\mathbf{u}_o - \mathbf{u}) \tag{2.10}$$

where $\mathbf{u}_a, \mathbf{u}_o$ are the surface velocities, ρ_a, ρ_o are the reference densities, C_a, C_o are the drag coefficients, and $\mathbf{R}_a, \mathbf{R}_o$ are rotation matrices for atmosphere (subscript a) and ocean (subscript o) (McPhee, 1975). Following Zhang & Hibler (1997), the momentum balance (2.8) neglects the advection of momentum. The resulting discretized equations are solved using a line successive relaxation method (Zhang & Hibler, 1997).

The stress tensor $\boldsymbol{\sigma}$ is related to the deformation rate tensor $\dot{\boldsymbol{\varepsilon}} = \frac{1}{2}\left[\nabla\mathbf{u} + (\nabla\mathbf{u})^T\right]$ by the constitutive relation

$$\boldsymbol{\sigma} = 2\eta\dot{\boldsymbol{\varepsilon}} + \left(\left(\zeta - \eta\right)\dot{\varepsilon}_I - \frac{P_r}{2}\right)\mathbf{I} \tag{2.11}$$

where P_r is the replacement pressure, $\mathbf{I}$ is the Identity Matrix, η and ζ are the shear and bulk viscosities, and $\dot{\varepsilon}_I = \dot{\varepsilon}_{11} + \dot{\varepsilon}_{22}$ is the first strain rate invariant (i.e. divergence). The bulk viscosity $\zeta = P/(2\Delta_{\dot{\varepsilon}})$ and the shear viscosity $\eta = \zeta/e^2$ in turn can be calculated from the ice strength P, the axis ratio e of the elliptical yield curve, and the deformation measure $\Delta_{\dot{\varepsilon}} = \sqrt{\dot{\varepsilon}_I^2 + e^{-2}\dot{\varepsilon}_{II}^2}$, where $\dot{\varepsilon}_{II} = \sqrt{(\dot{\varepsilon}_{11} - \dot{\varepsilon}_{22})^2 + 4\dot{\varepsilon}_{12}^2}$ is the second strain rate invariant (or maximum shear at a point). The replacement pressure $P_r = 2\Delta_{\dot{\varepsilon}}\zeta$ is calculated after regularizing ζ with the smooth formulation of

Lemieux & Tremblay (2009) to avoid spurious creep (Hibler & Ip, 1995).

The single-category model is based on the two continuity equations

$$\frac{\partial A}{\partial t} = -\nabla \cdot (\mathbf{u}A) + S_A \tag{2.12}$$

$$\frac{\partial H}{\partial t} = -\nabla \cdot (\mathbf{u}H) + S_H \tag{2.13}$$

for the prognostic variables ice concentration A and ice volume per grid cell area $H = Ah$. The variables change with time according to advection by the horizontal velocity $\mathbf{u}$ and the respective source terms S_A and S_H. The thermodynamic fluxes are calculated using a 0-layer model (Semtner, 1976). Note that Bitz $et\ al.$ (2001) analyzed the impact such simple thermodynamics have on an ITD model compared to more complex thermodynamics. They found that ice concentration is almost indistinguishable from the one simulated with more complex thermodynamics but there are non-negligible changes in ice thickness and growth rates, which should be kept in mind for the interpretation of the results presented below.

Ice Thickness Distribution

One main focus of our investigation is the subgrid-scale ice thickness distribution $g(h, \mathbf{x}, t)$ (Thorndike $et\ al.$, 1975), a probability density function for thickness h following the evolution equation

$$\frac{\partial g}{\partial t} = -\nabla \cdot (\mathbf{u}g) - \frac{\partial}{\partial h}(fg) + \Psi, \tag{2.14}$$

where f is the thermodynamic growth rate and Ψ a function describing the mechanical redistribution of sea ice during ridging or lead opening.

The mechanical redistribution function Ψ creates open water when the sea ice flow is divergent and ridges when the sea ice flow is convergent. The function Ψ depends on the total strain rate and the ratio between shear and divergent strain. In convergent motion, the ridging mode

$$\omega_r(h) = \frac{n(h) - a(h)}{N} \tag{2.15}$$

gives the effective change of ice volume for thickness between h and $h + \mathrm{d}h$ as the normalized difference between the ice $n(h)$ generated by ridging and the ice $a(h)$ participating in ridging. Following Lipscomb $et\ al.$ (2007), the

participation function is $a(h) = b(h)g(h)$, and the relative amount of ice of thickness h is weighted by an exponential function

$$b(h) = b_0 \exp[-G(h)/a^*], \qquad (2.16)$$

where $G(h) = \int_0^h g(h)\mathrm{d}h$ is the cumulative thickness distribution function, b_0 is a normalization factor, and a^* determines the relative amount of thicker and thinner ice that take part in ridging. The ice generated by ridging (from an original thickness h_1 to a new ice thickness h) is calculated as

$$n(h) = \int_0^\infty a(h_1)\gamma(h_1, h)\mathrm{d}h_1, \qquad (2.17)$$

where the density function $\gamma(h_1, h)$ can be written as:

$$\gamma(h_1, h) = \begin{cases} \frac{1}{k\lambda} \exp\left[\frac{-(h-h_{\min})}{\lambda}\right] & h \geq h_{\min} \\ 0 & h < h_{\min}. \end{cases} \qquad (2.18)$$

In this parameterization, the normalization factor $k = \frac{h_{\min}+\lambda}{h_1}$, the e-folding scale $\lambda = \mu h_1^{1/2}$ and the minimum ridge thickness $h_{\min} = \min(2h_1, h_1 + h_{\mathrm{raft}})$ all depend on the original thickness h_1. The maximal ice thickness allowed to raft is constant $h_{\mathrm{raft}} = 1\mathrm{m}$ and μ is a tunable parameter.

In the numerical implementation these equations are discretized into a set of thickness categories using the delta function scheme proposed by Bitz *et al.* (2001). A smoother linear remapping scheme (Lipscomb, 2001) is available but not used. Its effect will be discussed in section 2.4.1. For each thickness category in an ITD configuration, the volume conservation law equation (2.13) is evaluated as in the single-category model, but with the net surface ice-atmosphere heat flux calculated from the values for ice and snow thickness in the current category. There are no conceptual differences in the thermodynamics between the single-category and ITD configurations. The only difference is that in the ITD configuration, new ice of thickness H_0 is created only in the thinnest category; all other categories are limited to basal growth. The conservation of ice area (2.12) is replaced by the discretized evolution equation for the ITD (2.14). The thickness category limits of the discretization in space are given in Table 2.1. The total ice concentration and volume can then be calculated by summing up the values for each category.

In the single-category model ridge formation is treated implicitly by limit-

Table 2.1: Bin limits for ITD configurations

# of categories	bin limits in m									
5	0.0	0.64	1.39	2.47	4.57					
20	0.0	0.16	0.33	0.50	0.67	0.86	1.06	1.28	1.52	1.79
...	2.10	2.46	2.89	3.42	4.06	4.85	5.82	7.01	8.46	10.2

ing the ice concentration to a maximum of one (Hibler, 1979). In this simple case ($A = 1$), the concentration can no longer increase and convergence leads then to an increase in ice thickness (i.e. a "ridge").

Ice Strength Parameterizations

Rothrock (1975) derived a parameterization for the ice strength P

$$P = C_f C_p \int_0^\infty h^2 \omega_r(h) \mathrm{d}h \qquad (2.19)$$

from considerations of the amount of potential energy gained and frictional energy dissipated during ridging. The physical constant $C_p = \rho_i(\rho_w - \rho_i)\hat{g}/(2\rho_w)$ is a combination of the gravitational acceleration $\hat{g}$ and the densities ρ_i, ρ_w of ice and water, and C_f is a scaling factor relating the work against gravity to the work against friction during ridging.

Hibler (1979) proposed a simpler ice strength parameterization for a single-category model that is still widely used today. In this model the ice strength P is parameterized as

$$P = P^* A\, h\, e^{-C^*(1-A)} \qquad (2.20)$$

where P depends only on average ice concentration and thickness per grid cell, the compressive ice strength parameter P^* and the ice concentration parameter C^*. In the following we will refer to the ice strength parameterization of Hibler (1979) as H79 and that of Rothrock (1975) as R75.

Note that the parameterization R75 is a function of the ITD in each grid cell, while H79 is applicable both for ITD and single-category models. In contrast to H79, which builds on the plausible assumption that thick and compact ice has more strength than thin and loosely drifting ice, the R75 parameterization clearly contains more physical assumptions about energy conservation. For that reason R75 is often considered to be more physically realistic than H79.

2.2.4 Optimization Approach

Optimized Parameters

We define three groups of control parameters for our optimization that we think are most important for adjusting the modeled sea ice to observations. Group 1 contains parameters that are not directly related to the choice of ITD parameterizations: the albedo of cold and melting snow and ice, the air and water drag coefficients, the aspect ratio e of the elliptical yield curve, and the thickness of newly formed ice H_0. Group 2 contains parameters only relevant to the H79 ice strength formulation: the ice compressive strength parameter P^* and the ice concentration constant C^*. Finally group 3 contains parameters of the R75 strength formulation: the ice strength parameter C_f, and the ice redistribution coefficients μ and a^*.

Optimization Runs

For our comparisons we have three goals in mind: (1) evaluate the differences of model configurations with and without an ITD with respect to reproducing observed sea ice fields; (2) account for the influence of the number of ice thickness categories; (3) account for the influence of the ice strength parameterization. The quality of each model configuration is measured by means of a cost function. For an unbiased comparison of model quality, we first tune each model configuration in order to minimize the total cost function F.

We use the MIT general circulation model (MITgcm), in a coupled ocean / sea-ice configuration, forced with prescribed atmospheric reanalysis data. In this configuration, which is a coarser version of Nguyen *et al.* (2011), we implemented the ITD model in the MITgcm sea ice model (Losch *et al.*, 2010). The model region is the Arctic face of a global cubed sphere configuration with an average resolution of 36 km. Similar sea ice models are currently being used in configurations with horizontal resolutions between 5 km for regional simulations (Dupont *et al.*, 2015) and around 50 km for global reanalysis (Chevallier *et al.*, 2016). Our model is therefore representative of a broad group of medium resolution models. All model runs start from a 5-year spinup with periodic forcing of the year 1979. The model is then run from 1979 to 2009.

The initial choice of model parameters follows Nguyen *et al.* (2011), but we use a more recent atmospheric forcing data set following the recommen-

dations of Lindsay *et al.* (2014): The NCEP Climate System Forecast Reanalysis (NCEP-CSFR Saha *et al.*, 2010) produced the best results for our configuration in a comparison of different reanalysis products (i.e. the smallest model-data misfit prior to the formal optimization, not shown).

Starting from the tuned set of parameters of Nguyen *et al.* (2011), we adjust the parameters of group 1 with one optimization step to account for the differences in forcing, grid resolution and other model details. This setup without ITD parameterization is referred to as the "Baseline" hereafter. Next we tune a case with an ITD using five ice thickness categories, a number recommended by Bitz *et al.* (2001). In order to determine the parameters to be adjusted when switching to an ITD, we perform three different optimizations with the non ITD specific parameters of group 1 ("ITD5-g1"), the ITD and R75 specific parameters of group 3 ("ITD5-g3") or both sets together ("ITD5-g13"). Table 2.2 lists which parameters are modified in which experiment. The best result (minimum cost function F) is obtained when only tuning the ITD specific parameters of group 3 (Table 2.3). Therefore we continued from Baseline by tuning parameters of group 3 for two different numbers of ice thickness categories (5 and 20) with the R75 ice strength parameterization to arrive at the configurations "ITD5R" and "ITD20R".

Tuning the strength-specific parameters of group 2 yields the configuration noITD with a single-category thickness representation. In order for those optimizations to satisfy criterion (2.7), we require the linearization error to be smaller than 10% of the observation uncertainty on average. This requirement was satisfied in one step for noITD and two steps for each of ITD5R and ITD20R. This optimization approach decreases the cost function values of the ITD configurations by $25\% - 30\%$ (Table 2.3).

To assess the role of the strength parameterization in the context of an ITD model, we evaluated two additional model runs with an ITD and the simpler H79 ice strength parameterization: "ITD5H" and "ITD20H". For those runs we assume that the parameters, which have already been tuned using our cost function, give sufficiently good results in this new combination. Therefore we forego further optimization for the runs ITD5H and ITD20H and instead use the parameters from the respective R75 runs with the values P^* and C^* from noITD.

This approach implies that the thickness of newly formed ice is $H_0 = 0.5649$, the value resulting from the optimization of the Baseline configuration, in all ITD configurations. Arguably, this high value may prevent the

Table 2.2: Optimized parameters

Parameter		starting values	Baseline	noITD	ITD5R	ITD20R
albedo dry ice	α_{Id}	0.7000	0.71	-	-	-
albedo wet ice	α_{Iw}	0.7060	0.7119	-	-	-
albedo dry snow	α_{Sd}	0.8652	0.8556	-	-	-
albedo wet snow	α_{Sw}	0.8085	0.7903	-	-	-
air drag	$c_{d,a}$	1.14e-3	1.657e-3	-	-	-
water drag	$c_{d,w}$	5.563e-3	6.647e-3	-	-	-
axis ratio	e	2.0	1.523	-	-	-
lead opening	H_0	0.5	0.5649	-	(0.3546)	(0.3292)
ice strength (H79)	P^*	2.264	-	2.299	-	-
ice strength (H79)	C^*	20.0	-	15.92	-	-
ice strength (R75)	C_f	14.0	-	-	13.926	14.07
ridging participation	a^*	0.04	-	-	0.04058	0.04249
ridge shape	μ	4.5	-	-	3.029	3.104

[a] '-' means no change from the last column, values in bracket are from additional optimizations for H_0

Table 2.3: Cost function values

	Concentration	Thickness	Winter Drift	Summer Drift	Total
Baseline	1.71	0.75	0.52	1.06	4.04
noITD	1.69	0.75	0.50	1.03	**3.97**
ITD5 no tuning	1.84	0.81	1.20	2.00	5.84
ITD5-g1	1.79	0.85	1.06	1.74	5.44
ITD5-g3	1.62	0.75	0.69	1.23	4.28
ITD5-g13	1.67	0.78	0.81	1.39	4.66
ITD5R	1.57	0.72	0.56	1.20	**4.05**
ITD5R-H0	1.49	0.79	0.54	1.22	4.03
ITD20 no tuning	1.91	1.17	0.88	1.56	5.53
ITD20R	1.71	0.90	0.45	1.09	**4.15**
ITD20R-H0	1.63	0.87	0.42	1.11	4.04
ITD5H	1.57	0.63	0.45	0.95	**3.59**
ITD20H	1.77	0.61	0.46	0.91	**3.76**

[b] Experiment names as defined in Table 2.4

Table 2.4: Optimized Runs

	initiated from	optimized parameters
Baseline	(Nguyen *et al.*, 2011)	group 1
ITD5-g1	Baseline	group 1
ITD5-g3	Baseline	group 3
ITD5-g13	Baseline	group 1+3
noITD	Baseline	group 2
ITD5R	Baseline	group 3
ITD20R	Baseline	group 3
ITD5H	ITD5R	group 2 taken from noITD
ITD20H	ITD20R	group 2 taken from noITD
ITD5R-H0	ITD5R	H_0
ITD20R-H0	ITD20R	H_0

ITD model from representing the behavior of thin ice realistically, especially since the thinnest category for ITD20 contains only ice thinner than 16 cm. To investigate the effect of this artifact on our analysis, we additionally optimize only H_0 for the two configurations ITD5R and ITD20R. We find that it is possible to further decrease the model-data misfit by tuning H_0 as shown in Table 2.3 for runs "ITD5R-H0" and "ITD20R-H0", but that our qualitative results are not affected. Tuning of H_0 also does not reduce the value of H_0 to be within the limits of the thinnest category for ITD20R (see Table 2.2). We thus conclude that it is not necessary to contain newly formed ice in the thinnest thickness category in order to minimize model-data differences. An overview of the different optimized runs is given in Table 2.4.

2.3 Results

Based on the cost function, both combinations of ITD and H79 give best results and even the configuration noITD has a smaller cost function value than the two configurations with ITD and R75. This result is described in more detail in section 2.3.1. We then investigate separately the influence of the ITD (section 2.3.2) and the strength parameterization (section 2.3.3) on the quality and characteristics of the model results in order to explain why the configurations with R75 have difficulties fitting the data. Especially for the ice strength parameterization, we find a strong dependence on the thickness resolution in the ITD. For this reason, we account for the different number of thickness categories throughout this section.

The simulated sea ice climate in our experiments is very close to the one described by Nguyen *et al.* (2011). Due to our more specific tuning, we can even improve the fit to sea ice observations compared to their already very good model state, but still suffer from biases in thickness and concentration, that are common to many comparable models (Chevallier *et al.*, 2016). We therefore assume that our model provides a good representation of Arctic sea ice and we focus our analysis on the differences in the fit to observations, as expressed by our cost function, that are caused by changes in the model setup.

2.3.1   Cost function

The total error calculated from the cost function F is slightly larger for both ITD5R and ITD20R when compared to noITD and significantly larger than both model configurations ITD5H and ITD20H. An overview of the cost function values can be found in Table 2.3.

To investigate the individual strengths and weaknesses of the different model configurations in more detail, we split up the total cost function values into four contributions for each of the individual datasets (Table 2.3). The difference between the four different ITD configurations (ITD[5,20][R,H]) and noITD are shown in Figure 2.1. The ITD configurations using R75 improve the fit to some datasets, but this reduction in cost function is outweighed by increases in differences in others. For instance, ITD5R has a clearly better fit to concentration data than noITD and a slightly better fit to thickness, but the fit to the drift data is much worse than in noITD. ITD20R, on the other hand, has in total a comparable and in winter even a slightly better fit to the drift data than noITD, but the fit to thickness and concentration is much worse compared to ITD5R. Part of this behavior can also be observed for ITD5H and ITD20H: In this case the fit to thickness and drift is similar, but the fit to concentration is much better for ITD5H than for ITD20H. These observations are a first hint of the strong influence of the number of thickness categories on the simulated sea ice concentration for a general ITD model, but also on all other sea ice characteristics for the R75 strength parameterization.
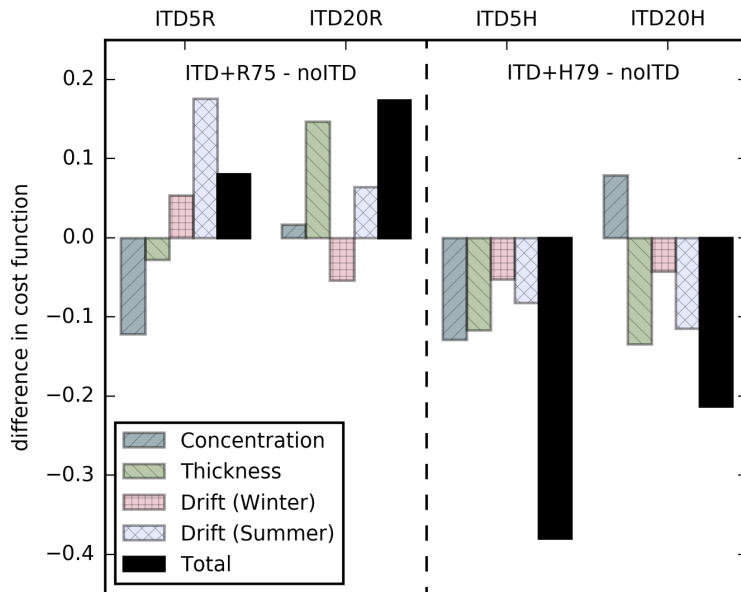
Figure 2.1: Difference in cost function values (ITD configuration - noITD) between different model configurations with an ITD and noITD. Shown are contributions of single datasets and total values.

2.3.2 ITD

We isolate and assess the effect of the ITD model by first comparing the configuration noITD with ITD5H and ITD20H, all of which use the same strength parameterization H79.

The more complex ITD model reduces the misfit for ice concentration especially in the marginal ice zone for the entire year, see Figure 2.2 for summer results; winter results are not shown. All model configurations generally overestimate the concentration especially in the North Atlantic, where the ice edge extends too far south and south east. While this overestimation is found in many medium resolution models (Chevallier *et al.*, 2016), the ITD configurations largely reduce this misfit when compared to noITD. In contrast, the summer ice concentration in the central Arctic and in the straits of the Canadian Arctic Archipelago is higher with an ITD model (Figure 2.2). This is because most ice in the ITD model is in the thicker ice categories and thicker ice takes longer to melt. In the noITD model, sea ice melt leads to sea ice concentration changes even for thicker ice because a linear ice thickness distribution between 0 and $2h$ is assumed so that there is always thin ice
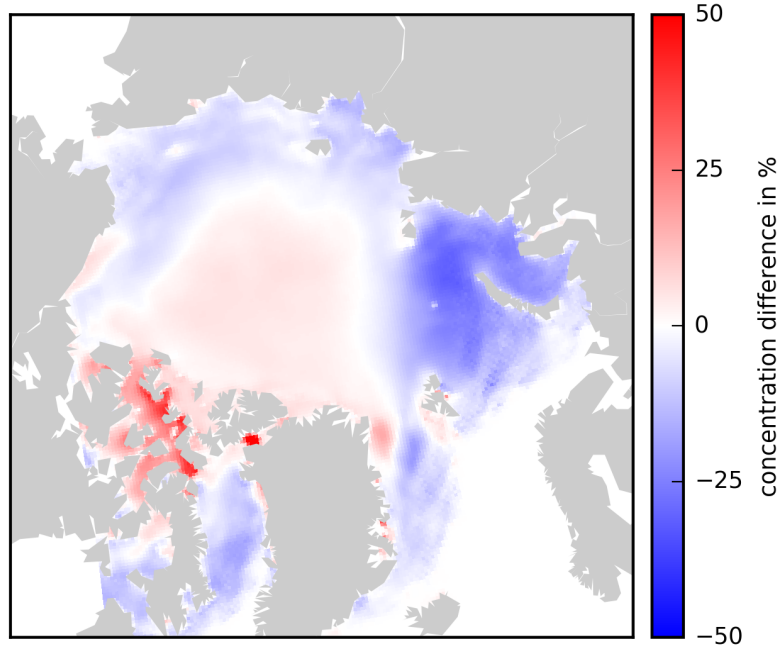
Figure 2.2: Mean difference in ice concentration (ITD5H - noITD) between an ITD configuration using 5 thickness categories and noITD, both with the H79 strength formulation, in Summer (July to September)

available for fast melting.

The ice thickness generally increases with number of ice thickness categories, with much stronger tendencies in the straits of the Canadian Arctic Archipelago. The difference in ice thickness between ITD5H - noITD is 0.11 ± 0.20 m (mean and standard deviation) for ice thinner than 4 m in ITD5H, and the comparable difference between ITD20H - noITD is 0.17 ± 0.25 m. These differences grow to 1.14 ± 1.67 m for ITD5H and 1.45 ± 1.49 m for ITD20H, if only ice thicker than 4 m in the ITD run is taken into account. Ice of this thickness is found mainly in the straits of the Canadian Arctic Archipelago and north of Greenland.

We now explicitly compare the ITD5 and ITD20 configurations for both strength parameterizations R75 and H79 in order to investigate the impact of the number of thickness categories. For ITD20 we observe generally a larger total ice volume compared to ITD5: First, if there is ice in an ITD5 configuration with a concentration of less than one, the concentration is in almost all cases higher in the corresponding ITD20 run. Second, the higher
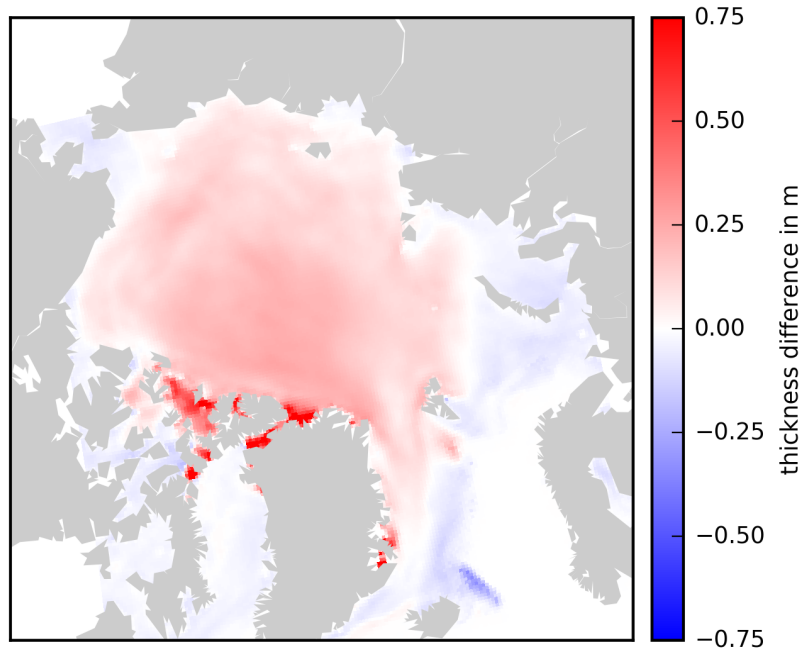
Figure 2.3: Mean difference in ice thickness H (ITD20H - ITD5H) between ITD configurations with 20 and 5 thickness categories, both using the H79 strength formulation, in Winter (December to May)

thickness observed for an ITD model compared to noITD is further increased, with the differences between ITD20 and ITD5 (Figure 2.3) showing a similar pattern as the differences between an ITD5 configuration and noITD (not shown).

The differences in ice drift are less clear. We find mostly higher drift speeds in the configurations ITD20R than in ITD5R, while we find the exact opposite for ITD20H and ITD5H. This ambiguous result can be explained by the effect of ice thickness resolution on the ice strength parameterization (see subsection 2.3.3, below).

2.3.3 Ice Strength

In this section, the effects of the different strength parameterizations on an ITD model are compared in greater detail. In this context, the role of the number of thickness categories is emphasized.

We find that the non-linearity in the R75 parameterization leads to higher fluctuations in the ice strength on the near-grid scale. For both ITD5 and

ITD20, the most prominent difference between the strength formulations is found in the ice thickness of very thick ice north of Greenland and the Canadian Archipelago. Ice exceeding four meters in thickness, which mainly exists in those regions, is on average thicker by more than seventy centimeters in the R75 runs when compared to H79; but ice thinner than two meters, especially common in the peripheral regions of the Arctic, is slightly thinner on average with R75 when compared to H79 (Figure 2.4). As a possible explanation for these observations, we see generally larger ice strength gradients with R75 than with H79, with the most prominent differences north of Greenland and Ellesmere Island (results not shown). The calculation of the ice strength following R75 depends non-linearly on the local distribution of ice into different thickness categories, so that to some degree higher small-scale fluctuations are expected. But the magnitude of those strength gradients can lead to stronger gradients in the velocity fields, especially for otherwise immobile ice. Due to this process we find in the runs using R75 higher convergence rates for ice thicker than $3\,\mathrm{m}$ (Figure 2.5). This increased ridging especially in regions of already thick ice dynamically creates peak ice thicknesses much higher than observed.

The differences in concentration and drift between R75 and H79 are less clear for all ITD configurations. The differences in sea ice concentration for ITD5 and ITD20 for a climatological August are plotted in Figure 2.6; the patterns are very similar throughout the year. The ice in the marginal ice zone between Siberia and Svalbard, in winter and spring even down to Iceland, is less compact for R75 than for H79. At the same time, the ice concentration is larger for R75 in the other marginal seas, most notably in the Beaufort and Chukchi Seas and in the Baffin Bay. In the central Arctic, the differences in concentration depend on the number of thickness categories: in the ITD5 configurations, the ice is more compact for R75 than H79; but in the ITD20 configurations, the ice in summer is slightly less compact for R75 compared to H79. The ice drift is slower for R75 in large parts of the central and western Arctic and faster in the outflow of the transpolar drift and in Fram Strait (not shown). In the remaining Arctic regions we find a similar ambiguity as in the concentration fields: For R75, the ice tends to be slightly slower in the ITD5 configurations and slightly faster in the ITD20 configurations when compared to H79. Those changes can be traced back to similar patterns in the ice strength with the ice being weaker for R75 where it is faster and vice versa (not shown).
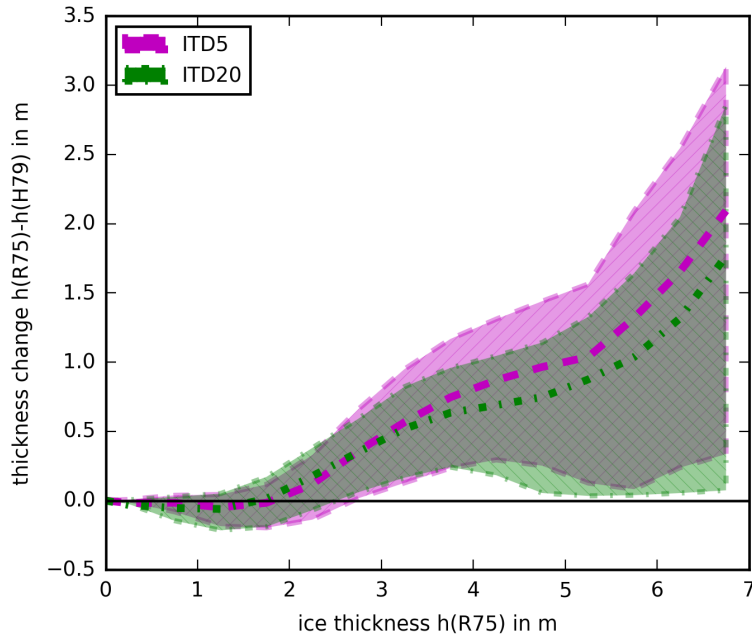
Figure 2.4: Mean difference in ice thickness ($h(\text{R75})$ - $h(\text{H79})$) between ITD configurations using R75 and H79 with the same number of thickness categories. The data is binned for ice thickness in the R75 configurations. Purple for ITD5, green for ITD20 with shaded range between 25th and 75th percentile.
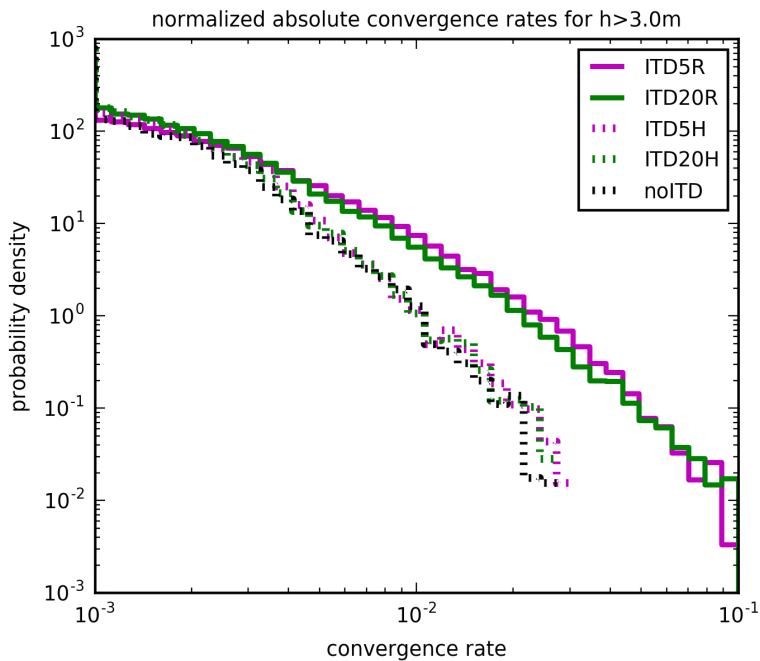
Figure 2.5: Frequency distribution of absolute convergence rates for configurations ITD5R, ITD20R, ITD5H, ITD20H, noITD; only accounting for ice thicker than 3m.
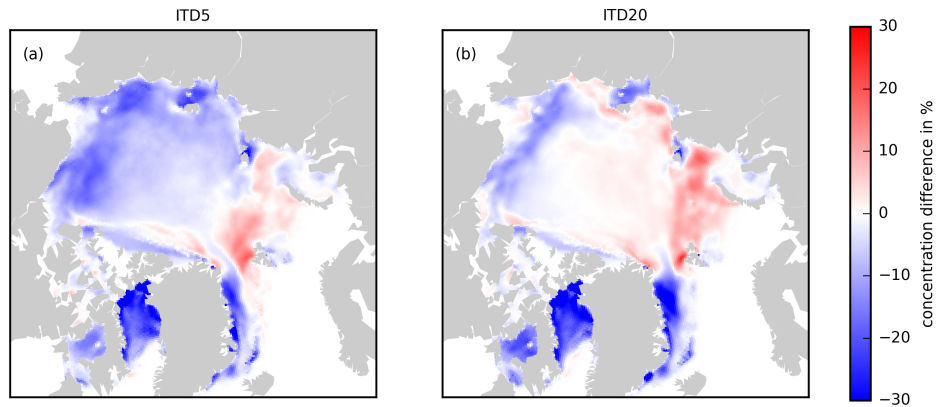
Figure 2.6: Mean change in August ice concentration (A(H79) - A(R75)) between ITD configurations using H79 and R75 for (a) 5 thickness categories and (b) 20 thickness categories

We explain those differences by the effects of two different mechanisms. On the one hand, the mean ice state with R75 is characterized over large parts of the central and western Arctic by larger thicknesses and often also slightly higher concentrations. Physically, those changes in the mean ice state generally lead to higher ice strength and thereby slower drift. On the other hand, the ice strength is a non-linear function of thickness distribution for R75, which makes the differences to the linear H79 formulation not uniform. To illustrate this we compare the strength values for both R75 and H79 computed from the ice states of model simulations using R75. For ice with a compressive strength (R75) higher than $40,000\,\mathrm{Nm}^{-2}$, the strength values calculated by R75 are higher than those for H79, and the differences grow linearly with the ice strength over a large range (Figure 2.7). In contrast, in the range below $30,000\,\mathrm{Nm}^{-2}$, the ice strength values calculated by R75 are lower than those for H79.

Finally, the R75 ice strength depends more strongly on the actual distribution of ice thicknesses than on the averaged characteristics of the sea ice. Figure 2.8 shows the difference in ice strength together with the difference in ice thickness between ITD5 and ITD20 simulations for both strength parameterizations. The ice thickness is mainly larger for the ITD20 model for both H79 and R75. As expected following the simple relationship (2.20) and
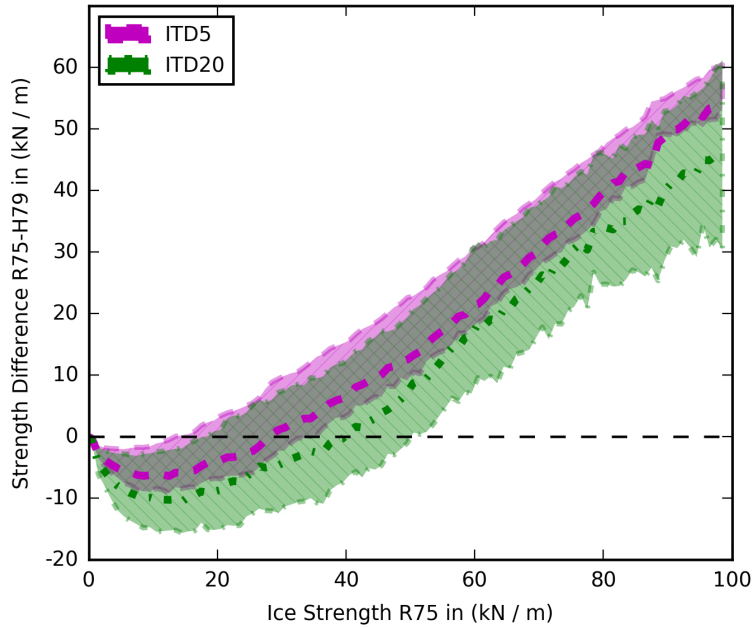
Figure 2.7: Mean difference in ice strength between R75 and H79 calculated for the same ITD. Differences are evaluated for 5 (magenta) and 20 (green) thickness categories, results are binned for ice strength after R75 with the shaded area between the 25th and 75th percentile.

the physical understanding that thicker ice is more difficult to deform, H79 calculates higher ice strength for the thicker ice in ITD20 over most thickness bins. The impact of the ice thickness on the ice strength reduces for ice thicker than three meters, most likely because of the increasing effect of the replacement pressure method (Hibler & Ip, 1995), which tends to reduce the ice strength of thick, immobile pack ice. In contrast, while for R75 the mean thickness is also mostly higher in the ITD20 configuration than in ITD5, the average ice strength is lower. So for this ice strength formulation, finely resolving the thin ice categories (and thereby weakening the ice pack) has a larger impact on the ice strength than the physical property that thicker ice should be more difficult to deform.

2.4 Discussion

The H79 ice strength formulation can be justly criticized because it is not derived from first principles. Therefore, the option of using the physically motivated R75 formulation is often thought of as a great advantage of an
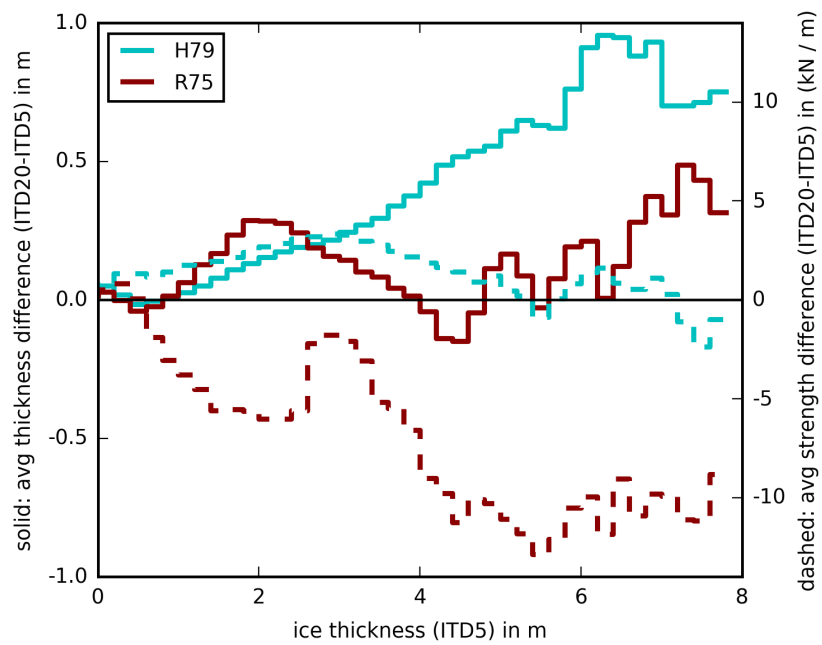
Figure 2.8: Average difference (ITD20 - ITD5) in ice strength (dashed) and ice thickness (solid) between ITD configurations using 20 and 5 thickness categories evaluated for H79 (cyan) and R75 (red). Differences are evaluated for different ice thicknesses, binned into thickness bins of the ITD5 simulations, as described in section 2.3.3

ITD model. In contrast to that notion, our results suggest that simulating realistic drift fields with medium-resolution sea ice models with R75 strength is difficult. In particular, in our simulations the model performance did not improve over a sufficiently tuned single-category set-up after including an ITD parameterization together with the commonly used R75 strength parameterization. Somewhat counter-intuitively, the model performance was better for fewer thickness classes and the model especially improved when the ITD was combined with the H79 strength formulation.

2.4.1 ITD

Our model overestimates the concentration along the ice edge almost everywhere in the North Atlantic and most of the time. In both ITD5 runs this overestimation is greatly reduced. Bitz *et al.* (2001) described a similar effect and explained it by faster melting of thin categories in the ITD, which leads to more open water, that is, lower ice concentration, especially during the summer season. Somewhat in contrast, we find also higher summer ice concentrations for the ITD configurations, mostly in the central ice pack. We explain this also by the same effect of thin ice melting. The single-category approach of Hibler (1979) assumes a uniform distribution of thickness between 0 and $2h$ for the creation of open water, so that there can be more thin ice available in this configuration than in the ITD models, which may not have any ice in the thinnest category.

In addition, the effect of an ITD model on the ice edge depends strongly on the number of categories. Resolving the ice thickness distribution better (ITD20 vs. ITD5 configurations) leads to higher ice concentrations in the marginal ice zone with the consequence of a larger ice edge position error than in the noITD model. We find that the increase in total ice volume and the associated ice export with more thickness classes is too strong to be balanced by the increased melting in the marginal ice zone that one would expect when the thinner categories are better resolved.

The mean ice thickness increases with the number of thickness classes (noITD < ITD5 < ITD20) (see also Holland *et al.*, 2006; Komuro *et al.*, 2012). This result is consistent with the physical reasoning that a better resolution of thin ice in the pack allows for more ice growth, because heat fluxes and deformation (ridging) increase. In contrast, Massonnet *et al.* (2011) found in a comparison between model versions a decrease in ice thickness,

which they attributed to the use of an ITD model. We argue, that their analysis may have been confounded because in comparing different model versions they changed multiple model components and parameters, including a lower value for the thickness of new ice H_0 in the model version with the ITD, which also changes ice thickness and concentration fields.

We did not fully address the question of (numerical) convergence of the ITD model with the number of thickness classes. A fine resolution of the thin ice range was found to be necessary to reproduce observed heat fluxes (Bitz *et al.*, 2001) and a better resolution of the upper thickness range was required to reproduce total ice volume (Hunke, 2014). Based on our experiments with 5, the minimum number recommended by Bitz *et al.* (2001), and 20 classes, which were chosen to have a simulation with a nearly converged ITD model (Lipscomb, 2001), we find that the better resolved solution does not lead to the best model-data fit. More thickness classes increase the ice volume and eventually lead to an overestimation of thickness, apparently introducing a stronger bias in the solution than the effects of a coarse thickness resolution. It is unclear in how far these effects can be moderated by more realistic thermodynamics, as the thermodynamics can have a strong impact on ice thickness (Bitz *et al.*, 2001; Losch *et al.*, 2010).

The delta function scheme (Bitz *et al.*, 2001), which we use in our simulations, was criticized to be prone to produce numerical discontinuities in the ITD and to leave many thickness categories empty, thereby artificially reducing the thickness resolution (Lipscomb, 2001). A linear remapping scheme was implemented to overcome these issues (Lipscomb, 2001). We observe the same improvements in test simulations with the linear remapping scheme (smoother thickness distributions with fewer gaps, not shown), but also on average slightly thicker ice and higher ice concentration. The main results of our study, however, remain intact: the quality of the model output, measured by the cost function, is higher for ITD configurations with H79 than for noITD, which in turn is better than the combinations of ITD and R75; and notably we observe the same dependency of the ice strength on the number of thickness categories (not shown).

2.4.2 Ice Strength

Bitz *et al.* (2001) found that for R75 the ice is weaker if a given thickness distribution is better resolved. This is probably so because the strength of the

ice pack is determined mostly by the amount of thin ice and if the thin end of the thickness distribution is better resolved, thinner ice can lead to smaller ice strength. H79 misses this sensitivity to thin ice because of linearity. We show that for R75 this effect can be strong enough in a realistic model set-up to outweigh the opposing effect of thicker ice resulting from more thickness categories (Figure 2.8). Although this behavior may be physical and could be seen as an advantage of R75 over H79, it reduces the ability to reproduce large-scale satellite observations in our experiments.

The differences in modeled ice drift patterns in our simulations are mostly caused by the different ice strength formulations, because other drivers such as the wind forcing were the same for all experiments. Because the number of thickness categories has such a strong impact on the solutions with R75, we cannot distinguish a clear change of drift patterns due to an ITD that would be independent of the choice of strength parameterization. In a comparison of different ocean-sea ice reanalysis products to satellite observations of ice drift — unfortunately they used a different observational data set, which makes a direct comparison of their results to ours difficult — Chevallier *et al.* (2016) identified the choice of atmospheric forcing and differences in drag coefficients as the most important model parameters and confirmed the strong role of the wind stress in determining the drift patterns of sea ice (Hunke *et al.*, 2011). Our results indicate that when those leading-order effects are held constant, changing the formulation of ice strength is a powerful way of affecting the model-data misfit for sea ice drift.

Holland *et al.* (2006) attributed the increased ice thickness with an ITD model to the larger ice growth rates generally produced by an ITD. We can now distinguish the effects of the strength parameterization from the choice of thickness representation in the model to show that while an ITD leads to a general increase in the overall thickness, the choice of R75 is mainly responsible for excessively large maximal thicknesses north of Greenland and Ellesmere Island. These are caused by the strong small-scale gradients in the ice strength for R75 that allow higher deformation rates in very thick ice, so that already thick ice can be ridged further, eventually leading to much higher maximal thickness values than observed.

Although the derivation of R75 is arguably more physical than that of H79, it leads to a poorer model-data misfit. In the following we speculate about the reasons for this counter-intuitive result: Rothrock (1975) already mentioned two issues with known energy sinks in his derivation of the work

necessary for ridge formation: (1) fracturing of ice was neglected following an argument of Parmerter & Coon (1973) and (2) frictional loss in shearing was neglected and assumed to be at most of the order of frictional losses in compression based on the notion of a Coulomb friction model. To estimate the work against friction in compression, Rothrock (1975) made strong assumptions about complicated processes of ice interaction without having enough data available to constrain them. He arrived at approximately similar contributions by gravitational and frictional work. This lead to a scaling factor $C_f = 2$, but later Flato & Hibler (1995) estimated this factor to be $C_f = 17$ based on a model comparison to observed buoy drift patterns. This large difference in C_f between estimates by theory and numerical model comparisons together with a re-evaluation of energy dissipation in shear (Pritchard, 1981) suggest to us that important physical effects are not properly included in the approach of R75.

Fundamental questions about the form of a new ice strength parameterization are unclear. For example, Hopkins (1998) found in model simulations of ridging processes that pressure ridge formation leads to a scaling of the ice strength proportional to $h^{3/2}$. Hibler (1980) also supports a scaling with $h^{3/2}$ by physical reasoning, but in the absence of sufficient observational data his theory is based in important parts on physical intuition. Note, however, that Hopkins (1998) considers only ice breaking in flexure, not in crushing. The load that ice can withstand before it is crushed grows linear in h (Rothrock, 1975). Further, ice strength scaling with h^2 was found in numerical simulation of ridge formation with a different experimental set-up (Hopkins *et al.*, 1991). The R75 ice strength scales with $h^{3/2}$, while the ice strength after H79 is linear in the mean thickness h (Lipscomb *et al.*, 2007), but neither appear to cover all observational evidence. We emphasize that there still exists great uncertainty in the exact nature of such a scaling. Our results indicate that the linear relationship (Hibler, 1979) might be better suited to represent Arctic-wide averages.

2.4.3   Qualitative Assessment of Our Results

Measuring the quality of our model results with the cost function (2.1) allows us to assess the overall performance of a given configuration in a detailed and quantifiable way. To this end, we evaluate the reproduction of large-scale sea ice features, such as sea ice extent, thickness and drift — as opposed to the

details of the ocean state. Three of the four data products (thickness and both drift products) are limited to certain seasons in a few years, and two of them (thickness and drift from Kimura *et al.* (2013)) are also limited to the central Arctic. Still the combination of the four products allows a year-round coverage of the whole Arctic in those years. In our analysis, we implicitly assume that large errors in one sea ice property (e.g. thickness) would affect other sea ice properties (e.g. drift and concentration) in a detectable manner. Additionally, the availability of the concentration data for the entire thirty-year simulation period provides some measure against overfitting the model to the short period 2002 - 2008 covered by the other satellite products.

Are the results presented in section 2.3 sensitive to the exact choice of observations included in the cost function? We tested this by evaluating the cost function for any combination of three (out of four) sets of observations and found that the main conclusion of the paper is robust to the exact choice of observations. In all cases, the ITD configurations together with the strength parameterization H79 lead to a better fit to the observations than the single-category configuration noITD with the strength parameterization H79. The noITD case in turn leads to a better fit than the ITD with the ice strength parameterization R75 (Table 2.3).

Our modeling approach is based on a simple single-category ice model (in fact, it is a two-category model: ice and no-ice (Hibler, 1979)) without internal heat capacity (linear internal temperature profile) and without considering a brine parameterization (Bitz & Lipscomb, 1999). Both of these omissions will lead to a larger seasonal amplitude in ice thickness and to the absence of a lag between the net surface heat fluxes and the seasonal cycle of ice thickness. When we minimize the cost function (2.1), the biases in ice thickness will be compensated by adjustments in the optimal choice of surface albedo for sea ice and snow. While it is true that we are compensating for a winter bias in ice growth (induced by the lack of thermal inertia) by including another bias in summer melt (via the albedo), the fact that we are mainly interested in the ice strength parameterization — something that is important only during one season (mid to late winter) when the ice interactions are significant (Steele *et al.*, 1997; Richter-Menge, 1997) — suggests that our conclusions are not sensitive to the presence or absence of sea ice thermal inertia. Moreover, the absence of a lag between surface atmospheric forcing and sea ice thickness will only be important for a few weeks near the onset of the melt season (the delayed ice growth in fall occurs at a time when

the ice interactions are small, (Richter-Menge, 1997)); this will therefore result in second order changes in the cost function over the full winter season. For these reasons, we believe that the simpler treatment of thermodynamic will not impact the main conclusions.

The choice of forcing data generally has a large impact on model results (Lindsay *et al.*, 2014). Prior to optimization, we chose the best forcing data set based on our cost function. A different forcing data set may change the magnitude of ice thickness or the regional distribution of ice and it will guide the optimization to a different set of optimized parameter values, but the internal mechanics of the model that are responsible for the differences between the parameterizations are not affected.

2.5   Conclusions

A rigorous model-data comparison for an ITD model and two different strength parameterizations leads us to the following conclusions: Sea ice models with an ITD parameterization can outperform single-category models in reproducing observed concentration, thickness, and drift fields. Somewhat unexpectedly, the best fit to observations is achieved with an ITD model following Thorndike *et al.* (1975) combined with a simple ice strength parameterization (Hibler, 1979). The more sophisticated ice strength parameterization by Rothrock (1975) leads to the poorest agreement to observations, even compared to the single-category model: Problems associated with this parameterization over-compensate the positive effect of an ITD model on the overall model.

It is not obvious why the Arctic-wide behavior of sea ice is reproduced with the least accuracy for the ice strength parameterization after Rothrock (1975) in our simulations. We found the modeled physics to produce implausibly large peak ice thicknesses, probably due to very high deformation of already thick ice and also a very strong dependence of the modeled ice strength on the number of thickness categories. This points to potential issues in both the physical assumptions in the formulation and the numerical discretization procedure. A short term improvement may be achieved by using the ITD parameterization together with the H79 strength formulation for medium resolution models. But because of the lack of physical justification for this parameterization, this short-term solution may turn out to be

insufficient for sea ice simulations in climate change scenarios.

The increasing availability of satellite data make possible detailed, quantitative analyses of model parameterizations. These can be further enhanced by additional data sources such as EM-Bird thickness measurements (Haas *et al.*, 2009) or ice age (Hunke, 2014). We argue that in order to realistically reproduce Arctic sea ice it is necessary to re-evaluate the ice strength formulation as a major link between ice volume and ice drift.

3. Reproduction of Observed Local Ice Thickness Distributions in an Arctic Sea Ice Model

Abstract A key parameterization in sea ice models describes the sub-grid scale ice thickness distribution. Although the positive impact of this parameterization on Arctic models is well documented, the evaluation of the produced distributions has been hindered for a long time by a shortage of reliable observations. We use a combination of historic and recent observations of local sea ice thickness to evaluate how well the model reproduces the physical processes shaping individual thickness distributions. To this end we evaluate modeled thickness distributions both in regional averages and single grid points and focus especially on the reproduction of regional, seasonal and decadal variability in the observations. We find that the model reproduces the observed regional and seasonal differences between thickness distributions, but underestimates decadal changes. The thickness distributions in single grid cells are a good reproduction of regional average conditions, but the variability on the grid scale is smaller in the model than in observations. We conclude that the ice thickness distribution parameterization provides good results for most current basin-scale models that aim to reproduce average ice properties in medium resolution. Further, we propose to calculate the modal thickness as an additional model diagnostic that allows to distinguish more clearly between thermodynamic and dynamic effects in the thickness evolution.

3.1 Introduction

The Arctic is changing rapidly. Especially the ice cover is in a transition from a perennial to a seasonal state (Overland *et al.*, 2013). For this reason, accurate sea ice models become increasingly important: (1) climate predictions depend on sea ice models to realistically represent both the feedback processes in the Arctic and the connections between Arctic phenomena and lower latitudes. (2) The reduced sea ice cover sparks economic interest in marine operations like shipping or offshore exploration. For their safety, these activities require reliable information about the ice cover.

For both applications, small openings in the ice pack are very important, starting from small cracks up to larger leads between floes or linear kinematic features in the ice more than 100km long. The ocean and the atmosphere exchange the largest part of heat and water in the Arctic in exactly those small stretches of open water. And for shipping in an ice covered ocean, leads mark divergent regions in the ice pack and often prescribe the most efficient

or only possible routes. These sub-grid scale features are not wide enough to be fully resolved even in very-high resolution sea ice models and need to be parameterized.

Thorndike *et al.* (1975) presented a sub-grid scale Ice Thickness Distribution (ITD) parameterization as an early and still one of the most important steps to tackle this problem. By now, this theory is used in many current climate models (Stroeve *et al.*, 2014) and numerous studies demonstrated how the ITD improves the representation of sea ice in models (Holland *et al.*, 2006; Massonnet *et al.*, 2011; Komuro & Suzuki, 2013; Ungermann *et al.*, 2017). In addition, more sophisticated parameterizations were developed based on this theory, e.g. more detailed thermodynamics (Bitz *et al.*, 2001) or melt pond parameterizations (Flocco & Feltham, 2007).

But despite the broad success of this parameterization, the insufficient availability of reliable observations hindered evaluations of the modeled ITDs for a long time. Some of the first Arctic models with an ITD parameterization compared ITDs from single grid cells of an Arctic model to observations from submarines (Hibler, 1980; Flato & Hibler, 1995), but only a few data points could be compared to the models and the strong differences between individual measurements led to mixed results for the reproduction of the observations in the model. In an investigation of the impact of the ITD parameterization on a fully coupled climate model, Bitz *et al.* (2001) also included a comparison against submarine data. But again, since the observations were not enough to really constrain the model development, they focused mostly on relative changes in the model with and without the parameterization instead of on thickness comparisons between model and observations. More recent evaluations of Arctic ocean – sea ice models often used large sets of different observations to assess the model. Part of such sets were also observed ITDs, e.g. from moorings (Dupont *et al.*, 2015) or airborne sounding (Herzfeld *et al.*, 2015). Both of these studies showed that the models could reproduce the observed ITDs, but the authors only compared model results to averages over observations during multiple years or over a larger region.

A different set of studies investigated how far ITD parameterizations can reproduce specific observed changes in clearly defined ITDs. Lindsay (2003) used the large amount of observations of atmospheric properties and sea ice deformation obtained during the Surface Heat Budget of the Arctic Ocean (SHEBA) experiment to force an ITD model of the immediate surroundings of the drift camp, but did not have any observations of the ITDs apart

from their initial state to validate the results. Bellchamber-Amundrud *et al.* (2002) used a coastal draft distribution model that was forced with meteorological observations from the coast and evaluated against draft observations from moorings. They identified excessive ridging in their model, but could otherwise largely reproduce the observations. Further, Kubat *et al.* (2010) evaluated a new redistribution model against high-resolution field observations in the Gulf of St. Lawrence. They found their model to reproduce very accurately the observed changes in the ice thickness distribution, but their experiments spanned only a few days.

In summary, it has been shown that ITD models can reproduce different observations of Arctic ITDs. But at the same time, most studies acknowledge mismatches of model results to observations either in the generation of open water, or in the amount of very thick ice produced by ridging, or in the amount of ridging taking place in shear. Depending on the region of the Arctic, each of these aspects can dominate the evolution of local ITDs. While it has been shown that these biases can be adjusted to reproduce single observations, it is still unclear if a single configuration using similar parameterizations can reproduce the many different ice conditions of the whole Arctic.

Over the last decades the amount of high-resolution sea ice thickness observations has increased continuously, with airborne ElectroMagnetic (EM) sounding of ice thickness complementing the Upward-Looking Sonar (ULS) measurements from submarine cruises, so that a detailed evaluation is finally possible. The aim of this study is to investigate in how far ITD parameterizations can reproduce regional, seasonal and decadal variability in Arctic ITDs. In the evaluation of the model results, I focus on three aspects: (1) Does the model reproduce regional averages of observed distributions? (2) Does the model reproduce single observations at the grid scale? And (3) which mechanisms and model parameters have the highest impact on the modeled ITDs? The data set I use and a description of the ITD model are presented in section 3.2. The relevant model – observation comparisons and the results of sensitivity studies are presented in section 3.3. These results are discussed in section 3.4, and the main conclusions are drawn in section 3.5.
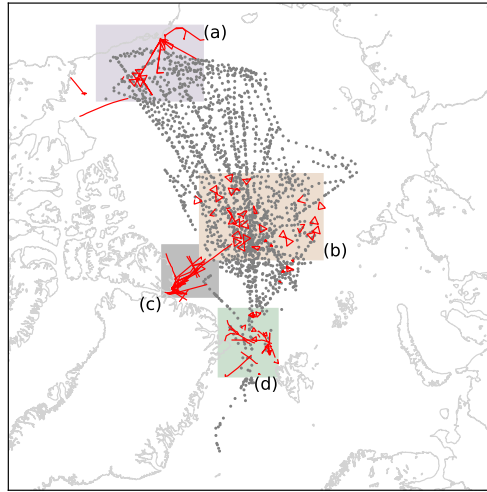
Figure 3.1: Overview of available observations: orange lines for EM-Bird flights, gray dots for ULS submarine track segments. Shaded areas are the model regions for comparison in (a) Beaufort Sea, (b) Central Arctic, (c) Lincoln Sea, (d) Fram Strait.

3.2   Methods

3.2.1   Observations

As early as 1958, submarines sailing under the Arctic sea ice have been equipped with Upward-Looking Sonar (ULS) that measure the draft of the sea ice. Lindsay (2013) collected large amounts of submarine-based ULS data and calculated draft distributions for each 50km segment of submarine track. These data cover a large part of the Arctic Ocean and span from 1975 to 2005. Over the last 15 years, many measurement campaigns where airborne electromagnetic sounding were used to measure the combined ice and snow thickness complemented this ULS-dataset (e.g. Haas *et al.*, 2008, 2010). The lengths of the individual flight tracks in those campaigns differ, but are also in the order of 50km. In this study, I focus on a subset of these observations in four regions (1) Beaufort Sea, (2) Lincoln Sea, (3) Fram Strait and (4) Central Arctic as shown in Figure 3.1. The sampled observations cover different seasons and different decades, the ULS data used in this study are from the years 1986 – 1997 and the EM data are from the years 2001 – 2012. Table 3.1 summarizes the exact years and seasons of the different observations.

ULS and EM soundings are very precise at measuring the thickness of

Table 3.1: Overview of different sets of observations

	region[1]	years	months	source	# obs[2]	# campaigns[3]
(S1)	Beaufort Sea	1986–1994	Apr	ULS	32	6
(S2)	Beaufort Sea	1993–1997	Sep, Oct	ULS	54	4
(S3)	Central Arctic	1989–1997	Sep	ULS	117	6
(S4)	Central Arctic	1986–1994	Apr, May	ULS	202	14
(S5)	Fram Strait	1987–1991	Apr, May	ULS	42	2
(S6)	Beaufort Sea	2007–2011	Apr	EM	25	7
(S7)	Lincoln Sea	2004–2012	Apr, May	EM	30	9
(S8)	Central Arctic	2001–2011	Aug, Sep	EM	37	3
(S9)	Fram Strait	2004–2011	Aug	EM	15	3
(S10)	Fram Strait	2003-2011	Apr, May	EM	12	4

[1] Regions as defined in Figure 3.1

[2] submarine track segments / individual EM-flights

[3] submarine cruises / EM measurement campaigns

undeformed ice, but have known biases for ridged ice. Rothrock & Wensnahan (2007) found the ULS data to overestimate the thickness by 29cm ± 25cm over large sample sizes. One important source of error is that the sensors record the fastest reflection of the emitted acoustic signal. This way the maximal draft over the footprint of the sensor is observed instead of the mean draft, and especially for rough, strongly deformed ice, the ice draft is overestimated. The uncertainties in the EM data are as low as ± 10cm for level ice (Pfaffling *et al.*, 2007), but again the thickness of deformed ice is less certain. In contrast to the ULS data, the electromagnetic sounding measures a weighted mean over a large footprint. That way, the thickness of individual ridges is mostly smoothed out by the surrounding thinner ice and EM data thereby underestimate the thickness of ridges (Reid *et al.*, 2006).

For a comparison of ULS and EM observations, I convert the ice draft to combined ice and snow thickness using the time-dependent values for snow thickness and snow density of Warren *et al.* (1999) and constant values $\rho_w = 1027\text{kg/m}^3$ and $\rho_i = 928\text{kg/m}^3$ for the densities of water and ice. Finally, both measurement techniques have difficulties to distinguish thin ice from open water. For this reason, the open water fraction is excluded from the analysis in this study.

3.2.2 Model Equations

Sea Ice Dynamics

The vector $\boldsymbol{u}$ of sea ice velocity is calculated according to the momentum balance

$$m\frac{\partial \boldsymbol{u}}{\partial t} = mf_C \boldsymbol{k} \times \boldsymbol{u} + \boldsymbol{\tau}_a + \boldsymbol{\tau}_o - m\hat{g}\Delta_H + \nabla \cdot \boldsymbol{\sigma}, \qquad (3.1)$$

where $m = \rho_i H_i + \rho_s H_s$ is the ice and snow mass per unit area, calculated from the respective densities ρ_i, ρ_s and grid cell area averaged thicknesses H_i, H_s of ice and snow. The different forcing terms on the right hand side of (3.1) are: the horizontal Coriolis force, calculated from the Coriolis parameter f_C and the vertical unit vector $\boldsymbol{k}$; the stress from atmosphere $\boldsymbol{\tau}_a$ and ocean $\boldsymbol{\tau}_o$; the sea surface tilt Δ_H with the gravitational acceleration $\hat{g}$; and the divergence of the internal ice stress $\boldsymbol{\sigma}$. The stresses from atmosphere and ocean on the ice are calculated using the quadratic laws

$$\boldsymbol{\tau}_a = \rho_a c_{d,a} |\boldsymbol{u}_a - \boldsymbol{u}| \boldsymbol{R}_a (\boldsymbol{u}_a - \boldsymbol{u}) \qquad (3.2)$$

$$\boldsymbol{\tau}_o = \rho_o c_{d,o} |\boldsymbol{u}_o - \boldsymbol{u}| \boldsymbol{R}_o (\boldsymbol{u}_o - \boldsymbol{u}) \qquad (3.3)$$

where ρ_a and ρ_o are the reference densities, $c_{d,a}$ and $c_{d,o}$ the drag coefficients, $\boldsymbol{u}_a$ and $\boldsymbol{u}_o$ the velocities, and $\boldsymbol{R}_a$ and $\boldsymbol{R}_o$ rotation matrices for the atmosphere (underscript a) or ocean (underscript o) (McPhee, 1975).

To be able to solve the momentum balance (3.1), the internal ice stress $\boldsymbol{\sigma}$ depends on the strain rate $\dot{\boldsymbol{\varepsilon}} = \frac{1}{2}\left[\nabla \boldsymbol{u} + (\nabla \boldsymbol{u})^T\right]$. I use the constitutive equation

$$\boldsymbol{\sigma} = 2\eta\dot{\boldsymbol{\varepsilon}} + \left((\zeta - \eta)\dot{\varepsilon}_I - \frac{P}{2}\right)\boldsymbol{I} \qquad (3.4)$$

for the viscous-plastic rheology (Hibler, 1979). Here the bulk viscosity $\zeta = \frac{P}{2\Delta_{\dot{\varepsilon}}}$ and the shear viscosity $\eta = \frac{\zeta}{e^2}$ are calculated from the ice pressure P, the axis ratio e of the elliptical yield curve, and invariants for divergence $\dot{\varepsilon}_I = \dot{\varepsilon}_{11} + \dot{\varepsilon}_{22}$ and shear $\dot{\varepsilon}_{II} = \sqrt{(\dot{\varepsilon}_{11} - \dot{\varepsilon}_{22})^2 + 4\dot{\varepsilon}_{12}}$ of the strain rate. Finally, $\boldsymbol{I}$ is the identity matrix and $\Delta_{\dot{\varepsilon}} = \sqrt{\dot{\varepsilon}_I^2 + e^{-2}\dot{\varepsilon}_{II}^2}$ is a measure of deformation.

In the sensitivity studies, four more parameterizations are included: (1)

The compressive ice strength

$$P = P^* A h e^{-C^*(1-A)} \qquad (3.5)$$

is calculated linearly in ice thickness h and decreases nearly exponentially with lower sea ice concentration A (Hibler, 1979). P^* and C^* are tuning parameters. (2) A gross closing rate of the ice pack is calculated from the sum of the divergence and the amount of shear, multiplied with a factor $0 \leq C_s \leq 1$. This factor determines how much of the shearing motion can be translated to closing of leads, and thereby ridging (Flato & Hibler, 1995). (3) The thickness of newly frozen ice is set to H_0 (Hibler, 1979). A large initial thickness can be criticized as going against physical principles, since the thickness of newly frozen ice increases more or less continuously in reality, beginning with an "initial thickness" of at most a few centimeters when frazil ice and small platelets start to form in the water. But this parameter allows to control how quickly open water freezes and offers a very rough parameterization of the many small-scale processes that take place during the freeze-up of open leads until the new ice is somehow consolidated. And (4) during ridging, a factor $0 \leq F_S \leq 1$ of the snow on the undeformed ice pack stays on the ridged ice, the rest is pushed into the water during the process (Flato & Hibler, 1995).

Ice Thickness Distribution

Thorndike *et al.* (1975) defined the thickness distribution $g(h)$ as the relative fraction of ice of thickness between h and $h + \mathrm{d}h$. This distribution can change by advection, thermodynamics or through ridging processes. The latter mechanical changes are described following the theory of Thorndike *et al.* (1975), but using the smooth functions of Lipscomb *et al.* (2007) in this framework: First, a participation function

$$a(h) = \frac{1}{b_0} \exp\left(\frac{-G(h)}{a^*}\right) g(h) \qquad (3.6)$$

determines how much of the ice of thickness h takes part in each ridging event. Here b_0 is a normalization factor, $G(h) = \int_0^h g(\hat{h}) \, \mathrm{d}\hat{h}$ is the cumulative thickness distribution and a^* is the participation parameter that scales the relative participation of thin and thick ice. And second, a redistribution

function

$$\gamma(h_{in}, h_{out}) = \gamma_0 \exp\left(\frac{-(h_{out} - h_{\min})}{\mu\sqrt{h_{in}}}\right) \qquad (3.7)$$

describes how much ice is ridged into thickness h_{out}, if unit area of ice of thickness h_{in} is ridged. Here, γ_0 is a normalization factor, μ is a scaling parameter, and $h_{\min}$ gives the minimal thickness into which ice can be ridged.

3.2.3 Model Data

An Arctic configuration of the MIT general circulation model (MITgcm) is compared against the observational data. The model setup in this study is based on previous Arctic configurations using the ITD parameterization and the Hibler-type strength (Ungermann *et al.*, 2017). The ITD is discretized into ten thickness categories. This configuration was chosen as a compromise between computational costs and sufficient thickness resolution.

In this configuration, sensitivity studies are performed for the influence of ten different parameters on the shape of the ITD produced. The tested parameters are the two redistribution parameters (1) a^*, that determines which ice takes part in ridging processes and (2) μ, that determines the shape of the produced ridges; (3) the compressive ice strength parameter P^* and (4) the ice concentration parameter C^*, of the ice strength parameterization; the drag coefficients (5) $c_{d,a}$ and (6) $c_{d,o}$ for the ice with respect to atmosphere and ocean; (7) the axis ratio e of the elliptical yield curve, which determines the ratio between shear strength and compressive strength P in the VP-rheology; (8) the shear coefficient C_s, which determines how much energy during shear deformation is used to build pressure ridges; (9) the thickness of newly formed ice H_0; and (10) the snow fraction F_s that remains on the ice after ridging.

The results of those sensitivity studies informed a manual adjustment of the parameters. The final values were chosen to improve the representation of the ITD in the model without departing too far from the mean sea ice state of the tested configurations from (Ungermann *et al.*, 2017) and are summarized in Table 3.2. In addition, I infer the sensitivity of the ITDs to individual parameter changes from the differences between the two perturbation runs for each parameter. I calculate the mean area between the regional cumulative thickness distributions as an established measure of similarity of histograms

Table 3.2: Parameter values in sensitivity analyses and final configuration

	Baseline	Perturbation Range	F inal
μ	3.029	2.0	2.0
a^*	0.041	0.02	0.03
P^*	2.299×10^4	7.0×10^4	2.2×10^4
C^*	15.92	8.0	10.0
$c_{d,a}$	1.657×10^{-3}	0.5×10^{-3}	1.9×10^{-3}
$c_{d,o}$	6.647×10^{-3}	1.0×10^{-3}	6.5×10^{-3}
e	1.523	0.8	1.8
C_s	0.5	0.5	0.85
H_0	0.5649	0.3	0.6
F_s	0.5	0.5	0.6

(Rubner *et al.*, 2000).

Model results are compared to observations of either ice draft (ULS) or combined ice and snow thickness (EM). In the MITgcm, local ice and snow profiles and the density of the ocean surface are active model variables, while the densities of ice and snow are kept constant. With this information, both the ice draft

$$h_d = \frac{\rho_i}{\rho_w} h_i + \frac{\rho_s}{\rho_w} h_s \qquad (3.8)$$

and the total ice and snow thickness

$$h_t = h_i + h_s \qquad (3.9)$$

can be calculated from the thicknesses h_i, h_s and densities ρ_i, ρ_s of ice and snow (subscripts i and s respectively) and the surface density ρ_w of the ocean. The observations allow to assess both regionally averaged ITDs and single, localized measurements. For these comparisons, the modeled thickness distributions are first averaged over the regions and months of the year defined in Table 3.1. Second, model snapshots are sampled every ten days, so that each track segment of the ULS data and single flight of the EM data can be matched with the nearest grid cell.

3.3 Results

3.3.1 Regional Ice Thickness Distributions

The model captures the regional differences of ITDs very accurately, but it sometimes overestimates seasonal changes in the ITDs (Figure 3.2). Decadal variability in the modeled ITDs is small.

The model shows a broad range of different ice conditions in different regions, similar to the observations. But the model reproduces the observations generally better for certain ice types than for others. When the observations cover mostly first-year ice, as in the Beaufort Sea and in the Central Arctic during the 2000s, the agreement between model and observations is very accurate. The total average area between the cumulative histograms is $0.64m \pm 0.21m$, while the average over the observations in the Beaufort Sea is $0.41m \pm 0.06m$. In regions with a larger amount of multi-year ice, the model still captures the overall properties of the ice pack, but the agreement with the exact shape of the observed ITDs tends to be lower especially for bi-modal distributions. Similarly, the modeled changes in the ITD between different seasons match mostly first-year ice behavior: The model slightly underestimates the changes in the Beaufort Sea, while it strongly overestimates the annual cycle in the Central Arctic and in the Fram Strait.

Differences between decades are small in the model. I compare averaged ITDs centered at 1990 and 2005 for regions and seasons as in the observations S1, S2, S3, S4, S5, S7 and S9 (see Table 3.1). Over this time, the modal thicknesses in the model distributions do not change on average ($0m \pm 0.02m$). In this evaluation, S5 is excluded because the distribution is very flat around its mode. Over the same time, the mean thicknesses of the distributions decrease by $0.06m \pm 0.12m$ in the model. In comparison, for the three regions with observations in different decades, the estimated loss in mean ice and snow thickness is 0.88m (S1 and S6, Beaufort Sea), 1.79m (S3 and S8, Central Arctic) and 1.37m (S5 and S10, Fram Strait).

The model underestimates both modal and mean thickness compared to observations, but the differences are smaller for the mean than for the mode. On average, the modal thicknesses of the ten regions are thinner by $0.66m \pm 0.89m$ in the model than in the observations, while the same difference for the mean thicknesses is only $0.25m \pm 0.47m$, indicating that the distributions in the model are skewed compared to the observations:
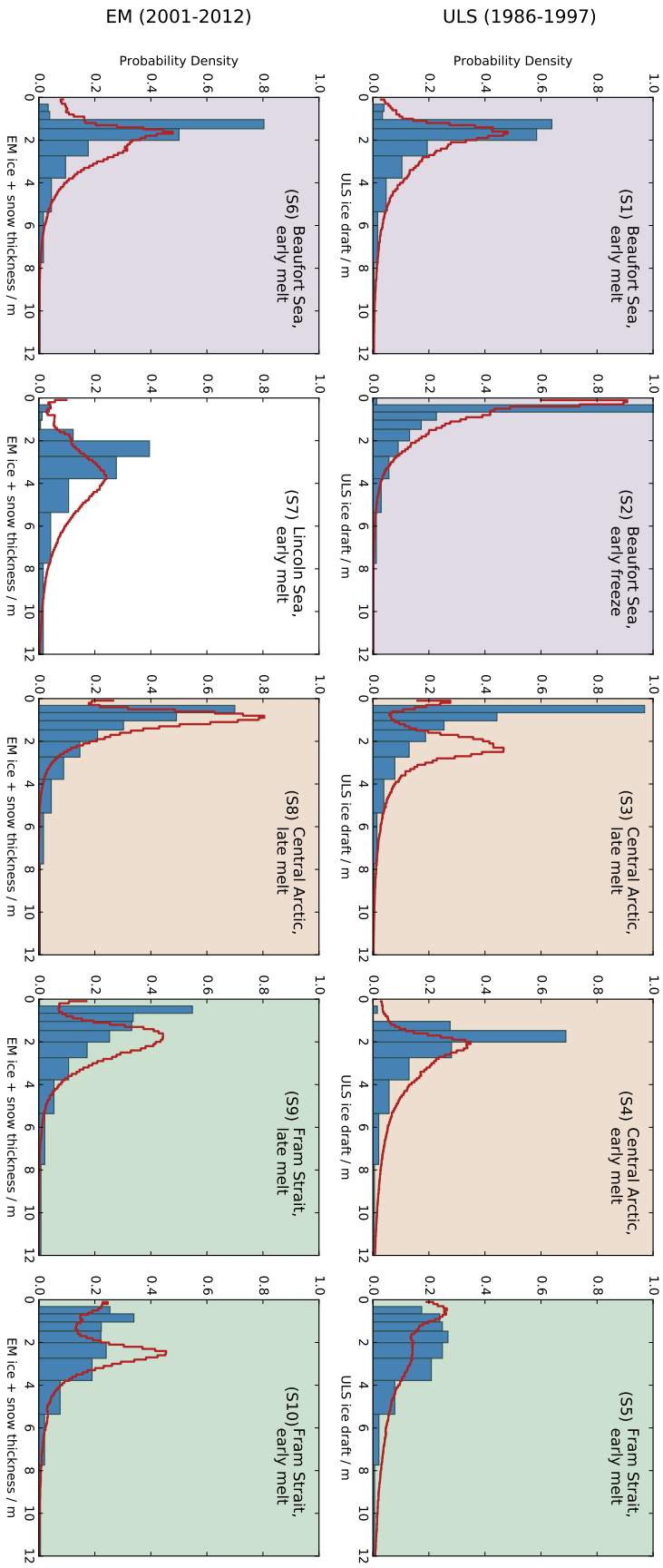
Figure 3.2: Regional ITDs from model (blue bars) and observations (red line). Observations are ice draft from submarine ULS (1)–(5), ice + snow thickness from airborne EM sounding (6) – (10). Exact regions and times of comparisons are specified in Figure 3.1 and Table 3.1.
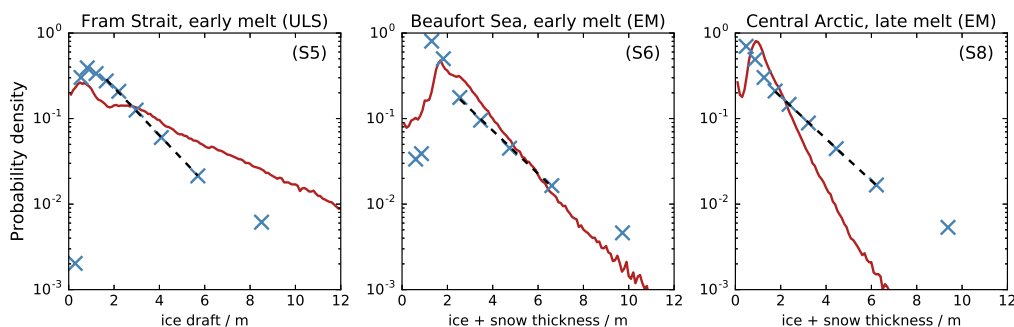
Figure 3.3: Semi-logarithmic plot of average ice thickness against probability mass in each category for three regional ITD. Blue crosses for model values, red lines for observations. The dashed black lines emphasize the accordance to an exponential fit.

The high amount of unrealistically thin ice in the modeled mode is partially offset by too much ridged ice and the lack of ice thinner than the mode.

The exponential tails in the distributions further highlight these differences in the shape of the ITDs. Both the observed and the modeled ITD show an exponential tail, but the rate parameters (or the slopes in the semilogarithmic plot) are different. In Figure 3.3, the thickness distributions of three different regions are plotted on semi-logarithmic axes. The specific regions were chosen for an overview of the range of tails that are present in the model and the observations, the thickness distributions in other regions show comparable exponential decay. While the qualitative behavior of the tail agrees between model and observations, the rate parameter of the modeled tail differs in most regions from the observations.

3.3.2 Grid-Scale Ice Thickness Distributions

The model results from single grid cells are often very similar to the regional averages presented in section 3.3.1. Figure 3.4 compares histograms from 20 different observations to model results from the nearest grid point. In general, the model distributions in single grid cells look physically plausible with mostly a single, dominant mode of thermodynamically grown ice and an exponentially decreasing tail of deformed ice. But the points are selected because they highlight the variability in the observations: nearly flat, uni- and bi-modal distributions. The modeled ITDs are less variable in shape than the observations. Without any smoothing by averaging, this comparison is more sensitive to biases in the ITD parameterizations than the comparison

of regional mean values. Especially when data from the same regions and seasons in Figure 3.4 are evaluated, the differences between model results at different points are small, compared to the observed range of distributions.

3.3.3   Sensitivity Studies

Sensitivity studies for tested parameters show that the redistribution during ridging and the deformation in shear are most important in shaping the modeled ITD. Figure 3.5 summarizes the sensitivity of the regional ITDs to the different parameters.

Adjusting the ridging parameterization, especially the redistribution of thicknesses during ridging (μ), can produce the largest changes in the modeled ITD. But note that the two tuning parameters involved in ridging have a drastically different impact on the ITD: adjusting the participation of ice in ridging (a^*) produces almost no changes in the ITDs at all. For the two parameters changing the behavior in shear deformation (e and C_s), a difference in impact is much smaller (than for μ). The sensitivity of the ITDs to both e and C_s is still larger than the sensitivity to P^* or $c_{d,a}$. These two parameters are among the most common parameters used to tune comparable sea ice models towards large-scale observations (Nguyen *et al.*, 2011), but these results indicate that they are not the best choice to tune regional ITDs.

3.4   Discussion

3.4.1   Regional Ice Thickness Distributions

I show that with the ITD parameterization regional and seasonal differences in ITDs can be reproduced and matched with corresponding observations. To my knowledge, it has not been shown in this detail that an ITD model is not only able to reproduce average ice conditions in a single region (e.g. Dupont *et al.*, 2015; Herzfeld *et al.*, 2015), but also to reproduce very different regional and seasonal ITDs in the same configuration. The model tends to produce distributions with a thin peak and an exponentially decaying tail of thicker, ridged ice. This leads to good model–observation fits for conditions of relatively uniform first-year ice as in the Beaufort Sea. At the same time, this tendency leads to a poor representation of bi-modal distributions with
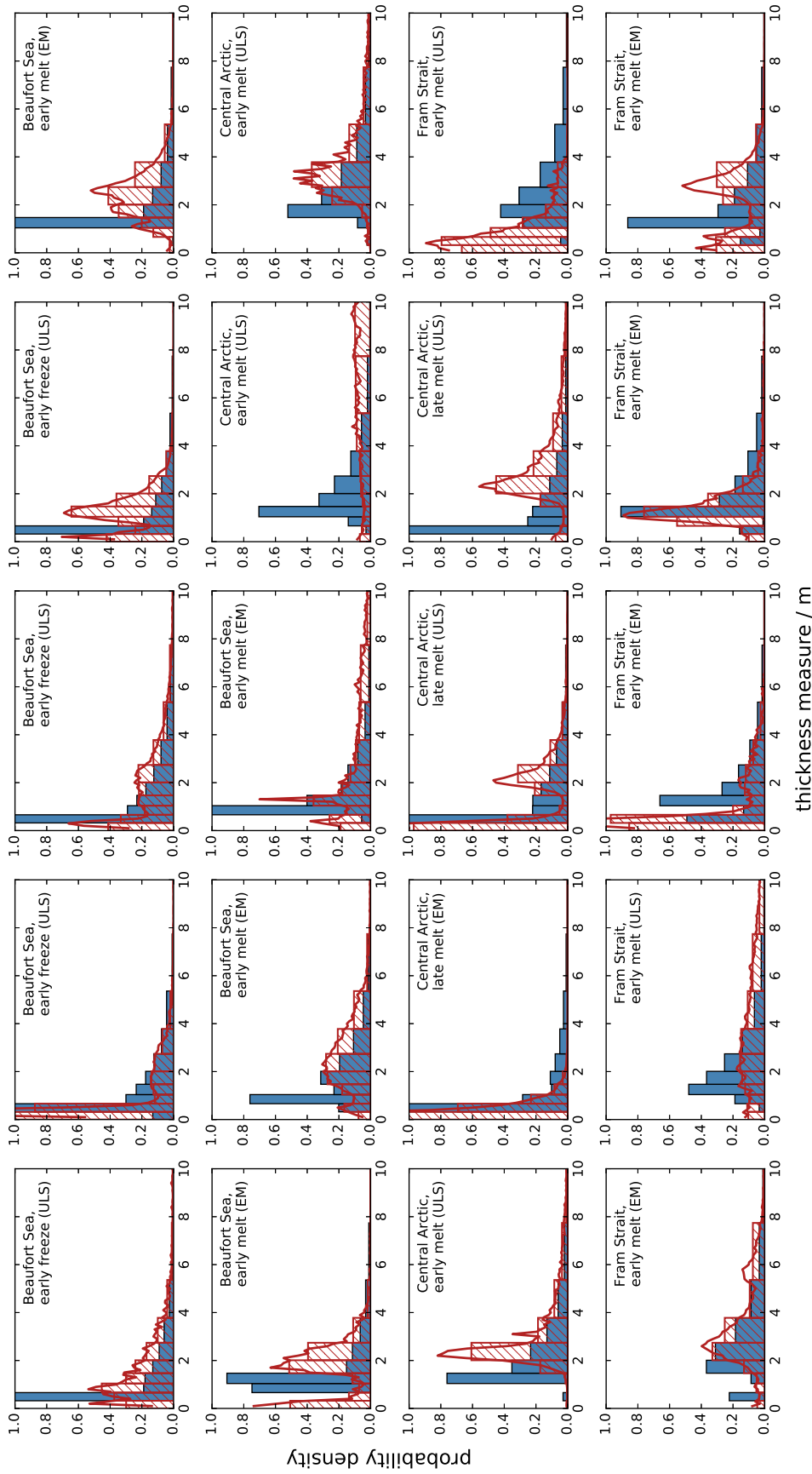
Figure 3.4: Choice of 20 ITD from single flights for EM-data or 50km submarine cruise tracks for ULS-data (red line: measurements, red hatched bars: rebinned into model bins) and the modeled ITD of the nearest grid cell (blue bars). Points are taken from regions as indicated in the label.

59
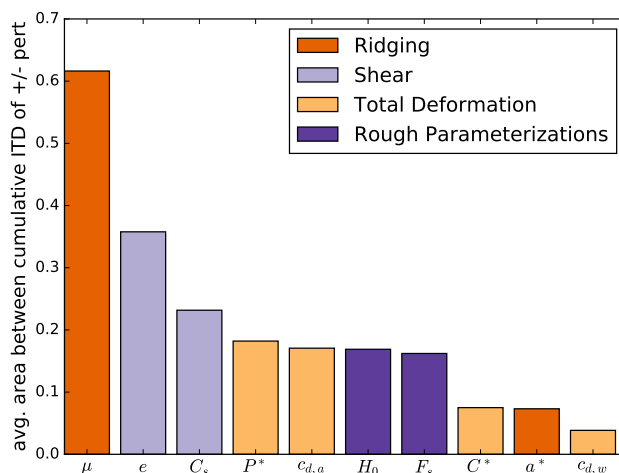
Figure 3.5: Sensitivity of the ITDs to each parameter. The mean areas between the cumulative thickness distributions of the respective perturbation experiments are plotted as colored bars; the color coding refers to different physical mechanisms.

multiple ice types, that are common e.g. in Fram Strait.

The changes in modeled ITDs over 15 years are small. The thinning in mean ice and snow thickness calculated from the observations probably overestimates the real changes, since the (older) ULS data generally overestimate mean ice thickness while the (younger) EM data underestimate mean ice thickness. But Rothrock *et al.* (2008) evaluated a larger set of observations with a higher precision and give a decrease of 0.54m in sea ice draft for the time span from 1990 to 2005 as an Arctic mean, still larger than even the largest values modeled in this study.

Over the time span of my investigation, one of the largest changes in the Arctic was the reduction in the multi-year ice fraction (Polyakov *et al.*, 2012), which can explain the different behavior of model and observations. The MITgcm currently does not distinguish first-year ice from multi-year ice, even though their physical properties differ greatly (Timco & Weeks, 2010). Armour *et al.* (2011) showed that sea ice models without such a distinction can reproduce mean ice properties from observations, but produce distorted climate sensitivities when the relative fraction of first-year ice and multi-year ice is not variable. My results, namely that the seasonal and regional differences can be reproduced, but that there is only small variability with changing forcing situations over the decades, support this finding.

I argue that including the modal thickness as model diagnostics can help

to constrain uncertain coefficients in different parameterizations, because the model used in this study (and probably models in general) can better simulate observed mean thickness than observed modal thickness. Sea ice models are often evaluated against mean sea ice thickness (e.g. Chevallier *et al.*, 2016; Stroeve *et al.*, 2014). Apparently, tuning the models towards this target can introduce compensating biases in the thermodynamics and the ridging schemes: for example, too much ridged, thick ice can be offset by a prominent and too thin mode, or too much very thin ice. Herzfeld *et al.* (2015) use a model with much more sophisticated thermodynamics than the MITgcm, but arrive at ice draft distributions with similar characteristics as those presented in Section 3.3. Therefore I assume that such compensating biases exist both for simple and very sophisticated model parameterizations of thermodynamic processes. With the current amount of available observations, including the modal thickness as a model diagnostic allows to better distinguish between thermodynamic changes of the mean ice thickness and purely mechanical changes. This provides a simple and cheap option to constrain the development and tuning of these two important parts of any sea ice model.

I interpret the clear exponential decay of the tail of the simulated distributions as an indication for a good model of the physical processes inherent to ridging. The exponentially decreasing tail of thick ice is a common feature of observed Arctic ice thickness distribution (Wadhams & Davy, 1986). Similar tails are simulated by Bellchamber-Amundrud *et al.* (2002) with a ridging model similar to the one used here but with constant redistribution, and by Godlovitch *et al.* (2012) using a stochastic model, also with constant redistribution. Their results indicate that the exponential tails are not created by the exponential redistribution functions used in this study. Instead, these results confirm that the appropriate physical mechanisms are included in the ITD parameterization.

3.4.2 Grid-Scale Ice Thickness Distributions

The evaluation of grid-cell ITDs shows that mean conditions are reproduced, but that the variability between points close to each other is low. My results corroborate previous evaluations of point-wise ITDs: Hibler (1980) provided ITDs taken from single grid cells of his model and the evolution of this parameterization was often based on the comparison of columnar ITD mod-

els with observations (Schramm *et al.*, 1997; Bellchamber-Amundrud *et al.*, 2002). Their results agree with mine in that with the ITD parameterization the sea ice simulations are consistent with observed Arctic ITDs and that the parameterization can be tuned to a specific set of observations. But with the currently available data, I can further show that the parameterization simulates ITDs in single grid cells that are very similar to the regional mean states and underestimate the observed variability on the grid scale.

I speculate about two explanations for the smaller grid-scale variability in the model: (1) The distinction between ice types is insufficient; (2) localization of deformation events is missing. The first explanation is in line with the arguments presented in section 3.4.1: The ice properties are chosen to represent the Arctic-wide mix of different ice types. Especially in regions where different ice types should be present in single grid cells, this approach will lower the range of possible behavior of the ice and might make the ITDs more uniform. The second explanation might be given in terms of the localization of deformation in viscous-plastic sea ice models: With coarse and medium resolution, such models underestimate the absolute deformation rate and especially the localization of the deformation (Dansereau *et al.*, 2017; Spreen *et al.*, 2017). A stronger localization of deformation events also leads to more heterogeneity in the simulated fields and hence might allow ITDs in different grid cells to develop more independently from each other. Spreen *et al.* (2017) show that the localization of deformation increases in VP models with high resolution. With this in mind, a high-resolution VP model with an active ITD parameterization may be necessary to better distinguish the effects of deformation localization on local ITDs.

3.4.3 Sensitivity Studies

The sensitivity studies emphasize how important the deformation properties in shear are for sea ice models. Both of the investigated shear parameters are used in many current model studies with their original values of $e = 2$ (Hibler, 1979) and $C_s = 0.5$ (Flato & Hibler, 1995), although these choices were only weakly motivated. More recent studies found that decreasing the value of e leads to improved representation of different Arctic-wide sea ice features (Miller *et al.*, 2005; Bouchat & Tremblay, 2017; Ungermann *et al.*, 2017). In addition, Kwok & Cunningham (2016) analyzed deformation fields and thickness changes from coinciding satellite observations. They found

that the major part of mechanical ice thickness redistribution is caused by deformation in shear, not by deformation in convergence. My results support the notion that deformation in shear is a key factor in shaping different ITDs in the Arctic. At the same time, this implies that it is possible to use the abundance of ITD observations to constrain poorly constrained parameters like e in future studies.

In addition, I hypothesize that changes in modeled local ITDs are always connected to changes in the basin-scale circulation. The ITD in a single grid-cell is the result of all processes along the Lagrangian path of the ice parcel. Therefore, changes in basin-scale patterns can have a larger impact on ITDs than changes in local processes. In the evaluation of the sensitivity runs, no parameter perturbation produced a change in the ITDs without a clear change in Arctic wide thickness and drift patterns (not shown), even though the processes that shape ITDs are inherently local in their effect. The large role of shear deformation also supports this hypothesis, since the axis ratio e effects primarily the dynamic behavior of the sea ice (e.g. Bouchat & Tremblay, 2017), and it also produces the second-largest changes in ITDs.

3.5 Conclusions

From a comparison of modeled ITDs against observations from different regions, seasons and decades in the Arctic, I draw the following conclusions: The currently used form of ITD parameterizations allows to consistently simulate basin-wide sea ice in the Arctic. Observed regional and seasonal variations in ITDs in the Arctic are, to a large degree, reproduced in regional averages and snapshots from single grid cells. The modeled ITDs depend on the overall drift and thickness patterns and hence on parameters that are not directly related to the ITD parameterization.

At the same time the parameterization appears to be incomplete, which limits its use for specific applications: The changes between different decades are small in the model and there is so far no mechanism implemented to distinguish between first-year and multi-year ice. Therefore, the parameterization might underestimate the climate sensitivity of the Arctic ice cover in longer climate change scenarios. Additionally, the grid cell ITDs mostly follow the regional mean without the observed variability. The parameterization was developed to describe tens of kilometers of pack ice. For local

process studies of, for example, sea ice-ocean interaction, or sea ice biology, it may not provide sufficient sub-grid scale information.

For future work, the shape of the modeled ITDs, and especially the modal thickness provide a new, and easy to implement model diagnostic. This diagnostic allows to separate more clearly thermodynamic and dynamic effects in thickness patterns, and can thereby reduce potentially compensating biases in these two parameterizations. In addition, it might allow to constrain poorly constrained model parameters like the axis ratio e of the elliptical yield curve.

4. Is the thin ice fraction really the key factor for the ice strength parameterization?

Abstract The choice between two common ice strength parameterizations can have a large effect on the reproduction of satellite observations of Arctic sea ice concentration, thickness and drift in viscous-plastic sea ice models. One parameterization calculates the ice strength from a multi-category ice thickness distribution and the other uses a two-category thickness model. With the latter parameterization the ice strength depend linearly on mean thickness, but with the multi-category model this dependence is quadratic on average. The aim of this study is to determine which of the differences between the two parameterizations are crucial for their impact on basin-scale models. A rederivation of the multi-category strength in the limiting case of only two thickness categories allows to perform Arctic model simulations that allow to distinguish effects of mean dependences on thickness and concentration from effects of the choice of thickness representation. The results show that a two-category strength is better suited for Arctic sea ice simulations than a multi-category strength and that the mean dependence of strength on thickness is only second order. In the original derivation of the multi-category strength, energy stored and dissipated during ridging is assumed to determine the large-scale ice strength. This assumption emphasizes the role of the thin ice fraction computing the ice strength, which we find to be detrimental to model performance. When calculating the ice strength, a larger role of energy dissipated in shear can explain both that the mean ice thickness determines the ice strength and that the ice strength is linear in the ice thickness.

4.1 Introduction

The climate is changing, and the Arctic is one of the regions, where those changes are most prominent (Overland *et al.*, 2013). Sea ice is a key factor in this rapid reaction to changing conditions, and it is necessary to understand its behavior to explain and correctly predict the future changes and their impact on the global climate system (Overland *et al.*, 2016). In addition, the sea ice cover plays a key role in every human activity in the Arctic, from the smallest communities to large shipping and construction operations (Meier *et al.*, 2014). But despite this importance on many different levels, many of the large-scale properties of the pack ice are still highly uncertain and a matter of ongoing research (Stroeve & Notz, 2015).

The yield strength of the ice pack is a central parameter for both climate

models and engineering applications. The maximum internal pressure that the ice can withstand before failing and deforming permanently. For sea ice models, the yield strength determines how the ice moves under a given forcing (Spreen *et al.*, 2017). And for any man-made structure in Arctic waters, knowledge of the yield strength is necessary to predict maximal forces that can be exerted by the ice (Timco *et al.*, 2017).

Today, many different parameterizations for the ice strength exist with the two most common ones attributed to Rothrock (1975) and Hibler (1979). Rothrock (1975) equated the work necessary to build a pressure ridge in the pack ice to the sum of the rise in the potential energy of the system and the energy lost to friction in the ridging process. Based on these processes, he derived an expression for the ice strength directly from the redistribution of sea ice between ice of different thicknesses. Such a model relies fundamentally on keeping track of sea ice in a number of ice thickness categories. The basic assumption behind this model is that the work associated with ridge formation is the dominant sink of energy when sea ice deforms. Another consequence of this model is that the thickness of the weakest ice determines the strength of geophysical sea ice (Rothrock, 1975). In contrast, Hibler (1979) defined the ice strength of sea ice in terms of the mean sea ice thickness over a given area (a grid cell in a finite element model). In this simpler model, the distribution of sea ice between different ice thickness categories is not necessary, reducing the computational cost and allowing for longer integrations. In his model the ice thickness distribution reduced to two categories - ice with cell-averaged thickness H and open water or thin ice with negligible volume, where the fraction of the surface area covered by either ice type is denoted by A. The mean ice thickness $\bar{h}$ can then be expressed in terms of the cell-averaged ice thickness and the ice area fraction ($\bar{h} = \frac{H}{A}$).

Apart from the use of the multi-category framework (Rothrock, 1975) or the two-category approach (Hibler, 1979), there are other conceptual differences between the two formulations: The ice strength parameterization of Hibler is linear in the mean ice thickness $\bar{h}$, while the original expression of Rothrock (in the limit of a two-category model as in Hibler) is proportional to h^2. Hibler (1980) continued to develop the multi-category ice strength and included more realistic ridge geometries, arriving at an expression that is proportional to $h^{1.5}$. There have been efforts to constrain the ice strength parameterizations by discrete element simulations of the ridging process (Hopkins, 1998), satellite observations (Tremblay & Hakakian, 2006) or both direct and

indirect observations in the ice pack (Timco *et al.*, 2017). But for all these approaches, many assumptions are needed to transfer the direct results of the experiments to parameterizations describing an effective yield strength of the ice pack on large scales. Therefore, any general laws for the ice strength in models inferred from these results are still highly uncertain.

In addition to the unknown dependence of ice strength on ice thickness, Wilchinsky & Feltham (2006) noted that models using the multi-category ice strength of Rothrock (1975) produce a larger misfit to observed Arctic-wide ice draft distributions than models using the mean-thickness ice strength of Hibler (1979). This result was confirmed in an evaluation of simulated model diagnostics against satellite observations of sea ice concentration, thickness and drift (Ungermann *et al.*, 2017): Again, model configurations with the Hibler two-category strength outperformed model configurations using the Rothrock multi-category strength, even when all other parts of the configurations were kept strictly the same. So far it is unclear if this modeling result is due to the different exponents in the thickness dependence of the strength parameterizations, or due to the use of mean thickness or a thickness distribution in the calculation of the ice strength.

The aim of this study is to determine the main reason why multi-category strength parameterizations deteriorate the reproduction of Arctic-wide sea ice observations in models. For this goal it is necessary to differentiate between the effects of different mean dependencies on ice thickness and concentration, and the effects of calculating the ice strength from the Ice Thickness Distribution (ITD) instead of the mean thickness. To this end I present the different ice strength parameterizations together with the assumptions made in their respective derivations in section 4.2.1. This allows to rederive the multi-category strength after Rothrock in the limit of a two-category ice model in section 4.2.2, to facilitate a direct comparison to the Hibler strength. Model configurations using the different ice strength parameterizations are described in section 4.2.3 and the effective dependence of the multi-category strength formulations in these configurations on mean ice thickness and concentration are evaluated in section 4.3.1. Using these results, the observed changes in Arctic model configurations using the Rothrock strength compared to the Hibler strength are separated in section 4.3.2 into contributions of the multi-category formulation compared to a two-category formulation and contributions of different dependencies on mean ice thickness and concentration. Finally, these results are discussed in section 4.4 and the most

important conclusions are given in section 4.5.

4.2 Methods

4.2.1 Ice Strength Parameterizations

In his derivation of an expression for the ice strength, Rothrock (1975) started from the framework for the thickness distribution presented by Thorndike *et al.* (1975). The ice thickness distribution $g(h)$ is defined so that $\int_{h_1}^{h_2} g(h)\,\mathrm{d}h$ gives the relative fraction of ice with thicknesses between h_1 and h_2. This definition implies that

$$\int_0^\infty g(h)\,\mathrm{d}h = 1 \tag{4.1}$$

where the upper limit can also be replaced by $h_{\max}$, the maximal ice thickness present in the respective area. An equivalent way of presenting the ice thickness distribution, that will be helpful in the derivation, is the cumulative thickness distribution

$$G(h) = \int_0^h g(\tilde{h})\,\mathrm{d}\tilde{h}. \tag{4.2}$$

Thorndike *et al.* (1975) described the change of the ITD during ridging by two functions:

First, a participation function

$$a(h) = b(h)g(h) \tag{4.3}$$

describes the relative participation of ice of thickness h in a ridging event. This is done by multiplying a weighting function $b(h)$ with the local ITD $g(h)$, to avoid more ice of a certain thickness taking part in ridging than is actually present. The weighting function b should emphasize the thin end of the thickness distribution, since this part of the ice pack ridges most easily in compression. The participation function a is defined to give the relative fractions of ice taking part in ridging, so it is normalized to

$$\int_0^\infty a(h)\,\mathrm{d}h = 1, \tag{4.4}$$

by a scalar factor in the weighting function b.

Second, the actual build-up of ridges is described by a redistribution function $\gamma(h_{\text{in}}, h_{\text{out}})$ that determines how much ice is ridged into thickness h_{out}, when a unit area of ice of thickness h_{in} takes part in ridging. With this redistribution function, the thickness distribution

$$n(h) = \int_0^h a(h_i)\gamma(h_i, h) \, \mathrm{d}h_i. \tag{4.5}$$

of ice created by ridging can be calculated as the integral over the ridges that are produced by all ice thicknesses in the local ITD that take part in ridging. It is assumed that the produced ridges contain exactly the amount of ice that took part in ridging, so that volume conservation can be expressed as

$$\int_0^\infty h\, n(h) \, \mathrm{d}h = \int_0^\infty h\, a(h) \, \mathrm{d}h \tag{4.6}$$

which can be achieved by normalizing the redistribution function γ.

From these two functions, the ridging mode

$$w_r(h) = \frac{-a(h) + n(h)}{\omega} \tag{4.7}$$

can be formed, which describes the overall change in the thickness distribution due to ridging. In the case of pure convergence, the reduction of total ice cover by this ridging mode must equal the influx of ice into the grid cell. For this reason, the corresponding term in the evolution equation of the ITD is a product of the ridging mode and the divergence. Conservation of area in compression is then obtained for the simple condition

$$\int_0^\infty w_r(h) \, \mathrm{d}h = -1, \tag{4.8}$$

which is met with the scalar normalization factor $\omega = \int_0^\infty n(h) - a(h) \, \mathrm{d}h$ in equation (4.7).

In this framework, Rothrock calculated the change in potential energy of the ice by ridging as

$$C_p \int_0^\infty h^2 w_r(h) \, \mathrm{d}h \tag{4.9}$$

where $C_p = \hat{g}\frac{(\rho_w - \rho_i)\rho_i}{2\rho_w}$ is a factor calculated from the gravitational acceler-

ation $\hat{g}$ and the densities ρ_i, ρ_w of ice and water. Including a factor C_f to account for frictional processes, which are assumed to be proportional to the change in potential energy, the total rate of energy lost to the deformation of the ice in unit strain is

$$P = C_f C_p \int_0^\infty h^2 w_r(h) \, \mathrm{d}h. \qquad (4.10)$$

Finally, Rothrock (1975) argued that this term can equivalently be seen as ice strength: The general form of the energy lost in deformation $\sigma_I \dot{\varepsilon}_I + \sigma_{II} \dot{\varepsilon}_{II}$ must be equal to the energy loss calculated in (4.10). In the special case of pure convergence ($\dot{\varepsilon}_{II} = 0$) the ice deforms only when $\sigma_I = P$.

Hibler (1979) followed a simpler route and presented a two-category model: This model only keeps track of open water and ice instead of the detailed ITD in every grid cell. In this case, the only information about the ice thickness h is the mean ice thickness $\bar{h}$. In this simpler context, Hibler presented an alternative parameterization for ice strength

$$P_H = P^* A \bar{h} e^{-C^*(1-A)} \qquad (4.11)$$

that only depends on mean ice thickness $\bar{h}$ and concentration A per grid cell. Here, P^* is the ice compressive strength parameter, that gives the ice strength of a full ice cover with 1m thickness, and C^* is a scaling parameter that determines how quickly the ice strength decreases with open water fraction.

4.2.2 Multi-category Ice Strength for a Two-Category Model

For a better comparison of the parameterizations (4.10) and (4.11), I derive a closed-form solution of equation (4.10) in the limit where I have only two ice categories (ice and no ice). In this case, I let

$$a(h) = \begin{cases} \frac{2}{G^*} \left(1 - \frac{G(h)}{G^*}\right) g(h) & 0 \le G(h) \le G^* \\ 0 & G(h) > G^* \end{cases} \qquad (4.12)$$

be the participation of ice in ridging, where G^* is a cumulative ice concentration below which the ridging occurs (Rothrock, 1975). And let

$$\gamma(h_i, h_o) = \begin{cases} \frac{1}{2(H^* - h_i)} & 2h_i \leq h_o \leq 2\sqrt{H^* h_i} \\ 0 & h_o < 2h_i \vee h_o > 2\sqrt{H^* h_i} \end{cases} \tag{4.13}$$

be the redistribution process with H^* a scaling parameter for the maximum ridge height (Hibler, 1980). To be able to solve the integrals analytically, the thickness distribution g of ice with mean thickness $\bar{h}$ is assumed to be uniform between $h = 0m$ and $h = 2\bar{h}$. With these definitions and using the notation

$$I_- = G^* - (1 - A)$$
$$I_+ = G^* + (1 - A),$$

the ice strength derived analytically ($P_{R,ana}$, see equation 4.10) can be written as

$$P_{R,ana} = \frac{2\bar{h}I_-^2 \left(-32A^2 H^* \sqrt{2\frac{H^*\bar{h}}{A}I_-} + 35AH^*\bar{h}I_- + 21\bar{h}^2 I_-^2\right)}{7A^2 \left(8AI_- \sqrt{2\frac{H^*\bar{h}}{A}I_-} - 15AH^* I_+ + 25\bar{h}I_- I_+ - 20G^*\bar{h}I_-\right)}. \tag{4.14}$$

Details of this derivation are presented in the appendix 4.A.1.

In addition, it is also possible to evaluate the integrals in equation (4.10) numerically. This allows to relax the assumptions made to arrive at the result (4.14) and investigate cases for which no closed-form solution exists. In this manner, different choices of redistribution functions can be tested. For instance, Lipscomb *et al.* (2007) proposed to use the following participation and redistribution functions:

$$a_L(h) = \frac{e^{\frac{-G(h)}{a^*}}}{a^*(1 - e^{\frac{-1}{a^*}})} g(h) \tag{4.15}$$

$$\gamma_L(h_i, h_o) = \frac{h_i}{(h_{min} + \mu\sqrt{h_i})\mu\sqrt{h_i}} e^{\frac{-(h_o - h_{min})}{\mu\sqrt{h_i}}} \tag{4.16}$$

In these formulations, the parameter a^* has a role that is equivalent to the

participation parameter G^*, μ is the equivalent of the redistribution parameter H^*, and h_{min} is a minimal thickness produced by ridging, which is assumed to be equal to the minimum of $2h_i$ and $h_i + 1m$. In the following, I use P_R to denote ice strength calculated using equation (4.10) with the ridging functions (4.12) and (4.13), and use P_L to denote ice strength calculated using equation (4.10) with the functions (4.15) and (4.16).

I also test the impact of the choice of ice thickness distribution $g(h)$ around the mean thickness $\bar{h}$. To this end, three different distributions are assumed for the integration: (1) a uniform distribution $g_{uni}(h) = \frac{A}{2\bar{h}}$ between $h = 0$ and $h = 2\bar{h}$, (2) a triangular distribution $g_{tri}(h) = \frac{8A}{9\bar{h}^2}(\bar{h} - h)$ between $h = \frac{\bar{h}}{2}$ and $h = 2\bar{h}$ to test the impact of empty thin ice categories as an extreme case, and (3) a log-normal distribution g_{ln} with the mean $\bar{h}$ and the mode $\frac{2}{3}\bar{h}$ that is set to $g_{ln} = 0$ for all thicknesses $h > 3\bar{h}$. The different distributions are plotted in Figure 4.1.
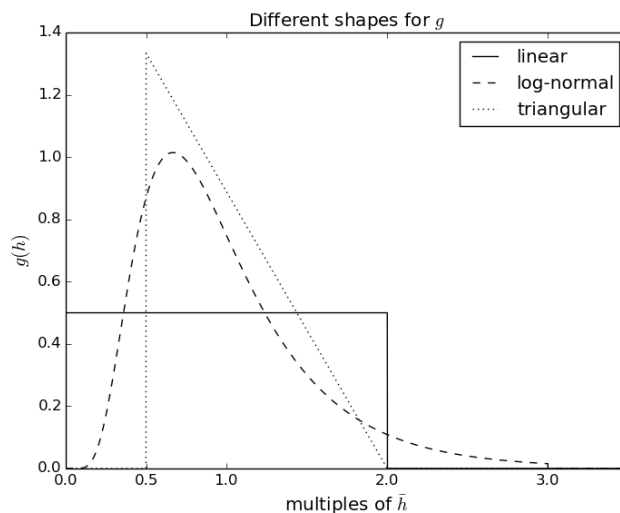
Figure 4.1: Different choices for the thickness distribution $g(h)$ expressed as a function of the mean ice thickness $\bar{h}$.

4.2.3 Comparison of Arctic Configurations

I use the method presented in Ungermann *et al.* (2017) to evaluate the performance of the different ice strength parameterizations in the MIT general circulation model (MITgcm). This method consists of two parts: A cost function calculates the misfit between model and satellite observations of sea ice as a measure of the quality of model results. Each configuration under-

goes an individual parameter optimization to ensure that comparisons are between equally-well tuned configurations.

The cost function uses satellite observations of sea ice concentration (EU-METSAT Ocean and Sea Ice Satellite Application Facility, 2011), sea ice thickness (Kwok & Cunningham, 2008), and sea ice drift (Lavergne *et al.*, 2010; Kimura *et al.*, 2013). The uncertainties in sea ice concentration, thickness and drift are provided with the measurements, taken as the minimum of 40% of the signal or 1m, and taken from detailed analyzes, respectively (EUMETSAT Ocean and Sea Ice Satellite Application Facility, 2011; Sumata *et al.*, 2014, 2015). The cost function value

$$F = \sum_{i=1}^{N} \frac{(y_i - x_i)^2}{N_d(y_i)\xi_i^2} \tag{4.17}$$

is calculated as the root mean square of the misfit between the model results x_i and the observed values y_i, weighted by the pointwise measurement uncertainty ξ_i. Then, the different observations are weighted in the cost function by the number $N_d(y_i)$ of observations in each data set, so that each satellite product has the same weight in the final cost function value. A more detailed description of the dataset and method can be found in Ungermann *et al.* (2017).

The choice of a quadratic cost function allows to optimize parameter values automatically towards this target using a Green's function approach. A description of the method used in the context of the MITgcm can be found in Menemenlis *et al.* (2005); and a description of the mathematical background on which the method is based can be found in Menke (2012). Green's functions are used to obtain a linear estimate of the model dependency on a chosen set of parameters. Using this linearized operator instead of the full non-linear model, it is possible to find an optimal perturbation for these parameters that minimizes the quadratic cost function. Using this routine, I tune the parameters relevant for the strength parameterizations in each configuration individually.

The model used in this study is a fully-coupled ocean – sea ice configuration of the MITgcm in the Arctic region. This configuration is well tuned to a large set of observations (Nguyen *et al.*, 2011; Ungermann *et al.*, 2017) and employs a mean grid resolution of 36km, making it representative of a broad class of climate models. The atmospheric forcing is taken from the NCEP

Climate System Forecast Reanalysis data (Saha *et al.*, 2010). Following this approach, I arrive at two different configurations for my comparisons:

$P_{R(\text{int})}$ Using the basic Rothrock strength P_R based on equation (4.10) with the participation functions (4.12), (4.13). The ice strength is determined by an integral over the ice thickness distribution. The tuning procedure gives values $G^* = 0.1456$, $H^* = 23.69\text{m}^{1/2}$ and $C_f = 13.42$.

$P_{R,\text{smooth}}$ Using the same strength as in configuration $P_{R(\text{int})}$, but fixing the value for the participation parameter at $G^* = 0.5$. This choice aims at reducing the impact of the thin ice fraction on the ice strength fields. Tuning gives $H^* = 29.35\text{m}^{1/2}$ and $C_f = 12.6$.

Two other configurations with commonly chosen parameterizations are included as reference, which were originally presented by Ungermann *et al.* (2017):

$P_{H(\text{mean})}$ Using an active ITD parameterization together with the classical two-category ice strength P_H after equation (4.11).

$P_{H,2\text{cat}}$ Using a simple two-category scheme for ice thickness together with P_H.

4.3 Results

The evaluation of the different strength parameterizations consists of two parts: first, I approximate the dependence of the somewhat unwieldy analytical strength parameterization (4.14) with simple functions and investigate to which degree these simpler laws depend on choices of parameterizations and coefficient values in section 4.3.1. Second, I compare the effects of different strength parameterizations in Arctic simulations in section 4.3.2, where I use the results of section 4.3.1 to distinguish clearly between the effects of multi-category vs. two-category strength and the effects of different mean dependencies on ice thickness and concentration.

4.3.1 Thickness and Concentration Dependence of Ice Strength

In a first step, I investigate if the behavior of the analytical ice strength (4.14) can be approximated by simple functions in thickness and concentration.

This allows to compare this newly derived ice strength parameterization more easily to the established two-category ice strength of Hibler (1979). Fits of different functions to the analytical ice strength (4.14) are plotted in Figure 4.2. In a second step, I compare how the quality of fit and the coefficient values of the fitted functions change with different choices for the distribution of $g(h)$ around $\bar{h}$ or for the participation and redistribution functions.
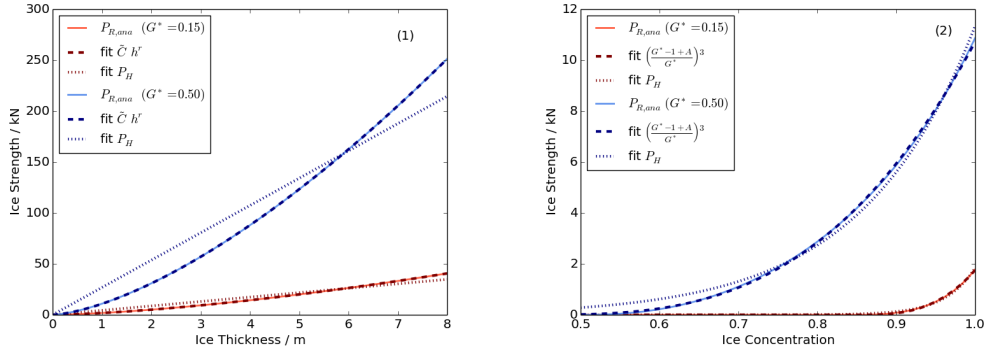
Figure 4.2: Thickness and concentration dependence for the closed-form solution of the multi-category ice strength $P_{R,ana}$ after Rothrock (1975) for two different choices of the participation parameter G^*. Fitted are the Hibler strength $P_{H(\text{mean})}$ and the new variant $P_{R(\text{mean})}$ with the exponent of h^r as an additional free parameter. Parameter values are $H^* = 25$m, $A = 1$ (subplot 1) and $h = 1$m (subplot 2).

These fits are performed for parameter combinations of $G^* \in \{0.05, 0.1, \ldots, 0.45, 0.5\}$ and $H^* \in \{10, 30, 50, 70, 90\}$. In a first order approximation, $P_{R,\text{ana}}$ should be proportional to $\bar{h}^{1.5}$ (Lipscomb et al., 2007). In almost perfect agreement to this estimate, the dependence on thickness can be modeled by an exponential function $P(h) = \widetilde{C} h^r$, where a least-squares fit produces an exponent of $r = 1.5 \pm 0.01$ in all tested cases. For the dependence of the $P_{R,\text{ana}}$ on the concentration, I find that the function $P(A) = \widetilde{C} \left(\frac{\widetilde{G}^* - 1 + A}{\widetilde{G}^*} \right)^3$ produces excellent fits for the dependence on sea ice concentration, where the relative difference between the fitted parameter $\widetilde{G}^*$ and the original value of G^* is less than 5% in all tested cases. Combining these two results, equation (4.14) can be approximated by

$$P_{R(\text{mean})} = C_P \bar{h}^{1.5} \left(\frac{G^* - (1 - A)}{G^*} \right)^3 \tag{4.18}$$

where C_P is a scaling coefficient equivalent to the ice strength parameter P^*.

The exact value of the ice strength parameter C_P depends strongly on the

thickness distribution $g(h)$. When numerically evaluating the ice strength P_R with parameters $G^* = 0.15$ and $H^* = 25$m for different assumed distributions $g(h)$ around the same mean thickness $\bar{h}$, the values for the ice strength parameter are fitted to $C_P = 1,780$Nm$^{1.5}$, $C_P = 10,429$Nm$^{1.5}$ and $C_P = 19,514$Nm$^{1.5}$ for the uniform, log-normal and triangular distribution, respectively. The thickness of the ice that takes part in ridging determines the work against gravity necessary for piling it up into a ridge, and thereby determines the ice strength. Taking the participation parameter to be $G^* = 0.15$ and solving the different distributions for the thickness with $G(h) = G^*$, the thickest ice that still takes part in ridging has a thickness of $0.3\bar{h}$ for the uniform distribution, and $0.51\bar{h}$ for the log-normal one. This thicker ice in the redistribution process (4.13) has a large impact on the calculated ice strength (equation 4.10).
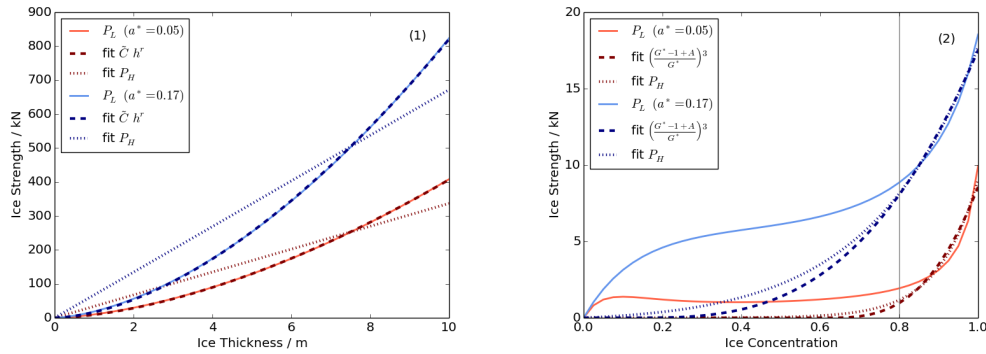
Figure 4.3: Thickness and concentration dependence for the numerical evaluation of the multi-category ice strength P_L after Lipscomb *et al.* (2007) for two different choices of the participation parameter a^*. The Hibler strength $P_{H(\text{mean})}$ and the new variant $P_{R(\text{mean})}$ with the exponent of h^r as an additional free parameter are fitted to P_L. In subplot 2 only values for $A \geq 0.8$ are fitted. Parameter values are $\mu = 3$m$^{1/2}$, $A = 1$ (subplot 1) and $h = 1$m (subplot 2), g is assumed log-normal.

A multi-category ice strength with smoother, exponential ridging functions can still be approximated by function (4.18), but introduces unexpected behavior for small sea ice concentrations. The strength P_L uses the smooth ridging functions (4.15) and (4.16) as a smooth approximation of the discontinuous functions (4.12) and (4.13). When fitting the function $P(h) = \widetilde{C}h^r$ to the results of P_L, the optimal exponents r range between 1.57 and 1.73 for parameter values $a^* \in \{0.03, 0.04, 0.05, 0.08\}$ and $\mu \in \{2., 3., 4., 6.\}$. So in this case, second-order effects start to show in the calculated values for ice strength, slightly increasing the exponent in h compared to the origi-

Table 4.1: Overview of different model configurations

	strength equations	calculated from	comment
$P_{R(\text{int})}$	(Rothrock, 1975)	ITD	
$P_{R(\text{mean})}$	(Rothrock, 1975)	$\bar{h}$	equation (4.18)
$P_{H(\text{mean})}$	(Hibler, 1979)	$\bar{h}$	
$P_{R,\text{smooth}}$	(Rothrock, 1975)	ITD	$G^* = 0.5$
$P_{H,2\text{cat}}$	(Hibler, 1979)	$\bar{h}$	2-category thickness

nal P_R. The decrease of the ice strength with lower concentrations is slower than predicted by the approximation (4.18) for sea ice concentrations smaller than 0.8, and shows a second local maximum for small concentrations around $A = 0.1$ for certain combinations of a^* and μ (Figure 4.3). Ice of concentrations lower than $A = 0.8$ is normally assumed to be in free drift, so there should be only little or no internal ice strength (Leppäranta, 2011). Still, I assume the unexpected dependence on concentration does not influence sea ice models strongly: for sea ice concentrations of less than $A = 0.8$, even the comparably high ice strength P_L is low enough to be negligible in the sea ice momentum balance.

4.3.2 Impact on Arctic Simulations

I compare the reproduction of Arctic sea ice observations in configurations using different ice strength parameterizations. In addition to the model configurations presented in section 4.2.3, a configuration $P_{R(\text{mean})}$ using the ice strength equation (4.18) will be included in the comparisons. Note that this configuration does also use an active ITD parameterization, but calculates the ice strength from the average thickness values. The tuning procedure presented in section 4.2.3 gives $C_P = 15.09\text{kN}$ and $G^* = 0.1597$. An overview of the compared configurations is presented in Table 4.1.

Comparing the cost function results of the tested configurations gives better (lower) total values for the configurations using two-category strength, than for the configurations using multi-category strength (Figure 4.4). This difference holds both for a comparison between $P_{R(\text{int})}$ and $P_{H(\text{mean})}$ and for a comparison between $P_{R(\text{int})}$ and $P_{R(\text{mean})}$. The latter comparison shows that reduced model skill when using a Rothrock strength (Wilchinsky *et al.*, 2006; Ungermann *et al.*, 2017) is caused by the use of a multi-category strength formulation, and not by different exponents in the thickness dependencies of
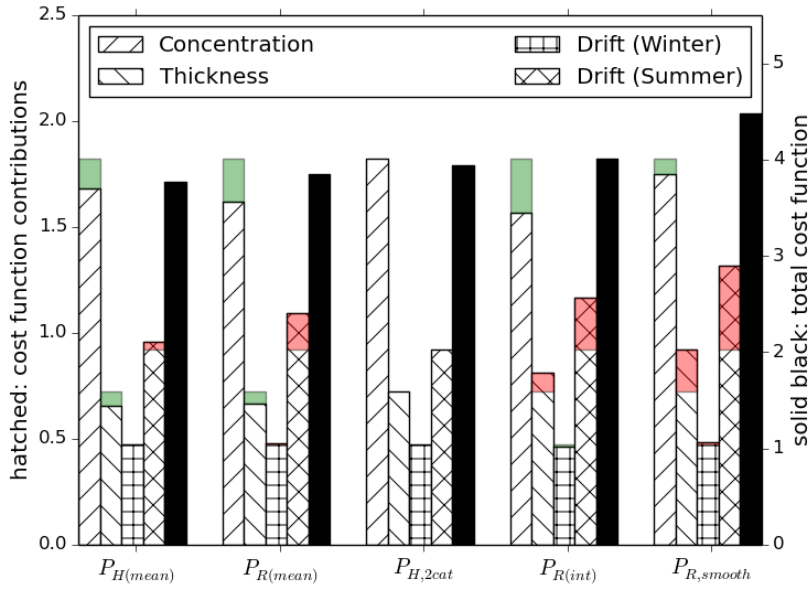
Figure 4.4: Comparison of the cost function results for configurations using an multi-category thickness scheme and respectively the mean-thickness Hibler-strength $P_{H(\mathrm{mean})}$, the newly derived mean-thickness strength $P_{R(\mathrm{mean})}$, the multi-category Rothrock-strength $P_{R(\mathrm{int})}$, and the multi-category strength $P_{R,\mathrm{smooth}}$ with a high participation parameter $G^* = 0.5$. As a reference the configuration $P_{H,2\mathrm{cat}}$ with a two-category thickness scheme is shown and differences to this configuration are color-coded. Note the different scales for single contributions (hatched, left scale) and total sum (black, right scale).

the ice strength.
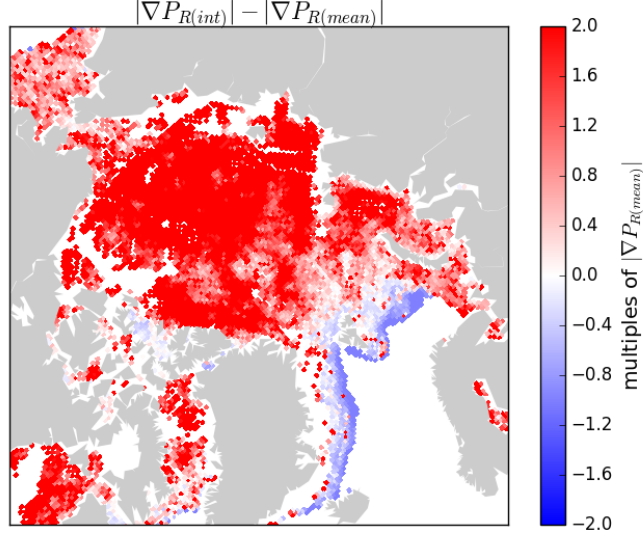
Figure 4.5: Difference between the norm of the average ice pressure gradient (normalized as $\frac{\|\nabla P_{R(\mathrm{int})}\| - \|\nabla P_{R(\mathrm{mean})}\|}{\|\nabla P_{R(\mathrm{mean})}\|}$) for the multi-category strength $P_{R(\mathrm{int})}$ minus the mean-thickness strength $P_{R(\mathrm{mean})}$.

One consistent difference between configurations is that the ice strength gradients are much larger for the multi-category strengths than for two-category strengths (see also Ungermann *et al.*, 2017). Comparing $P_{R(\mathrm{int})}$ and $P_{R(\mathrm{mean})}$ as an example, $\|\nabla P_{R(\mathrm{int})}\|$ is at least twice as large as $\|\nabla P_{R(\mathrm{mean})}\|$ under almost all ice conditions, often larger (Figure 4.5). My experiments indicate that these high strength gradients may be one of the main problems of the multi-category strength and I discuss this result further in section 4.4.2.

I tried to smooth the high strength gradients in multi-category parameterizations by increasing the participation parameter to $G^* = 0.5$, but this did not improve the model performance. A higher value of the participation parameter leads to a larger range of ice thicknesses taking part in ridging. Thereby, the ice strength should depend less strongly on the thinnest part of the ITD. Even though this change reduced the norm of the ice strength gradients on average (not shown), the resulting configuration $P_{R,\mathrm{smooth}}$ produces the largest (i.e. worst) cost function values. The extreme change in the participation parameter has a large effect on many different parts of the sea ice model when compared to the configuration $P_{R(\mathrm{int})}$: during summer, the sea ice concentration is reduced drastically over the whole Arctic and

the thickness is decreased moderately over the central Arctic for $P_{R,\text{smooth}}$. Still, the ice drift is slower in $P_{R,\text{smooth}}$ over the whole year in most of the ice covered area. These effects probably outweigh the positive impact it may have on the ice strength.
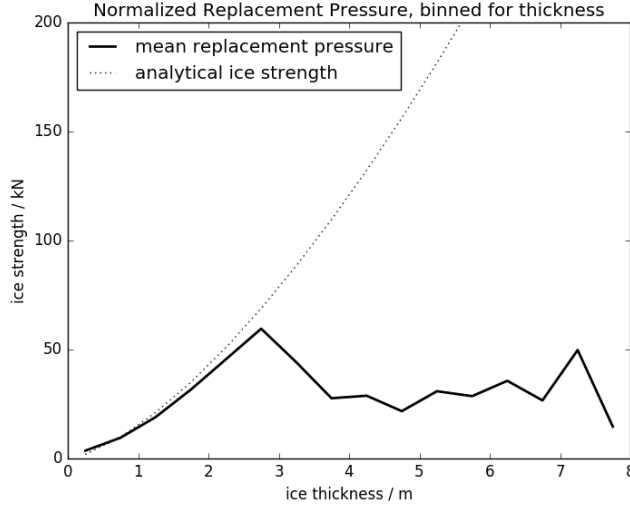
Figure 4.6: Mean modeled ice strength for different thicknesses as calculated in the Arctic by the mean-thickness strength formulation $P_{R(\text{mean})}$ together with the replacement pressure method. All strength values are rescaled to full concentration $A = 1$ using equation (4.18).

Note that, if the replacement pressure method is used, the relationship between ice strength and thickness, as calculated in Section 4.3.1 (equation 4.18), is only valid for ice thicknesses below 3m (Figure 4.6). The replacement pressure method was introduced to avoid non-physical viscous creep in the ice in the absence of all forcing (Hibler & Ip, 1995). Using the replacement pressure

$$P_r = P \frac{\Delta_{\dot{\varepsilon}}}{\Delta_{\dot{\varepsilon}} + \Delta_{\dot{\varepsilon},\text{min}}} \tag{4.19}$$

instead of the calculated ice pressure P in the stress calculations removes this creep from the equations, where $\Delta_{\dot{\varepsilon}}$ is a measure of deformation and $\Delta_{\dot{\varepsilon},\text{min}} = 2 \times 10^{-9}\text{s}^{-1}$ is a regularization parameter (details on the equations are given in appendix 4.A.2). I find that using this method also introduces a limiting feedback for the ice strength: since thick ice is generally stronger, it deforms less and the deformation measure $\Delta_{\dot{\varepsilon}}$ is small. In these situations the regularization (4.19) regulates the ice strength down. This result agrees with previous work, where ridging was found to be increased when using the

replacement pressure method (Kimmritz *et al.*, 2017).

4.4 Discussion

4.4.1 Thickness Dependence of Ice Strength

The results of this study suggest that there is no clear advantage of an ice strength proportional to $h^{1.5}$ over an ice strength proportional to h in large-scale models. The total cost function is lower with the ice strength $P_{H(\text{mean})}$ (proportional to h) than with the ice strength $P_{R(\text{mean})}$ (proportional to $h^{1.5}$). The total cost function value should be interpreted with care: P_R simulates an ice edge in better agreement with observations than P_H; but the ice velocities in the central ice pack are consistently lower for P_R than for P_H, which in turn reduces the agreement with drift observations. Additionally, the two strength parameterizations differ not only in their dependence on the ice thickness, but also in the dependence on ice concentrations, making any decision about the more accurate form of ice strength to thickness relation even more complicated.

Both physical reasoning (Hibler, 1980) and discrete element simulations of the ridge building process (Hopkins, 1998) indicate that when ridging is considered the only energy sink, the ice strength should be proportional to $h^{1.5}$. In contrast, Croasdale (2012) estimated the maximum pressure that the ice pack can exert on large structures in the Arctic. He identified four different processes that can limit this pressure and found that a thickness dependency on $h^{1.104}$ gives a best fit to the observations available for his analysis. In a review of this and similar analyzes of direct and indirect observations of maximum pressures in the ice pack, Timco *et al.* (2017) pointed out that current observations do not allow to derive general laws like these with certainty: Too many assumptions are necessary to translate the observations into values of peak pressure in the ice pack and especially the relative importance of different energy sinks in the failure process is still uncertain.

A lower exponent of ice thickness can be explained when shear deformation along linear kinematic features is the limiting process for sea ice strength. The assumption of Rothrock (1975) that the work done by the pressure force is equal to the sum of the potential energy increase and the energy loss to friction in ridging gives an ice strength proportional to h^2 (or $h^{1.5}$ with refined ridge geometries (Hibler, 1980)). But assuming a situation of pure shear (i.e.

$\dot{\varepsilon}_{II} \neq 0$, $\dot{\varepsilon}_I = 0$), the energy dissipated along shear lines is

$$D_{II} = \dot{\varepsilon}_{II}\boldsymbol{\sigma}_{II} \tag{4.20}$$

where $\boldsymbol{\sigma}_{II}$ is the area average over a grid cell of the depth integrated stress invariant, so

$$\begin{aligned} \boldsymbol{\sigma}_{II} &= \frac{1}{L}\int_0^L \int_0^{h'(x')} \boldsymbol{\sigma}'_{II}(x')\,\mathrm{d}z'\,\mathrm{d}x' \\ &= \boldsymbol{\sigma}'_{II}\,\bar{h} \end{aligned} \tag{4.21}$$

where 0 and L are the beginning and end of the shear line in a given grid cell, and quantities of the sub-grid scale are marked with a prime. Since the stress is assumed constant over a single grid cell, inserting equation (4.21) into the definition (4.20) gives an energy dissipated in shear

$$D_{II} = \dot{\varepsilon}_{II}\boldsymbol{\sigma}'_{II}\bar{h} \tag{4.22}$$

that depends only on the mean thickness of the ice along the shear line, and the thin ice fraction has no special importance. As a consequence, the same argument made by Rothrock (1975) can be used to show that the ice strength in such shear deformation also depends on the mean ice thickness in a given grid cell.

The frictional loss associated with shearing along large-scale linear kinematic features is a much larger energy sink in sea ice models than both potential energy rise and frictional loss in compression (Bouchat & Tremblay, 2014). Further, sea ice models that increase the shear strength relative to the compressive strength compared to the usual ratio of $e = 2$ in an elliptical yield curve simulate better thickness distribution, sea ice drift, sea ice concentration and deformation fields (Miller $et\ al.$, 2005; Ungermann $et\ al.$, 2017; Bouchat & Tremblay, 2017). Wilchinsky & Feltham (2006) explicitly accounted for the effects of sliding friction with a newly derived shape of the yield curve and improved the probability distribution function for ice thickness, ice speed and ice velocity angle with this method. In contrast, the derivation of Rothrock (1975) is based on the argument that the main energy sinks in sea ice deformation are directly connected to ridge formation. A larger role of shear deformation in the energy balance of sea ice could therefore imply an exponent of ice thickness closer to one in ice strength

parameterizations.

The assumptions of Rothrock (1975) about the work necessary for ridging lead to the large role of the thin ice fraction that is found to reduce model performance. The energy dissipated in shear depends on the mean thickness of the ice pack along the shear line, which should have no special connection to the thin ice fraction in any given grid cell. Adjusting the ice strength to account for this large impact of shear deformation could therefore not only explain the low exponents of ice thickness, but also the dependence on mean thickness that are found optimal to reproduce observations.

4.4.2   Weaknesses of the Multi-Category Strength

In this study I find that mean-thickness ice strength parameterizations give better results in an Arctic ocean – sea ice model than multi-category strength parameterizations. In this section I discuss possible reasons for the deficits of ice strength parameterizations based on a multi-category ice model.

Wilchinsky & Feltham (2006) found in multiple combinations of different rheologies and strength parameterizations that multi-category strength leads consistently to larger misfits to observed ice draft distributions. They argue that stability problems alone are not enough to explain this persistent bias. My study agrees with these results when the contributions of each individual dataset for the cost function are taken into account: While the ITD parameterization has an overall positive impact on the concentration field, multi-category strength parameterizations consistently produce a poorer fit to thickness observations (c.f. Figure 4.4).

I propose the high grid-scale gradients in the ice strength as one possible explanation for the poor fit of multi-category strength configurations to thickness observations. The thin categories of the ITD can change more easily on small scales than the mean ice properties. Since the multi-category strength depends strongly on the thin ice fraction, it is affected much more by these changes than a mean-thickness strength. I argue that the other forcing terms in the momentum balance, most importantly the wind and ocean currents, do not fluctuate as strongly on the grid scale. If the forcing in neighboring grid cells is very similar, large differences in ice strength introduce velocity gradients. These increased velocity gradients can lead to excess sea ice deformation with a large impact on Arctic-wide thickness distributions. In my experiments, neither smoother ridging functions (Lipscomb *et al.*, 2007) nor

a higher value for the participation parameter G^* can improve the thickness cost function results significantly, even if they slightly reduce the ice strength gradients. I see this as confirmation that the unrealistically large gradients are inherent to multi-category strength parameterizations.

Noisy fields of sea ice concentration, thickness and strength in models using the Rothrock strength led to unrealistically high thicknesses and strong numerical instabilities (Lipscomb *et al.*, 2007). The smooth ridging functions (4.15) and (4.16) were proposed to damp these effects to make the models more stable. However, the use of the smoother multi-category strength parameterization P_L instead of P_R does not significantly improve the results of the cost function, although this result was produced without resolving the plastic waves (Ungermann *et al.*, 2017). Unresolved plastic waves in viscous-plastic sea ice models can also lead to instabilities on the grid scale (Williams *et al.*, 2017), for example those described in Lipscomb *et al.* (2007). These unresolved plastic waves have so far been analyzed only in numerical models using the two-category strength of Hibler (Williams *et al.*, 2017), so it is unclear if multi-category strength parameterizations simply amplify this instability into the ice strength field, or if the behavior found in the present study is independent of the plastic waves.

4.5   Conclusions

The simple strength parameterization following Hibler (1979) leads to better reproductions of Arctic-wide sea ice observations in an ocean – sea ice model than the strength parameterization based on the simulated change in the ice thickness distribution proposed by Rothrock (1975). The key difference between the two parameterizations is that Hibler calculates the ice strength from the mean ice thickness per grid cell, while Rothrock uses a discretized ice thickness distribution for his calculations. The role of the different mean dependencies of the two ice strength parameterizations on ice thickness and concentration are of second order.

My results show that mean-thickness strength parameterizations perform generally better in basin-scale models than multi-category strengths. I find consistently much larger gradients in the ice strength for multi-category strength than for mean-thickness strength and argue that these lead to unrealistic sea ice deformation. I suggest that grid-scale fluctuations of the thin

ice fraction may cause these larger gradients in the ice strength, possibly amplifying known numerical instabilities caused by unresolved plastic waves in viscous-plastic sea ice models.

Additional arguments for a simple linear relationship between the ice strength and the ice thickness on large scales are: over the last years, different studies indicated that the ice strength should be proportional to a power of h^r with an exponent lower than $r = 1.5$, but the exact value for this exponent is still uncertain. In Arctic simulations, I find no clear advantage of an ice strength dependence on $h^{1.5}$ over an ice strength dependence on h. When the energy necessary for deformation of the ice pack is determined by ridging, the ice strength should be proportional to $h^{1.5}$. Assuming instead that energy dissipated in shear determines the work necessary for deformation, the ice strength should be linear in h. Therefore the relative importance of the different processes taking place in deformation of the ice pack on large scales determines if the exact value of the exponent in the thickness dependence is closer to $r = 1$ or to $r = 1.5$. Specifying the relative amounts of ridging and shear deformation will be the next step necessary for physically realistic and effective ice strength parameterizations.

Appendix 4.A   Derivations and Equations

4.A.1   Closed-Form Solution of Ice Strength for Two-Category Model

For a better comparison of the theory of Rothrock (1975) (equation 4.10) and the simpler ice strength of Hibler (1979) (equation (4.11)), I derive a closed-form solution for the ice strength (4.10) if there is only a mean ice thickness $\bar{h}$ known. This derivation is based on the three assumptions:

1. Ice of mean ice thickness $\bar{h}$ is uniformly distributed between $h = 0$ and $h = 2\bar{h}$

2. Ice takes part in ridging up to the fraction G^* of the cumulative thickness distribution, following Thorndike *et al.* (1975)

3. Ice of thickness h_{in} is ridged uniformly into thicknesses between $h_{out} = 2h_{in}$ and $2\sqrt{H^* h_{in}}$, following Hibler (1980)

If ice in a grid-cell has mean thickness $\bar{h}$ and covers a fraction A of the total area, then the first assumption leads to an ice thickness distribution

$$g(h) = \begin{cases} (1-A)\delta(h) & h = 0 \\ \frac{A}{2\bar{h}} & 0 < h \leq 2\bar{h} \\ 0 & h > 2\bar{h} \end{cases} \tag{4.23}$$

and a cumulative thickness distribution

$$G(h) = \begin{cases} (1-A) + \frac{Ah}{2\bar{h}} & 0 \leq h \leq 2\bar{h} \\ 1 & h > 2\bar{h}. \end{cases} \tag{4.24}$$

The second assumption states that ice of thickness h only takes part in ridging if

$$G(h) \leq G^*. \tag{4.25}$$

For an ice concentration $A > 1 - G^*$ this condition provides a maximal ice thickness

$$h_G = \frac{2\bar{h}}{A}(G^* - (1-A)) \tag{4.26}$$

$$\Leftrightarrow \quad G(h_G) = G^* \tag{4.27}$$

that takes part in ridging. At this point I introduce the notation

$$I_- = G^* - (1-A)$$
$$I_+ = G^* + (1-A)$$

which allows to write $h_G = \frac{2\bar{h}}{A}I_-$. The general form of the weighting function b after Thorndike *et al.* (1975) is

$$b(h) = b_0\left(1 - \frac{G(h)}{G^*}\right), \tag{4.28}$$

which can be written as

$$b(h) = \begin{cases} b_0\left(\frac{I_-}{G^*} - \frac{Ah}{2G^*\bar{h}}\right) & 0 \leq h \leq h_G \\ 0 & h > h_G \end{cases} \tag{4.29}$$

in this special case. Inserting (4.29) into equation (4.3) gives a normalization factor

$$b_0 = \frac{2G^*}{I_- I_+} \tag{4.30}$$

and a final participation function

$$a(h) = \begin{cases} \frac{2(1-A)}{I_+} & h = 0 \\ \frac{A}{\bar{h}(I_+)} - \frac{A^2 h}{2\bar{h}^2 I_- I_+} & 0 < h \leq h_G \\ 0 & h > h_G. \end{cases} \tag{4.31}$$

Finally the third assumption defines a redistribution function

$$\gamma(h_i, h_o) = \begin{cases} N_\gamma & 2h_i \leq h_o \leq 2\sqrt{H^* h_i} \\ 0 & h_o < 2h_i \vee h_o > 2\sqrt{H^* h_i} \end{cases} \tag{4.32}$$

for the tuning parameter H^* and a normalization coefficient N_γ that allows to fulfill the volume conservation (4.6). Inserting the special cases (4.31) and (4.32) into equation (4.5) gives the preliminary form

$$n(h) = \begin{cases} N_\gamma \frac{A}{2\bar{h}} I_+^{-1} \left(h - \frac{AH^* + 4\bar{h} I_-}{8\bar{h} H^* I_-} h^2 + \frac{A}{32\bar{h} H^{*2} I_-} h^4 \right) & h \leq 2h_G \\ N_\gamma I_+^{-1} \left(I_- - \frac{A}{5\bar{h} H^*} h^2 + \frac{A^2}{64\bar{h}^2 H^{*2} I_-} h^4 \right) & 2h_G < h < 2\sqrt{H^* h_G} \\ 0 & h \geq 2\sqrt{H^* h_G} \end{cases} \tag{4.33}$$

of the ITD of produced ridges, which can be inserted into (4.6) to solve for the normalization coefficient

$$N_\gamma = \frac{A}{2(AH^* - \bar{h} I_-)}. \tag{4.34}$$

The results (4.31),(4.33) and (4.34) allow to use the conservation of area (4.8) to calculate the normalization coefficient

$$\omega = \frac{8\sqrt{2} A I_- \sqrt{\frac{H^* \bar{h}}{A}} I_- - 15 A H^* I_+ + 25 \bar{h} I_- I_+ - 20 G^* \bar{h} I_-}{-15 I_+ (AH^* - \bar{h} I_-)} \tag{4.35}$$

necessary to define the ridging mode (4.7). Inserting (4.31), (4.33) and (4.35) into equation (4.10), the result is an analytical formulation for the ice strength

$$P = \frac{2\bar{h}I_-^2\left(-32A^2H^*\sqrt{2\frac{H^*\bar{h}}{A}I_-} + 35AH^*\bar{h}I_- + 21\bar{h}^2I_-^2\right)}{7A^2\left(8AI_-\sqrt{2\frac{H^*\bar{h}}{A}I_-} - 15AH^*I_+ + 25\bar{h}I_-I_+ - 20G^*\bar{h}I_-\right)}.$$

4.A.2 Equations of Sea Ice Motion

The motion of the sea ice is determined by the momentum balance

$$m\frac{\partial \boldsymbol{u}}{\partial t} = mf_C\boldsymbol{k} \times \boldsymbol{u} + \boldsymbol{\tau}_a + \boldsymbol{\tau}_w - m\hat{g}\Delta_H + \nabla \cdot \boldsymbol{\sigma}, \qquad (4.36)$$

which calculates the change in sea ice velocity $\boldsymbol{u}$ from the Coriolis force with f_C the Coriolis parameter and $\boldsymbol{k}$ a unit vector pointing vertically upward; the surface stress on the ice from air τ_a and water τ_w; the sea surface tilt Δ_H with $\hat{g}$ the gravitational acceleration; and the divergence of the internal ice stress $\boldsymbol{\sigma}$. Finally, $m = \rho_i H_i + \rho_s H_s$ is the ice and snow mass per unit area, where H_i, H_s are the grid cell averaged thicknesses of ice and snow and ρ_i, ρ_s the densities of ice and snow. Note that the advection of momentum is neglected in this balance. The surface stresses are calculated as

$$\boldsymbol{\tau}_a = \rho_a c_{d,a}|\boldsymbol{u}_a - \boldsymbol{u}|\boldsymbol{R}_a(\boldsymbol{u}_a - \boldsymbol{u}) \qquad (4.37)$$

$$\boldsymbol{\tau}_o = \rho_o c_{d,o}|\boldsymbol{u}_o - \boldsymbol{u}|\boldsymbol{R}_o(\boldsymbol{u}_o - \boldsymbol{u}) \qquad (4.38)$$

where ρ_a, ρ_o are the reference densities, $c_{d,a}$, cd, o are the drag coefficients, $\boldsymbol{u}_a$, $\boldsymbol{u}_o$ are the surface velocities and $\boldsymbol{R}_a$, $\boldsymbol{R}_o$ rotation matrices for atmosphere (subscript a) and ocean (subscript o) (**?**).

Using the viscous-plastic rheology with an elliptical yield curve, the strain rate tensor $\dot{\boldsymbol{\varepsilon}} = \frac{1}{2}\left[\nabla\boldsymbol{u} + (\nabla\boldsymbol{u})^T\right]$ is connected to the stress by the constitutive equation

$$\boldsymbol{\sigma} = 2\eta\dot{\boldsymbol{\varepsilon}} + \left((\zeta - \eta)\dot{\varepsilon}_I - \frac{P}{2}\right)\boldsymbol{I} \qquad (4.39)$$

where η and ζ are the bulk and shear viscosities, P is the ice pressure and $\boldsymbol{I}$

is the identity matrix. The strain rate can be expressed in its two invariants

$$\dot{\varepsilon}_I = \dot{\varepsilon}_{11} + \dot{\varepsilon}_{22} \tag{4.40}$$

$$\dot{\varepsilon}_{II} = \sqrt{(\dot{\varepsilon}_{11} - \dot{\varepsilon}_{22})^2 + 4\dot{\varepsilon}_{12}} \tag{4.41}$$

expressing divergence and maximum shear. Finally, the bulk viscosity $\zeta = \frac{P}{2\Delta_{\dot{\varepsilon}}}$ and the shear viscosity $\eta = \frac{\zeta}{e^2}$ depend on the axis ratio e of the elliptical yield curve, and the deformation measure

$$\Delta_{\dot{\varepsilon}} = \sqrt{\dot{\varepsilon}_I^2 + e^{-2}\dot{\varepsilon}_{II}^2}. \tag{4.42}$$

5. Summary and Conclusions

Summary

Chapter 2 explores in how far an active ice thickness distribution parameterization in combination with commonly used ice strength parameterizations can improve Arctic sea ice model simulations. A precise methodology is developed to clearly single out the effects of a single parameterization on the model. As a measure of model quality, a costfunction measures the misfit between model results and satellite observations for sea ice concentration, sea ice thickness and sea ice drift, weighted by the measurement uncertainty. Each of the model configurations that are compared is tuned individually with an automated parameter optimization, so that the comparison is between equally-well tuned configurations. I find that an ice thickness distribution parameterization improves model simulations overall, with the most prominent change in the position of the ice edge in the North Atlantic. At the same time, a multi-category ice strength parameterization reduces the agreement of the model results with observations, even undoing the positive impact of the ice thickness distribution parameterization. In addition, this multi-category strength depends strongly on the number of thickness categories which further complicates the use of this parameterization in sea ice models.

Chapter 3 focuses on the precision of the ice thickness distribution parameterization. Results of this parameterization are compared to a large amount of observed local ice thickness distributions in the Arctic. The model reproducing both regional and seasonal differences in the observed distributions to a large degree. However, the model shows a larger bias in modal thicknesses than in mean thicknesses, which indicates skewed distributions compared to

the observations. We argue that such a shift in the distributions is caused by biases in the thermodynamics and the dynamics of the sea ice model that cancel each other out for the mean thickness. Implementing the modal thickness as an additional model diagnostic allows to interpret these biases more clearly in the future. Finally, the model underestimates both differences between different decades and variability in different grid points next to each other. A distinction between multi-year and first-year ice could help the model to better match the observed variabilities and thereby improve the climate sensitivity of the sea ice cover.

Chapter 4 focuses on the different ice strength parameterizations and offers explanations why the two-category parameterization produces better results in Arctic sea ice models than the multi-category parameterization, even though the latter is physically derived from first principles. In this chapter, the multi-category strength is rederived in the limit of only two ice thickness categories to enable a clear comparison of individual features. A comparison of the resulting ice strength parameterizations shows that sea ice models improve when the ice strength depends on the mean thickness instead of on the thin ice fraction as in the multi-category approach. The exact functional dependence of the ice strength on the thickness is a second order effect. This dependence on mean thickness can be explained by taking into account that deformation in shear dissipates the largest amount of energy in the Arctic, while the multi-category ice strength parameterization calculates the ice strength based on the energy lost in compression.

Conclusions

The most general result of this thesis is that the inclusion of an ice thickness distribution parameterization does improve sea ice models overall. But at the same time, the associated multi-category strength parameterization leads to a poorer agreement of model results to observations of sea ice parameters and should be avoided in favor of a simpler two-category ice strength. Even if the multicategory ice strength is derived from first principles, a more ad hoc two-category ice strength parameterization gives better results for medium-resolution sea ice models (Question **Q1**, page 10).

The answer to the question **Q2** requires more detail. The ice thickness distribution parameterization both improves the large-scale features in sea ice models, and it also simulates realistic ice thickness distributions in single grid cells. These distributions match the observed regional and seasonal differences and show the exponentially decaying distribution of thick, ridged ice that can be found in most observations. Therefore, I conclude, that the parameterization of ridging provides an adequate description of the many complex processes involved. In conclusion, sea ice simulations on a basin-scale will improve through an ice thickness distribution parameterization, and it can be fully recommended as long as the additional computational cost is affordable.

The only drawback of this parameterization is that it underestimates the changes connected to decadal differences in atmospheric forcing. Even though the advantages provided by this parameterization are not affected, this can further reduce the climate sensitivity of the Arctic in models compared to reality. Especially for climate change scenarios in fully coupled ocean – sea ice – atmosphere simulations and predictions of future sea ice reduction, these small decadal changes should be taken into account for the evaluation of possible results.

Ice strength parameterizations based on the multi-category approach of Rothrock (1975) generally lead to poorer fits to Arctic sea ice thickness observations than a simple two-category ice strength. This bias is inherent to the multi-category formulation and does not depend on the functional dependence of the ice strength on ice thickness or concentration. I can explain this behavior with the physical assumptions that were made in the derivation of the multicategory strength. There, the deformation in compression of the ice pack is assumed to be the main process that determines the strength of

the ice pack while the impact of deformation in shear on the ice strength is underestimated.

The evaluation of the inner mechanics of these parameterizations leads directly to question **Q3** about possible further improvements. The simplest recommendation is to use sea ice models with an active ice thickness distribution parameterization and the basic two-category ice strength parameterization of Hibler (1979). Many sea ice models already employ the ice thickness distribution (e.g. CICE, LIM3, see Hunke *et al.*, 2011; Massonnet *et al.*, 2011) and I can support this choice by a rigorous comparison to observations that has not been done in this detail. While some of the models already combine the ice thickness distribution with a two-category ice strength (Massonnet *et al.*, 2011), I show for the first time the clear advantage this choice has over a multi-category strength and I can counter the argument that the multi-category strength parameterization should be physically more realistic.

The thickness resolution of the ice thickness parameterization should be high enough to calculate a modal thickness of the distributions and it should be included in the model diagnostics. The modal thickness should be a standard model diagnostic and the thickness resolution of the ice thickness distribution parameterization should be high enough to represent a modal thickness of the distributions. This allows to use thickness distribution observations in a simple yet effective way as an additional model constraint.

Any further development of the investigated parameterizations would take substantially more effort. Possible directions for future work to eliminate the identified flaws are outlined below.

Future perspectives

- The underestimation of the climate sensitivity can be seen as the most relevant problem of the ice thickness distribution parameterization. While sea ice models constantly improved the reproduction of many different observations, the observed decline in summer sea ice area in the Arctic is still not captured by most predictions. A possible step forward could be to implement a distinction between first-year ice and multi-year ice in the model, even though the atmospheric models have probably the largest margin for improvements in similar, fully coupled

predictions. In a simple variant, this distinction could be done by tracing the age of individual ice parcels and adjusting the mechanical and thermodynamic properties of the ice according to age. Alternatively, this could be done in a more process-oriented way, so that deformation events and the desalination over the course of a melting season change the sea ice properties directly.

- The difference between the multi-category strength parameterization and the two-category strength parameterization can be interpreted on a physical basis: the former assumes deformation in convergence as the main mechanism that determines the ice strength, while the latter can be explained by assuming deformation in shear as the main mechanism. Ideally, an ice strength parameterization would take both contributions into account when calculating the ice strength against deformation. In this case, either the thin ice fraction or the mean thickness could be more important for the ice strength, depending on the direction of the loading. A single parameterization that blends different physical processes like this would need a completely new design, starting from the physical assumptions. Even though parts of the theory presented by Rothrock (1975); Pritchard (1981); Wilchinsky & Feltham (2006) may be used, this would be an elaborate project.

- Integrating a more complex relationship between ice strength in compression and ice strength in shear into the model does not only influence the ice strength parameterization but also the yield curve. Adjusting the ice strength to properly account for different mechanisms in shear deformation and in compression might make it necessary to simultaneously modify the rheology of the sea ice model.

Additionally, in this thesis I developed a method to investigate the isolated impact a single parameterization can possibly have on a sea ice model. This method includes a semi-automatic parameter optimization routine that is easy to use and flexible in the definition of the target for the optimization, the Green's Function Approach. While I used this method for the evaluation of specific parameterizations in a sea ice model, the range of possible applications is far larger and it is simple to apply this method to any other parameter-dependent model and with different goals. Currently, it is already used in different contexts:

- Current PhD student Elena Gerwing reduced successfully the sea surface elevation bias in a global ocean model using this method. She took satellite observations of global sea surface elevation as the target of the optimization and adjusted a set of 5 ocean parameters using the Green's Function Approach.

- Giulia Castellani analyzed the effect of variable sea ice drag coefficients in a coupled ocean – sea ice model. She used the Green's Function Approach to adjust the free parameters of the new variable drag parameterization to the used model configuration, using a similar costfunction as presented in chapter 2.

This exemplifies that the Green's Function Approach can serve as a valuable tool to quickly adjust a set of model parameters towards any target and the existing scripts can be used with any numerical model, both for large scale circulation simulations and for process studies.

Overall summary

- I developed a method to measure the fit between model results to satellite observations for sea ice concentration, thickness and drift in a quantitative way and account for confounding effects of model tuning.

- Sea ice models give best results when combining an ice thickness distribution and a two-category thickness parameterization.

- An ice thickness distribution parameterization improves overall results in Arctic sea ice models and produces realistic thickness distributions both in regional averages and in single grid cells.

- Deformation in shear is more important for the strength of the ice pack than deformation in convergence, and ice strength parameterizations need to reflect this. As a consequence, multi-category ice strength parameterizations in sea ice models do not perform as well as two-category ice strength parameterizations.

Acknowledgements

After having finished this thesis, I would like to express my thanks to some people who greatly deserve it. First of all to Martin Losch, whose advice, guidance and sense of humor have not only made this thesis possible, but also made me more often than not enjoy working on it. And to Bruno Tremblay, who showed me the beauty in my work when I could not see it anymore.

Next I want to mention Thomas Jung, who supported myself and my work wherever he could. Frank Kauker accompanied me over the whole course of my project with helpful advice, it was always good to hear his opinion. And I would like to thank Christian Haas for the interesting discussions on my work and his review of this thesis.

I would like to thank my colleagues from the Climate Dynamics section, especially Nils Hutter, Camila Campos and Damien Ringeisen for their support and the friendly atmosphere in which I could pursue my research. And I would like to thank my friends from the ArcTrain program who made the time of my PhD as fun and exciting as it was.

Finally, all of this was only possible with the unwavering support of my family. Thank you so much!

List of Figures

List of Tables

Bibliography

ARMOUR, K. C., BITZ, C. M., THOMPSON, L., & HUNKE, E. C. 2011. Controls on Arctic sea ice from first-year and multiyear ice survivability. *Journal of Climate*, **24**(9), 2378–2390.

BELLCHAMBER-AMUNDRUD, T., MELLING, H., & INGRAM, G. 2002. Modelling the Evolution of Draft Distribution in the Sea Ice Pack of the Beaufort Sea. *In: Ice in the Environment: Proceedings of the 16th IAHR International Symposium on Ice.*

BITZ, C. M., & LIPSCOMB, W. H. 1999. An energy-conserving thermodynamic model of sea ice. *Journal of Geophysical Research*, **104**(C7), 15669.

BITZ, C. M., HOLLAND, M. M., WEAVER, A. J., & EBY, M. 2001. Simulating the ice-thickness distribution in a coupled climate model. *Journal of Geophysical Research*, **106**, 2441.

BLUNDEN, J., & ARNDT, D. S. 2017. State of the Climate in 2016. *Bulletin of the American Meteorological Society*, **98**(8), Si–S277.

BOUCHAT, A., & TREMBLAY, B. 2014. Energy dissipation in viscous-plastic sea-ice models. *Journal of Geophysical Research: Oceans*, **119**, 976–994.

BOUCHAT, A., & TREMBLAY, B. 2017. Using sea-ice deformation fields to constrain the mechanical strength parameters of geophysical sea ice. *Journal of Geophysical Research: Oceans*, **122**(7), 5802–5825.

CHEVALLIER, M., SMITH, G. C., DUPONT, F., LEMIEUX, J.-F., FORGET, G., FUJII, Y., HERNANDEZ, F., MSADEK, R., PETERSON, K. A., STORTO, A., TOYODA, T., VALDIVIESO, M., VERNIERES, G., ZUO, H., BALMASEDA, M., CHANG, Y.-S., FERRY, N., GARRIC, G., HAINES, K., KEELEY, S., KOVACH, R. M., KURAGANO, T., MASINA, S., TANG, Y., TSUJINO, H., & WANG, X. 2016. Intercomparison of the Arctic sea

ice cover in global oceansea ice reanalyses from the ORA-IP project. *Climate Dynamics*, **SI**(jan).

COON, M. D., MAYKUT, G., PRITCHARD, R. S., ROTHROCK, D. A., & THORNDIKE, A. S. 1974. Modeling the Pack Ice as an Elastic-Plastic Material. *AIDJEX Bulletin*, **24**, 1–106.

CROASDALE, K. R. 2012. Ice rubbling and ice interaction with offshore facilities. *Cold Regions Science and Technology*, **76-77**, 37–43.

DANSEREAU, V., WEISS, J., SARAMITO, P., LATTES, P., & COCHE, E. 2017. Ice bridges and ridges in the Maxwell-EB sea ice rheology. *The Cryosphere*, **11**(5), 2033–2058.

DING, Q., SCHWEIGER, A., L'HEUREUX, M., BATTISTI, D., PO-CHEDLEY, S., JOHNSON, N., BLANCHARD-WRIGGLESWORTH, E., HARNOS, K., ZHANG, Q., EASTMAN, R., & STEIG, E. 2017. Influence of high-latitude atmospheric circulation changes on summertime Arctic seaice. *Nature Climate Change*, **7**(4), 289–295.

DUPONT, F., HIGGINSON, S., BOURDALLÉ-BADIE, R., LU, Y., ROY, F., SMITH, G. C., LEMIEUX, J.-F., GARRIC, G., & DAVIDSON, F. 2015. A high-resolution ocean and sea-ice modelling system for the Arctic and North Atlantic oceans. *Geoscientific Model Development*, **8**(5), 1577–1594.

EUMETSAT OCEAN AND SEA ICE SATELLITE APPLICATION FACILITY. 2011. *Global sea ice concentration reprocessing dataset 1978-2009 (v1.1), [Online]. Norwegian and Danish Meteorological Institutes. Available from http://osisaf.met.no.*

EUROSTAT. 2017. *Energy balance sheets.* Publications Office of the European Union.

FELTHAM, D. L. 2008. Sea Ice Rheology. *Annual Review of Fluid Mechanics*, **40**(1), 91–112.

FICHEFET, T., & MORALES MAQUEDA, M. A. 1997. Sensitivity of a global sea ice model to the treatment of ice thermodynamics and dynamics. *Journal of Geophysical Research: Oceans*, **102**(C6), 12609–12646.

FLATO, G. M., & HIBLER, W. D. 1995. Ridging and strength in modeling the thickness distribution of Arctic sea ice. *Journal of Geophysical Research*, **100**(C9), 18611–18626.

FLOCCO, D., & FELTHAM, D. L. 2007. A continuum model of melt pond evolution on Arctic sea ice. *Journal of Geophysical Research*, **112**(C8).

FLOCCO, D., FELTHAM, D. L., & TURNER, A. K. 2010. Incorporation of a physically based melt pond scheme into the sea ice component of a climate model. *Journal of Geophysical Research: Oceans*, **115**(8), 1–14.

GODLOVITCH, D., ILLNER, R., & MONAHAN, A. 2011. Smoluchowski coagulation models of sea ice thickness distribution dynamics. *Journal of Geophysical Research*, **116**(C12).

GODLOVITCH, D., MONAHAN, A., & FLATO, G. 2012. An idealised stochastic model of sea ice thickness dynamics. *Cold Regions Science and Technology*, **78**, 14–30.

HAAS, C., PFAFFLING, A., HENDRICKS, S., RABENSTEIN, L., ETIENNE, J. L., & RIGOR, I. 2008. Reduced ice thickness in Arctic Transpolar Drift favors rapid ice retreat. *Geophysical Research Letters*, **35**(17), 1–5.

HAAS, C., LOBACH, J., HENDRICKS, S., RABENSTEIN, L., & PFAFFLING, A. 2009. Helicopter-borne measurements of sea ice thickness, using a small and lightweight, digital EM system. *Journal of Applied Geophysics*, **67**(3), 234–241.

HAAS, C., HENDRICKS, S., EICKEN, H., & HERBER, A. 2010. Synoptic airborne thickness surveys reveal state of Arctic sea ice cover. *Geophysical Research Letters*, **37**(9), 1–5.

HEIMBACH, P., MENEMENLIS, D., LOSCH, M., CAMPIN, J.-M., & HILL, C. 2010. On the formulation of sea-ice models. Part 2: Lessons from multi-year adjoint sea-ice export sensitivities through the Canadian Arctic Archipelago. *Ocean Modelling*, **33**(1), 145–158.

HERMAN, A. 2016. Discrete-Element bonded-particle Sea Ice model DESIgn, version 1.3a model description and implementation. *Geoscientific Model Development*, **9**(3), 1219–1241.

HERZFELD, U. C., HUNKE, E. C., MCDONALD, B. W., & WALLIN, B. F. 2015. Sea ice deformation in Fram Strait – Comparison of CICE simulations with analysis and classification of airborne remote-sensing data. *Cold Regions Science and Technology*, **117**, 19–33.

HIBLER, W. D. 1977. A Viscous Sea Ice Law as a Stochastic Average of Plasticity. *Journal of Geophysical Research*, **82**(27), 3932–3938.

HIBLER, W. D. 1979. A Dynamic Thermodynamic Sea Ice Model. *Journal of Physical Oceanography*, **9**(4), 815–846.

HIBLER, W. D. 1980. Modeling a Variable Thickness Sea Ice Cover. *Monthly Weather Review*, **108**(12), 1943–1973.

HIBLER, W. D., & IP, C. F. 1995. The effect of sea ice rheology on Arctic buoy drift. *Pages 255–264 of:* DEMPSEY, J. P., & RAJAPAKSE, Y. D. S. (eds), *Ice Mechanics.* New York: Am. Soc. of Mech. Eng.

HOLLAND, M. M., BITZ, C. M., HUNKE, E. C., LIPSCOMB, W. H., & SCHRAMM, J. L. 2006. Influence of the sea ice thickness distribution on polar climate in CCSM3. *Journal of Climate*, **19**(11), 2398–2414.

HOPKINS, M. A. 1998. Four stages of pressure ridging. *Journal of Geophysical Research*, **103**(C10), 21883.

HOPKINS, M. A., & THORNDIKE, A. S. 2006. Floe formation in Arctic sea ice. *Journal of Geophysical Research: Oceans*, **111**(11), 1–9.

HOPKINS, M. A., HIBLER, W. D., & FLATO, G. M. 1991. On the numerical simulation of the sea ice ridging process. *Journal of Geophysical Research*, **96**(C), 4809–4820.

HOURDIN, F., MAURITSEN, T., GETTELMAN, A., GOLAZ, J.-C., BALAJI, V., DUAN, Q., FOLINI, D., JI, D., KLOCKE, D., QIAN, Y., RAUSER, F., RIO, C., TOMASSINI, L., WATANABE, M., & WILLIAMSON, D. 2017. The Art and Science of Climate Model Tuning. *Bulletin of the American Meteorological Society*, **98**(3), 589–602.

HUNKE, E. C. 2010. Thickness sensitivities in the CICE sea ice model. *Ocean Modelling*, **34**(3-4), 137–149.

HUNKE, E. C. 2014. Sea ice volume and age: Sensitivity to physical parameterizations and thickness resolution in the CICE sea ice model. *Ocean Modelling*, **82**, 45–59.

HUNKE, E. C., LIPSCOMB, W. H., & TURNER, A. K. 2011. Sea-ice models for climate study: Retrospective and new directions. *Journal of Glaciology*, **56**(200), 1162–1172.

IPCC. 2013. *Climate Change 2013 - The Physical Science Basis. Contribution of Working Group I to the Fifth Assessment Report of the Intergovernmental Panel on Climate Change.* Cambridge, United Kingdom and New York, NY, USA: Cambridge University Press.

KAUKER, F., KAMINSKI, T., RICKER, R., TOUDAL-PEDERSEN, L., DYBKJAER, G., MELSHEIMER, C., EASTWOOD, S., SUMATA, H., KARCHER, M., & GERDES, R. 2015. Seasonal sea ice predictions for the Arctic based on assimilation of remotely sensed observations. *The Cryosphere Discussions*, **9**(5), 5521–5554.

KIMMRITZ, M., LOSCH, M., & DANILOV, S. 2017. A comparison of viscous-plastic sea ice solvers with and without replacement pressure. *Ocean Modelling*, **115**, 59–69.

KIMURA, N., NISHIMURA, A., TANAKA, Y., & YAMAGUCHI, H. 2013. Influence of winter sea-ice motion on summer ice cover in the Arctic. *Polar Research*, **32**, 1–8.

KOMURO, Y., & SUZUKI, T. 2013. Impact of subgrid-scale ice thickness distribution on heat flux on and through sea ice. *Ocean Modelling*, **71**, 13–25.

KOMURO, Y., SUZUKI, T., SAKAMOTO, T. T., HASUMI, H., ISHII, M., WATANABE, M., NOZAWA, T., YOKOHATA, T., NISHIMURA, T., OGOCHI, K., EMORI, S., & KIMOTO, M. 2012. Sea-Ice in Twentieth-Century Simulations by New MIROC Coupled Models: A Comparison between Models with High Resolution and with Ice Thickness Distribution. *Journal of the Meteorological Society of Japan*, **90**(A), 213–232.

KUBAT, I., SAYED, M., SAVAGE, S. B., & CARRIERES, T. 2010. Numerical simulations of ice thickness redistribution in the Gulf of St. Lawrence. *Cold Regions Science and Technology*, **60**(1), 15–28.

KWOK, R., & CUNNINGHAM, G. F. 2008. ICESat over Arctic sea ice: Estimation of snow depth and ice thickness. *Journal of Geophysical Research*, **113**(C8), C08010.

KWOK, R., & CUNNINGHAM, G. F. 2016. Contributions of growth and deformation to monthly variability in sea ice thickness north of the coasts of Greenland and the Canadian Arctic Archipelago. *Geophysical Research Letters*, **43**(15), 8097–8105.

LAVERGNE, T., EASTWOOD, S., TEFFAH, Z., SCHYBERG, H., & BREIVIK, L.-A. 2010. Sea ice motion from low-resolution satellite sensors: An alternative method and its validation in the Arctic. *Journal of Geophysical Research*, **115**(C10), C10032.

LEMIEUX, J.-F., & TREMBLAY, B. 2009. Numerical convergence of viscous-plastic sea ice models. *Journal of Geophysical Research*, **114**(C5).

LEPPÄRANTA, M. 2011. *The Drift of Sea Ice*. Berlin, Heidelberg: Springer Berlin Heidelberg.

LEVITUS, S., ANTONOV, J. I., BOYER, T. P., BARANOVA, O. K., GARCIA, H. E., LOCARNINI, R. A., MISHONOV, A. V., REAGAN, J. R., SEIDOV, D., YAROSH, E. S., & ZWENG, M. M. 2012. World ocean heat content and thermosteric sea level change (0-2000m), 1955-2010. *Geophysical Research Letters*, **39**(10), 1–5.

LINDSAY, R. W. 2013. *Unified Sea Ice Thickness Cilmate Data Record, 1975-2012.*

LINDSAY, R. 2003. Changes in the modeled ice thickness distribution near the Surface Heat Budget of the Arctic Ocean (SHEBA) drifting ice camp. *Journal of Geophysical Research*, **108**(C6).

LINDSAY, R., & SCHWEIGER, A. 2015. Arctic sea ice thickness loss determined using subsurface, aircraft, and satellite observations. *The Cryosphere*, **9**(1), 269–283.

LINDSAY, R., WENSNAHAN, M., SCHWEIGER, A., & ZHANG, J. 2014. Evaluation of Seven Different Atmospheric Reanalysis Products in the Arctic. *Journal of Climate*, **27**(7), 2588–2606.

LIPSCOMB, W. H. 2001. Remapping the thickness distribution in sea ice models. *Journal of Geophysical Research*, **106**(C7).

LIPSCOMB, W. H., HUNKE, E. C., MASLOWSKI, W., & JAKACKI, J. 2007. Ridging, strength, and stability in high-resolution sea ice models. *Journal of Geophysical Research: Oceans*, **112**, 1–18.

LOSCH, M., MENEMENLIS, D., CAMPIN, J.-M., HEIMBACH, P., & HILL, C. 2010. On the formulation of sea-ice models. Part 1: Effects of different solver implementations and parameterizations. *Ocean Modelling*, **33**(1), 129–144.

MANABE, S., & STOUFFER, R. J. 1980. Sensitivity of a global climate model to an increase of CO2 concentration in the atmosphere. *Journal of Geophysical Research*, **85**(C10), 5529–5554.

MASLOWSKI, W., & LIPSCOMB, W. H. 2003. High resolution simulations of Arctic sea ice, 1979 1993. *Polar Research*, **22**(1), 67–74.

MASSONNET, F., FICHEFET, T., GOOSSE, H., VANCOPPENOLLE, M., MATHIOT, P., & KÖNIG BEATTY, C. 2011. On the influence of model physics on simulations of Arctic and Antarctic sea ice. *The Cryosphere*, **5**(3), 687–699.

MAYKUT, G. A., & UNTERSTEINER, N. 1971. Some results from a time-dependent thermodynamic model of sea ice. *Journal of Geophysical Research*, **76**(6), 1550.

MCPHEE, M. 1975. Ice-Momentum Transfer for the AIDJEX Ice Model. *AIDJEX Bulletin*, **29**, 93–112.

MEIER, W. N., HOVELSRUD, G. K., VAN OORT, B. E., KEY, J. R., KOVACS, K. M., MICHEL, C., HAAS, C., GRANSKOG, M. A., GERLAND, S., PEROVICH, D. K., MAKSHTAS, A., & REIST, J. D. 2014. Arctic sea ice in transformation: A review of recent observed changes and impacts on biology and human activity. *Reviews of Geophysics*, **52**(3), 185–217.

MENEMENLIS, D., FUKUMORI, I., & LEE, T. 2005. Using Green's Functions to Calibrate an Ocean General Circulation Model. *Monthly Weather Review*, **133**(5), 1224–1240.

MENKE, W. 2012. *Geophysical Data Analysis: Discrete Inverse Theory.* Elsevier.

MILLER, P. A., LAXON, S. W., & FELTHAM, D. L. 2005. Improving the spatial distribution of modeled Arctic sea ice thickness. *Geophysical Research Letters*, **32**(18).

NGUYEN, A. T., MENEMENLIS, D., & KWOK, R. 2011. Arctic ice-ocean simulation with optimized model parameters: Approach and assessment. *Journal of Geophysical Research: Oceans*, **116**(4), 1–18.

OVERLAND, J. E., & WANG, M. 2013. When will the summer Arctic be nearly sea ice free? *Geophysical Research Letters*, **40**(10), 2097–2101.

OVERLAND, J. E., WANG, M., WALSH, J. E., & STROEVE, J. C. 2013. Future Arctic climate changes : Adaptation and mitigation time scales. *Earth's Future*, **2**, 68–74.

OVERLAND, J. E., DETHLOFF, K., FRANCIS, J. A., HALL, R. J., HANNA, E., KIM, S.-J., SCREEN, J. A., SHEPHERD, T. G., & VIHMA, T. 2016. Nonlinear response of mid-latitude weather to the changing Arctic. *Nature Climate Change*, **6**(11), 992–999.

PARMERTER, R. R., & COON, M. D. 1972. Model of pressure ridge formation in sea ice. *Journal of Geophysical Research*, **77**(33), 6565–6575.

PARMERTER, R. R., & COON, M. D. 1973. Mechanical Models of Ridging in the Arctic Sea Ice Cover. *AIDJEX bulletin*, **19**, 59–112.

PFAFFLING, A., HAAS, C., & REID, J. E. 2007. Direct helicopter EM Sea-ice thickness inversion assessed with synthetic and field data. *Geophysics*, **72**(4), F127–F137.

PITHAN, F., & MAURITSEN, T. 2014. Arctic amplification dominated by temperature feedbacks in contemporary climate models. *Nature geoscience*, **7**(February), 2–5.

PIZZOLATO, L., HOWELL, S., DAWSON, J., LALIBERTÉ, F., & COPLAND, L. 2016. The influence of declining sea ice on shipping activity in the Canadian Arctic. *Geophysical Research Letters*, **43**, 12,146–12,154.

Polyakov, I. V., Walsh, J. E., & Kwok, R. 2012. Recent changes of Arctic multiyear sea ice coverage and the likely causes. *Bulletin of the American Meteorological Society*, **93**(2), 145–151.

Polyakov, I. V., Pnyushkov, A. V., Alkire, M. B., Ashik, I. M., Baumann, T. M., Carmack, E. C., Goszczko, I., Guthrie, J., Ivanov, V. V., Kanzow, T., Krishfield, R., Kwok, R., Sundfjord, A., Morison, J., Rember, R., & Yulin, A. 2017. Greater role for Atlantic inflows on sea-ice loss in the Eurasian Basin of the Arctic Ocean. *Science*, **291**(April), 285–291.

Pritchard, R. S. 1981. Mechanical Behavior of Pack Ice. *Pages 371–405 of:* Selvadurai, A. P. S. (ed), *Mechanical Behaviour of Structured Media*. Elsevier.

Reid, J. E., Pfaffling, A., & Vrbancich, J. 2006. Airborne electromagnetic footprints in 1D earths. *Geophysics*, **71**(2), 63–72.

Richter-Menge, J. A. 1997. Towards improving the physical basis for ice-dynamics models. *Annals of Glaciology*, **25**, 177–182.

Richter-Menge, J. A., & Elder, B. C. 1998. Characteristics of pack ice stress in the Alaskan Beaufort Sea. *Journal of Geophysical Research: Oceans*, **103**(C10), 21817–21829.

Rothrock, D. A. 1975. The energetics of the plastic deformation of pack ice by ridging. *Journal of Geophysical Research*, **80**(33), 4514–4519.

Rothrock, D. A., & Wensnahan, M. 2007. The accuracy of sea ice drafts measured from U.S. Navy submarines. *Journal of Atmospheric and Oceanic Technology*, **24**(11), 1936–1949.

Rothrock, D. A., Percival, D. B., & Wensnahan, M. 2008. The decline in arctic sea-ice thickness: Separating the spatial, annual, and interannual variability in a quarter century of submarine data. *Journal of Geophysical Research: Oceans*, **113**(5).

Rubner, Y., Tomasi, C., & Guibas, L. J. 2000. The Earth Mover's Distance as a Metric for Image Retrieval. *International Journal of Computer Vision*, **40**(2), 99–121.

Saha, S., Moorthi, S., Pan, H. L., Wu, X., Wang, J., Nadiga, S., Tripp, P., Kistler, R., Woollen, J., Behringer, D., Liu, H., Stokes, D., Grumbine, R., Gayno, G., Wang, J., Hou, Y. T., Chuang, H. Y., Juang, H. M. H., Sela, J., Iredell, M., Treadon, R., Kleist, D., Van Delst, P., Keyser, D., Derber, J., Ek, M., Meng, J., Wei, H., Yang, R., Lord, S., Van Den Dool, H., Kumar, A., Wang, W., Long, C., Chelliah, M., Xue, Y., Huang, B., Schemm, J. K., Ebisuzaki, W., Lin, R., Xie, P., Chen, M., Zhou, S., Higgins, W., Zou, C. Z., Liu, Q., Chen, Y., Han, Y., Cucurull, L., Reynolds, R. W., Rutledge, G., & Goldberg, M. 2010. The NCEP climate forecast system reanalysis. *Bulletin of the American Meteorological Society*, **91**(August), 1015–1057.

Savage, S. B. 2008. Two-component sea-ice thickness redistribution model. *Cold Regions Science and Technology*, **51**(1), 20–37.

Schramm, J. L., Holland, M. M., Curry, J. a., & Ebert, E. E. 1997. Modeling the thermodynamics of a sea ice thickness distribution: 1. Sensitivity to ice thickness resolution. *Journal of Geophysical Research*, **102**(C10).

Schweiger, A., Lindsay, R., Zhang, J., Steele, M., Stern, H., & Kwok, R. 2011. Uncertainty in modeled Arctic sea ice volume. *Journal of Geophysical Research*, **116**(September).

Screen, J. A., & Francis, J. A. 2016. Contribution of sea-ice loss to Arctic amplification is regulated by Pacific Ocean decadal variability. *Nature Climate Change*, **6**(May), 856–861.

Semtner, A. J. J. 1976. A model for the thermodynamic growth of sea ice in numerical investigations of climate. *Journal of Physical Oceanography*, **6**, 379–389.

Spreen, G., Kwok, R., Menemenlis, D., & Nguyen, A. T. 2017. Sea-ice deformation in a coupled ocean-sea-ice model and in satellite remote sensing data. *The Cryosphere*, **11**(4), 1553–1573.

Steele, M., Zhang, J., Rothrock, D. A., & Stern, H. L. 1997. The force balance of sea ice in a numerical model of the Arctic Ocean. *Journal of Geophysical Research*, **102**(C9), 21061—-21079.

STROEVE, J. C., & NOTZ, D. 2015. Insights on past and future sea-ice evolution from combining observations and models. *Global and Planetary Change*, **135**, 119–132.

STROEVE, J. C., BARRETT, A. P., SERREZE, M. C., & SCHWEIGER, A. 2014. Using records from submarine, aircraft and satellite to evaluate climate model simulations of Arctic sea ice thickness. *The Cryosphere*, **8**, 2179–2212.

SUMATA, H., LAVERGNE, T., GIRARD-ARDHUIN, F., KIMURA, N., TSCHUDI, M. A., KAUKER, F., KARCHER, M., & GERDES, R. 2014. An intercomparison of Arctic ice drift products to deduce uncertainty estimates. *Journal of Geophysical Research: Oceans*, **119**.

SUMATA, H., KWOK, R., GERDES, R., KAUKER, F., & KARCHER, M. 2015. Uncertainty of Arctic summer ice drift assessed by high-resolution SAR data. *Journal of Geophysical Research: Oceans*, **120**, 5285–5301.

THOMAS, D. N., & DIECKMANN, G. S. (eds). 2009. *Sea Ice*. Oxford, UK: Wiley-Blackwell.

THORNDIKE, A. S., ROTHROCK, D. A., MAYKUT, G. A., & COLONY, R. 1975. The Thickness Distribution of Sea Ice. *Journal of Geophysical Research*, **80**(33), 4501–4513.

TIMCO, G. W., & WEEKS, W. F. 2010. A review of the engineering properties of sea ice. *Cold Regions Science and Technology*, **60**(2), 107–129.

TIMCO, G., SUDOM, D., FREDERKING, R., BARKER, A., & WRIGHT, B. 2017. A critical review of Arctic pack ice driving forces: New sources of data. *Cold Regions Science and Technology*, **138**, 1–17.

TREMBLAY, L. B., & HAKAKIAN, M. 2006. Estimating the Sea Ice Compressive Strength from Satellite-Derived Sea Ice Drift and NCEP Reanalysis Data. *Journal of Physical Oceanography*, **36**(11), 2165–2172.

TSAMADOS, M., FELTHAM, D. L., SCHROEDER, D., FLOCCO, D., FARRELL, S. L., KURTZ, N., LAXON, S. W., & BACON, S. 2014. Impact of Variable Atmospheric and Oceanic Form Drag on Simulations of Arctic Sea Ice. *Journal of Physical Oceanography*, **44**(5), 1329–1353.

TUCKER, W. B., & PEROVICH, D. K. 1992. Stress measurements in drifting pack ice. *Cold Regions Science and Technology*, **20**(2), 119–139.

TUHKURI, J. 2002. Laboratory tests on ridging and rafting of ice sheets. *Journal of Geophysical Research*, **107**(C9), 1–14.

TURNER, A. K., & HUNKE, E. C. 2015. Impacts of a mushy-layer thermodynamic approach in global sea-ice simulations using the CICE sea-ice model. *Journal of Geophysical Research: Oceans*, **120**(2), 1253–1275.

UNGERMANN, M., TREMBLAY, L. B., MARTIN, T., & LOSCH, M. 2017. Impact of the ice strength formulation on the performance of a sea ice thickness distribution model in the Arctic. *Journal of Geophysical Research: Oceans*, **122**(mar), 2017–2033.

VIHMA, T. 2014. Effects of Arctic Sea Ice Decline on Weather and Climate: A Review. *Surveys in Geophysics*, **35**(5), 1175–1214.

WADHAMS, P., & DAVY, T. 1986. On the spacing and draft distributions for pressure ridge keels. *Journal of Geophysical Research*, **91**(C9), 10697.

WANG, Q., DANILOV, S., JUNG, T., KALESCHKE, L., & WERNECKE, A. 2016. Sea ice leads in the Arctic Ocean: Model assessment, interannual variability and trends. *Geophysical Research Letters*, **43**(13), 7019–7027.

WARREN, S. G., RIGOR, I. G., UNTERSTEINER, N., RADIONOV, V. F., BRYAZGIN, N. N., ALEKSANDROV, Y. I., & COLONY, R. 1999. Snow depth on Arctic sea ice. *Journal of Climate*, **12**, 1814–1829.

WENDISCH, M., BRÜCKNER, M., BURROWS, J., CREWELL, S., DETHLOFF, K., EBELL, K., LÜPKES, C., MACKE, A., NOTHOLT, J., QUAAS, J., RINKE, A., & TEGEN, I. 2017. Understanding Causes and Effects of Rapid Warming in the Arctic. *Eos*, **98**(jan).

WILCHINSKY, A. V., & FELTHAM, D. L. 2006. Modelling the rheology of sea ice as a collection of diamond-shaped floes. *Journal of Non-Newtonian Fluid Mechanics*, **138**(1), 22–32.

WILCHINSKY, A. V., & FELTHAM, D. L. 2012. Rheology of Discrete Failure Regimes of Anisotropic Sea Ice. *Journal of Physical Oceanography*, **42**(7), 1065–1082.

WILCHINSKY, A. V., FELTHAM, D. L., & MILLER, P. A. 2006. A Multi-thickness Sea Ice Model Accounting for Sliding Friction. *Journal of Physical Oceanography*, **36**, 1719.

WILLIAMS, J., TREMBLAY, L. B., & LEMIEUX, J.-F. 2017. The effects of plastic waves on the numerical convergence of the viscousplastic and elasticviscousplastic sea-ice models. *Journal of Computational Physics*, **340**(jul), 519–533.

WINDNAGEL, A., SAVOIE, M., & MEIER, W. 2016. *Sea Ice Index Version 2 Analysis*. Tech. rept. National Snow and Ice Data Center, Boulder CO, USA.

ZHANG, J., & HIBLER, W. D. 1997. On an efficient numerical method for modeling sea ice dynamics. *Journal of Geophysical Research*, **102**, 8691–8702.

ZHANG, J., & ROTHROCK, D. A. 2001. A Thickness and Enthalpy Distribution Sea-Ice Model. *Journal of Physical Oceanography*, **31**(1), 2986–3001.